FACULDADE DE
CIÊNCIAS E TECNOLOGIA
UNIVERSIDADE NOVA DE LISBOA
Departamento de Física

Neural Correlations during Brain Activation in Arithmetical tasks – an approach using Electroencephalographic data

Leonor Lopes Ribeiro da Silva Girão

Dissertação apresentada na Faculdade de Ciências e Tecnologiea da Universidade Nova de Lisboa, para obtenção do Grau de Mestre em Engenharia Biomédica sob a orientação da Professora Doutora *Carla Quintão Pereira*

Setembro de 2010

Resumo

Este trabalho tem por objectivo o estudo da correlação entre diferentes regiões cerebrais durante a realização de uma tarefa de cálculo mental, e de como estas relações variam comparativamente a uma situação de repouso. Para tal, foram utilizados métodos lineares bem como não lineares, i.e., métodos que calculam a correlação linear entre dois sinais e métodos que calculam a correlação entre sinais sem partir de qualquer pressuposto a nível do tipo de relação que se encontra presente.

O primeiro algoritmo implementado foi a função de correlação cruzada, que estima a correlação linear entre dois sinais e o desfasamento entre estes, permitindo fazer inferências a nível de causalidade. Este algoritmo foi validado com a técnica de *surrogation*, de modo a testar a sua aplicabilidade neste tipo de sinais. Seguidamente, foram implementados dois algoritmos análogos entre si, o coeficiente de determinação e o coeficiente de regressão não linear. Ambos estes coeficientes medem a proporção de redução na variância que pode ser obtida estimando a relação entre ambas as variáveis através de uma determinada curva de ajuste, sendo que o primeiro método assume uma relação linear entre as variáveis e o segundo não parte de qualquer tipo de pressuposto relativamente à correlação entre as mesmas.

As principais diferenças observadas entre a situação de repouso e a situação de cálculo consistiram em que na situação de repouso verificou-se que havia mais zonas correlacionadas e durante a tarefa a sincronia entre regiões tornava-se localizada principalmente nas regiões frontais e parietais. Além disso, as estimativas obtidas através dos métodos lineares e do método não linear foram bastante semelhantes, o que sugere que neste caso as relações entre os diferentes circuitos cerebrais são maioritariamente lineares, e deste modo justifica-se a aplicação de algoritmos lineares neste tipo de análises em determinados casos.

Relativamente ao estudo dos atrasos e estimativas de causalidade, não foram obtidos resultados conclusivos.

Palavras-chave: EEG, Cálculo Mental, Correlação Linear e Não Linear

Abstract

The present study aims at examining the correlation among different brain areas while the subjects performed an arithmetical task, and how these differ from the mental relations in the same subjects during a resting state. In order to this, both linear and nonlinear methods were used, i.e., both algorithms capable of detecting linear relations and algorithms capable of detecting correlations without assuming any type of parametric relationship between the signals were implemented.

The first algorithm that was implemented was the cross-correlation function, which gives an estimate of how much two signals are linearly correlated, and estimates the delay between them, thus permitting to make inferences on causality. Furthermore, this algorithm was validated using the statistic method called *surrogation*, in order to test for the applicability of the algorithm on the signals that were to be processed. The next part of the study consisted on implementing two analogous algorithms, the coefficient of determination and the nonlinear regression coefficient. These coefficients both measure the fraction of reduction of variance that can be obtained by estimating the relationship between two signals according to a fitted line, the difference being that the former assumes a linear relation between both sets of samples and the latter doesn't previously assume any type of relationship between the signals.

The main differences in correlation that were observed between the state of mental rest and between the arithmetic task performance were that in the former more brain sites were correlated, whereas during the task this synchrony was mainly verified between frontal and parietal areas, showing a decrease in the other locations. Furthermore, the estimates provided by the linear and nonlinear algorithms were very similar, suggesting that in this case the relationships among different neural networks were mainly linear, and thus validating the application of linear methods in this type of analysis in particular cases.

Regarding the estimation of delays between signals and inferences on causality, no conclusive results were attained.

Keywords: EEG, Mental Calculation, Linear and Nonlinear Correlation

Acknowledgments

First of all, I would like to thank my thesis advisor, Professor Carla Quintão Pereira, not only for her precious advice, but also for all the availability and comprehension demonstrated in all moments.

I would also like to thank Professor Mário Forjaz Secca, for all his support throughout the course, and in particular in this final stage.

A special thank you to Professor Maria João Trindade, for the sympathy demonstrated towards my present condition.

I would also like to thank Filipa Borges, for having shared her knowledge with me.

To all my family, who has always supported and helped me in all possible ways.

A very special thank you to my friends. You know how much you mean to me.

Finally, thank you to my parents for believing in me, and for being such an example.

Contents

List of Figures

List of Tables

Acronyms

BOLD	blood oxygenation level dependence
CBF	cerebral blood flow
DTT	diffusion tensor tractography
ECoG	electrocorticography
EEG	electroencephalography
EPSP	excitatory postsynaptic potential
fMRI	functional magnetic resonance imaging
FT	Fourier transform
HIPS	horizontal segment of the intraparietal sulcus
IPSP	inhibitory postsynaptic potential
MEG	magnetoencephalography
MRI	magnetic resonance imaging
NIRS	near-infrared spectroscopy
OCD	obsessive compulsive disorder
PET	positron emission tomography
PSP	postsynaptic potential
PTO	parieto-occipital-temporal
SPECT	single-photon emission computed tomography
TES	transcranial electric stimulation
TMS	transcranial magnetic stimulation

Introduction

The subject of brain and cognition has been the focus of the attention of many investigators. From cognitive psychology to functional neuroimaging techniques, many have been the approaches taken to get further insight into this question. Techniques having high spatial resolution such as positron emission tomography (PET) and functional magnetic resonance imaging (fMRI) have permitted to identify some structures which become active in several mental tasks. However, no method has, until the present date, attained the high temporal resolution of the electrophysiological methods of electroencephalography (EEG) and magnetoencephalography (MEG), which permit to monitor the activity of the brain in a time-scale in the order of milliseconds. This characteristic of EEG and MEG makes them extremely useful tools particularly in studying relations among different brain areas, being it the reason why the EEG method has been selected for this study.

The present study consisted of processing EEG signals coming from 15 subjects both in an arithmetic task condition and in a resting state condition, and to compare the results obtained from both. With this protocol, the objective is to obtain further insight into mental activation in this type of cognitive activity.

This thesis is organized in five chapters: two theoretical chapters introducing the main aspects regarding this work, one chapter describing the methodology, one chapter presenting and discussing the results that were obtained, and a final conclusion.

In the first chapter, *Introduction to the Brain and Arithmetical thinking*, a brief description of the anatomy and physiology of the brain is presented. This is followed by an outline of the main theories regarding arithmetical thinking that have been presented until the present date by other authors.

The second chapter, *Brain Imaging methods – the special case of EEG*, summarizes the main imaging techniques that are available for the functional study of the brain, focusing, in particular, on EEG.

The third and fourth chapters, respectively, *Methodology* and *Results and Discussion*, describe

the procedures used in the present study and the results they have yielded. In the end of the fourth chapter these results will be discussed.

Finally, in the last chapter, *General Conclusions*, this work will be put in context with the state of art of this subject. This thesis will end by giving further suggestions for its continuation.

1

Introduction to the Brain and Arithmetical thinking

This chapter is aimed at introducing the theme of brain mechanisms underlying mental calculation, describing the main theories and findings on this subject until the present date, and to relate these to the present study. In order to this, a brief description of the brain's anatomy will be presented, followed by a section about the functional organization of the cerebral cortex and a section about brain activity during arithmetic processing. Finally, a brief description of the paradigm used in the present study will be presented, linking this with the findings previously outlined.

1.1 Anatomy of the Brain

1.1.1 The central nervous system

The brain is the centre of the nervous system in all vertebrate and most invertebrate animals (Shepherd 1994).

The nervous system and the endocrine system control the functions of the body. It is composed basically of specialized cells that receive sensory stimuli and which transmit them to effector organs, so that these work harmoniously together for the well-being of the individual. In addition to these functions, the nervous system of higher species has the ability to store sensory information received from past experiences. It is divided into two parts, the central nervous system and the peripheral nervous system. The first is formed by the brain and spinal cord whereas the latter consists of the cranial and spinal nerves and their associated ganglia.

The central nervous system is the main centre where correlation and integration of nervous information occur, and it is composed of a large number of excitable cells called neurons, which are

supported by specialized tissue called neuroglia. The long processes of a nerve cell are called axons or nerve fibres and the substance consisting of nerve fibres embedded in neuroglia is called white matter. The remaining part of the neurons embedded in neuroglia is called gray matter. These two substances form the interior of the central nervous system(Snell 2001).

As reported by Borges (2009), the central nervous system is composed by seven main parts, which are summarized in table1.1. and represented in figure1.1.

Table 1-1: The main parts of Central Nervous System and short description of their main functions.

The Main Parts of the Central Nervous System (CNS)	
Spinal Cord	Caudal part responsible for receiving and processing information from the limbs and trunk
Medulla oblongata	Situated immediately above the spinal cord, controls essentially autonomic functions like digestion, breathing and heart rate
Pons	Juxtaposed to the medulla,it is the carrier of information between the cerebral hemisphere and the cerebellum
Cerebellum	Mass behind the pons, it is the coordinator of voluntary muscle movement and plays a role in the learning of motor functions
Midbrain	Caudally adjoins the pons, it is responsible for sensory-motor function such as eye movement and visual/auditory reflexes.
Diencephalon	Rostrally positioned relatively to the midbrain, it is composed by the thalamus (where the major part of the sensory information is processed and relayed to the cortical areas) and the hypothalamus (regulator of autonomic, endocrine and visceral functions)
Cerebral Hemispheres	Composed in their outer portion by the cerebral cortex and internally by the basal ganglia (regulator of motor performance), the hippocampus (memory storage) and the amygdaloid nuclei (autonomic and endocrine responses of emotional states)

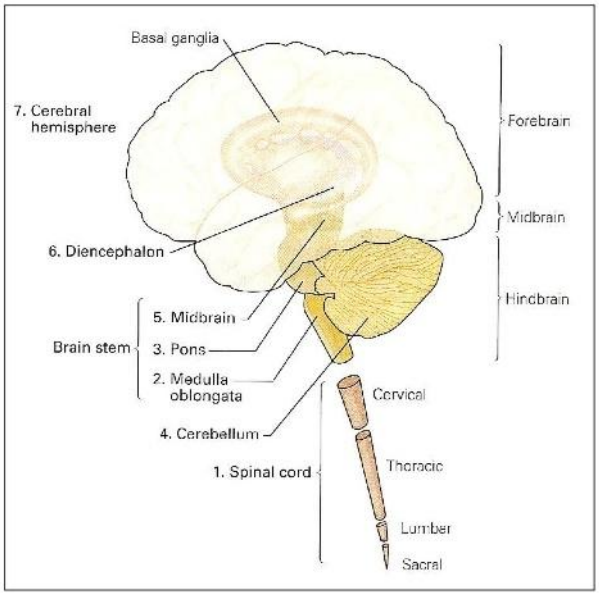

Figure 1-1: The seven main parts of the Central Nervous System (adapted from (Shepherd 1994)

1.1.2 The Brain

The brain is divided in three parts (figure 1.1): the hindbrain, the midbrain and the forebrain. Within the forebrain we can further distinguish the diencephalon and the cerebrum, which is the largest part of the brain and is formed by the two cerebral hemispheres (Snell 2001). The cerebral hemispheres are composed by an inner layer of white matter coated with a layer of grey matter, the cortex, which is the cerebral structure which is most related to the highest cognitive, perceptional and motor functions (Pereira 1998). In order to increase the surface of the cortex, the latter is thrown into folds, called gyri, separated by fissures, or sulci. A number of large sulci are used to separate the brain into lobes. The lobes are named according to the cranial bones under which they lie, and consist of: frontal, parietal, temporal and occipital lobes (see figure 1.2). The sulcis which serve as boundaries for this division are the central and parieto-occipital sulci and the lateral and calcarine sulci. Within each lobe, further structures can be distinguished. Because the lobes of the cerebral hemisphere are not clearly defined on the medial and inferior surfaces, a description will be presented of the divisions in the superolateral surface of each hemisphere, followed by an outline of some important areas in the medial and inferior surfaces of the hemispheres. These structures will be referred to in the following chapters.

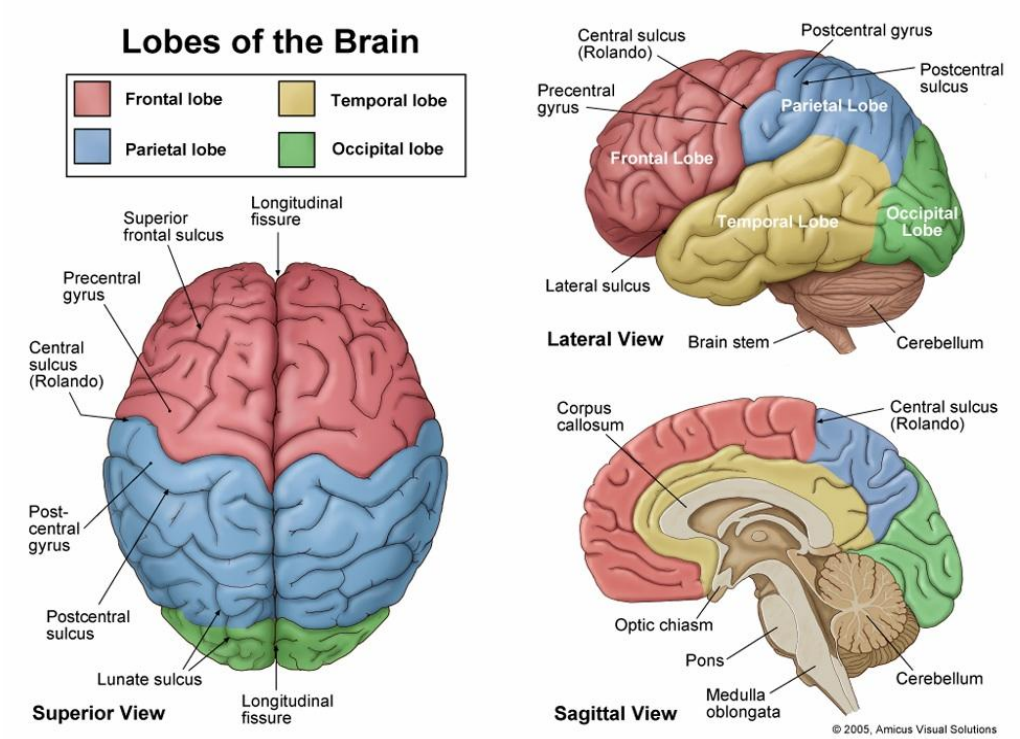

Figure 1-2: The lobes of the brain: Superior, Lateral and Sagittal views (illustrations 2005).

The frontal lobe is divided by three sulci into four gyri. These are the precentral sulcus, the superior frontal sulcus, the inferior frontal sulcus, the precentral gyrus, the superior frontal gyrus, the middle frontal gyrus and the inferior frontal gyrus (figure 1.2, figure 1.3).

The parietal lobe is divided by two sulci into three gyri. The intraparietal sulcus and the postcentral sulcus divide the lateral surface of the parietal lobe into superior parietal gyrus, inferior parietal gyrus and postcentral gyrus (figure 1.2, figure 1.3).

The temporal lobe is also divided by two sulci into three gyri. The superior temporal sulcus and the middle temporal sulcus divide the lateral surface of the temporal lobe into superior temporal gyrus, middle temporal gyrus and inferior frontal gyrus (figure 1.2, figure 1.3).

In the occipital lobe no similar divisions are considered. The occipital lobe occupies a small area behind the parieto-occipital sulcus (figure 1.2, figure 1.3).

In the medial and inferior surfaces of the hemisphere it is worth outlining the cingulate gyrus, which is separated from the superior frontal gyrus by the cingulate sulcus, and the precuneus, which is bounded anteriorly by the upturned posterior end of the cingulate sulcus and posteriorly by the parieto-occipital sulcus (Snell 2001).

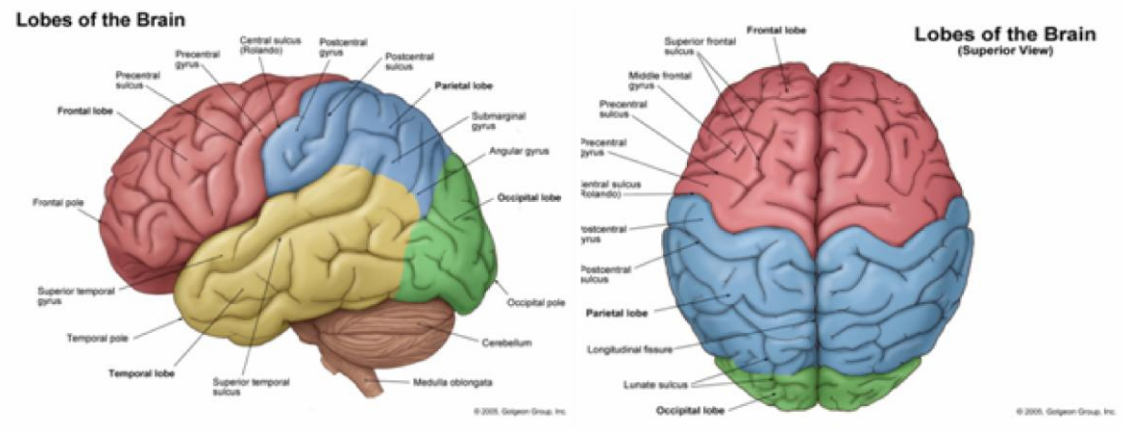

Figure 1-3: The lobes of the brain: Lateral and Superior views (illustrations 2005).

1.2 Functional organization of the cerebral cortex

Many studies carried out in the past century have suggested that the brain is divided into functional specialized areas (Shepherd 1994), although they all work interactively in order to carry out the higher cognitive functions of the human brain (Eric R. Kandel 2000). Some functional regions are represented in figure 1.4. In this section the main functional divisions of the cortex within each lobule will be outlined.

First of all, a distinction can be made between the sensory and motor areas and the association areas. Within the former we can further distinguish the primary sensory and motor areas and the secondary sensory and motor areas. Within the latter we can distinguish the prefrontal, the inferior temporal and the parietal-temporal-occipital areas.

The primary sensory and motor areas occupy about 20% of the cortex and are where most of the sensory information first arrives. Primary motor areas send commands to the muscles. The secondary sensory and motor areas are where the sensory information is further processed (Physpharm 2009).

The sensory and motor areas only occupy a small part of the brain. The remaining areas are known as the association areas, or association cortex. These areas have multiple inputs and outputs and are very much concerned with behaviour, discrimination and interpretation of sensory experiences (Snell 2001).

In the next section a brief description of the sensory and motor areas in each lobule will be presented, followed by an outline of the association areas.

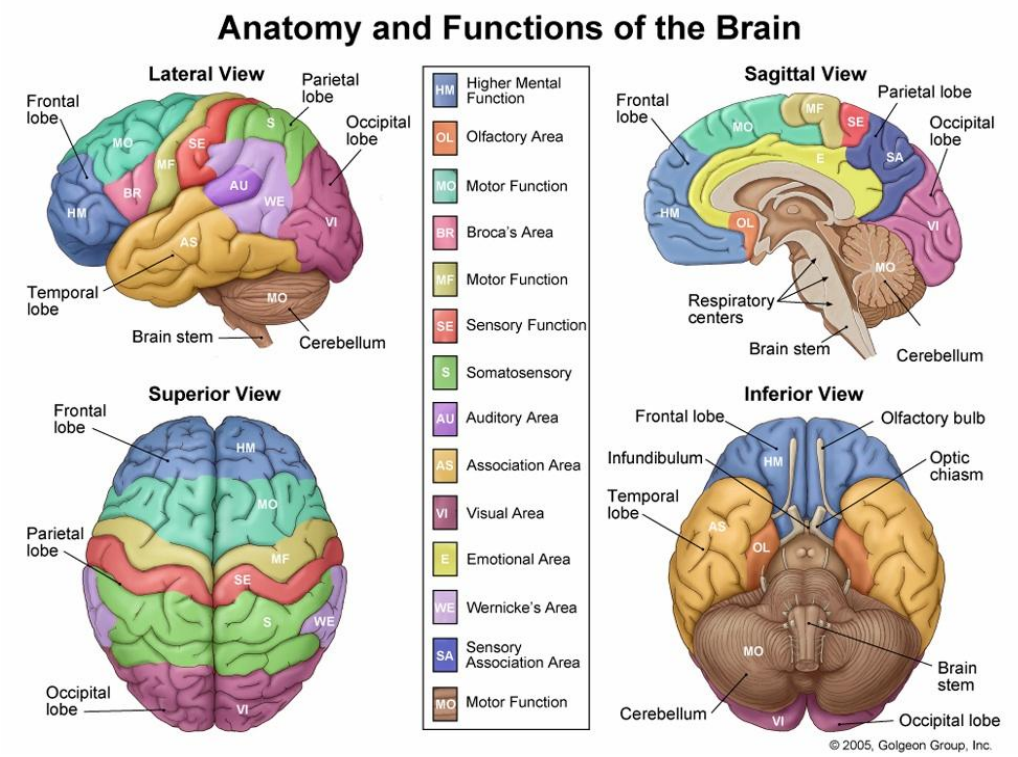

Figure 1-4: Anatomy and functions of the brain (illustrations 2005)

1.2.1 Sensory and motor areas

In the frontal lobe, the precentral area is situated in the precentral gyrus and comprises the motor or primary motor area in the posterior region and the premotor or secondary motor area in the anterior region (figure 1.5). The primary motor area is responsible for carrying out movements of different parts of the body. The area of cortex controlling a particular movement is proportional to the skill involved in performing the movement and not to the mass of muscle which participates in the movement. The function of the secondary motor area is to program the activity of the primary motor cortex. In the medial frontal gyrus is located the supplementary motor area, which is also responsible for producing movement. However its removal does not cause permanent loss of movement. The frontal eye field extends forward from the facial area of the precentral gyrus into the middle frontal gyrus and is considered to be related to the voluntary movements of the eyes, independently of visual stimuli. Finally, located in the inferior frontal gyrus is the motor speech area of Broca, or Broca's area. This area is very important in the language dominant hemisphere (which is the left hemisphere, in 90% of the population (Eric R. Kandel 2000) since it brings about the

formation of words by its connections with the adjacent primary motor areas. The ablation of this area will result in paralysis of speech.

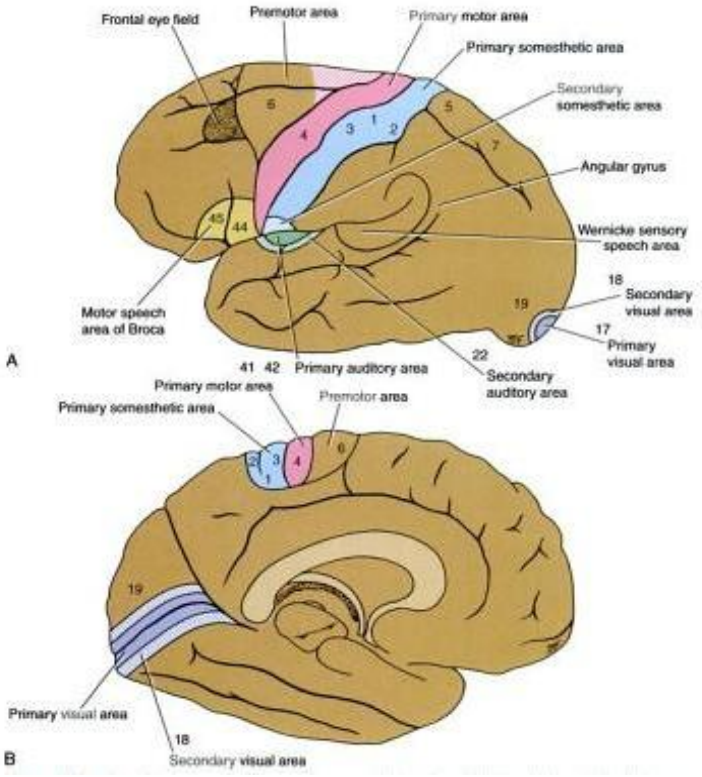

Figure 1-5: Sensory and motor areas. (adapted from (Snell 2001)).

In the parietal lobe, two sensory areas can be distinguished. These are the primary somesthetic area (or primary somatic sensory cortex) and the secondary somesthetic area (secondary somatic sensory cortex). The primary somesthetic area lies across the central sulcus and occupies the precentral gyrus behind the primary motor area. It receives sensory information from nerve projections from the body. Analogously to the primary motor area, the area controlling a particular part of the body is related to its functional importance rather that to its size. The face, lips, thumb and index finger have particularly large areas assigned to them. The secondary somesthetic area is located in the superior bank of the lateral fissure. It is much smaller and seems to be less important than the primary sensory area, and it responds to transient stimuli. However, the exact function of this area is not fully understood.

In the temporal lobe, we can distinguish the primary and secondary auditory areas and the sensory speech area of Wernicke (or Wernicke's area). The primary auditory area is located in the inferior wall of the lateral sulcus. The secondary auditory area lies posterior to the primary auditory area. Together, they are responsible for auditory functions. It is thought that the secondary area is

necessary for the interpretation of sounds and for the association of the auditory input with other sensory information. The sensory speech area of Wernicke lies mainly in the superior temporal gyrus of the dominant hemisphere for language and is connected to Broca's area (on the same hemisphere) by a bundle of nerve fibres called the arcuate fasciculus. It permits the understanding of the written and spoken language.

In the occipital lobe lie the primary and secondary visual areas and the occipital eye field. The primary visual area is located in the walls of the posterior part of the calcarine sulcus and is surrounded by the secondary visual area on the medial and lateral surfaces of the hemisphere. The secondary area is responsible for the integration of the visual information received by the primary visual area to past visual experiences, enabling one to recognize and appreciate what one is seeing. The occipital eye field is thought to exist in the secondary visual area in humans and its function is believed to be reflex and associated with movements of the eye when it is following an object (Snell 2001).

1.2.2 Association areas

The prefrontal cortex is an association area that lies anterior to the precentral area and is concerned with the individual's personality. It is responsible for associating experiences that are necessary for the production of abstract ideas, judgment, emotional feelings and planning. After lesions in this region, patients' emotions become altered. The planning function is carried out through the use of working memory (Physpharm 2009). Working memory is, as Baddeley (1992) defined it, "a brain system that provides temporary storage and manipulation of the information necessary for such complex cognitive tasks as language comprehension, learning and reasoning". It requires simultaneously both storage and processing of information, and can be divided into three subcomponents: the main component is the central executive component, which is an attentional-controlling system, and the other two slave systems are the visuospatial sketch pad, responsible for the manipulation of visual images, and the phonological loop, which stores and rehearses speech-based information in order to keep the contents in working memory. The frontal lobes have been reported to be important in the process of maintenance of the contents of working memory through verbal rehearsal mechanisms due to their relationship with working memory and attention (Baddeley 1992; Thalía Harmony 1999).

The inferior temporal association areas are large areas located on the underside of the cortex and are very much related to memory functions. The inferior and medial portions of the temporal lobe are involved in long term memory. The right side is more involved with pictorial memory (Physpharm 2009) and the left side in verbal memory (in individuals in which the left hemisphere is dominant for language) (Thalía Harmony 1999).

The parieto-occipital-temporal (PTO) areas are where the convergence of senses and attention occur. They are responsible for, as an example, locating objects in space by touch, sight, sound, etc (Physpharm 2009).

1.3 Arithmetics and the Brain – mental processes under number comprehension, production and calculation

The question of how the brain perceives, produces numbers and calculates is highly complex. It has been argued by many investigators, and is now widely assumed, that there is a tight relation between numerical abilities and language mechanisms (M. Caramazza 1985; Stanislas Dehaene 1992; Juliana V. Baldo 2006; Baldo and Dronkers 2007). However, there is strong evidence that numerical competence cannot be reduced to syntax and language skills. Thus, it has been proposed that there exists a numerical sense which enables one to understand the semantic of numbers and operations in terms of numerical quantities (Stanislas Dehaene 1992; Rochel Gelman 2005). To what extent this number sense is innate or developed in the course of life is another question in debate (S. Dehaene 1999; Simon 1999; Laure Zago 2001).

1.3.1 Mental representation of numbers

Before analyzing the process of mental calculation, let us focus on the way numbers are represented mentally. These two aspects have been considered as being separate by many authors (M. Caramazza 1985; Stanislas Dehaene 1992). In 1985, McCloskey and Caramazza proposed a model for the brain circuits used in arithmetic involving two different systems: a number-processing system and a calculation system, where the former "comprises the mechanisms for comprehending and producing numbers, whereas the calculation system consists of the facts and procedures required specifically for carrying out calculations". Tests carried out on brain-damaged patients who showed impairment at performing arithmetical tasks provided further insight into the organization and the functioning of these two systems (M. Caramazza 1985). McCloskey (1985) argued that we can distinguish the capacity to comprehend from the capacity to produce numbers, being that a patient with some impairment might be able to perform the former without being able to perform the latter and vice-versa (figure 1.6).

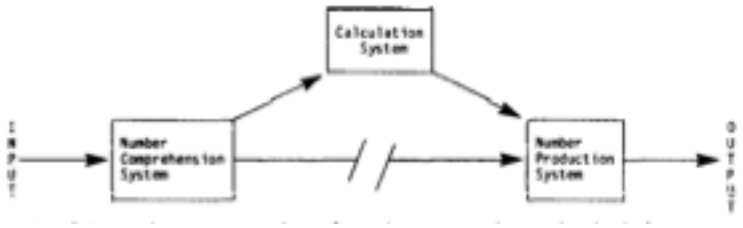

Figure 1-6: Schematic representation of number-processing and calculation systems (adapted from (M. Caramazza 1985)

Within each of these capacities, we can further distinguish the components for processing Arabic numbers (in digit form, e.g. 32) from the components for processing verbal numbers (either spoken or written, e.g. *thirty-two*). Within each of these subsystem there is a distinction between lexical-processing and syntactic-processing components, where lexical-processing refers to the capacity to comprehend or produce single digits (e.g. 2 or *two*) and syntactic-processing refers to the relations among the digits in order to comprehend or produce a number as a whole (e.g. 253 or*two hundred fifty three* involves understanding and processing 2x100+5x10+3).Finally, within the lexical-processing mechanisms of the verbal system (but not the Arabic system) a distinction has been made between the components for producing and comprehending spoken numbers and the components for producing and comprehending written numbers (figure 1.7). In any of the subsystems mentioned, it can occur that someone is impaired at processing one of them while the other remains intact, i.e, they are considered to be independent (M. Caramazza 1985). McCloskey and Caramazza (1985) reported several cases of impaired patients observed by previous investigators which illustrate these distinctions.For example, a patient was described who when presented an arithmetical problem visually or orally he could consistently chose the correct answer from a set of possible answers. However, when this patient was asked to say or write down the answer, he almost always answered incorrectly. This shows an ability to comprehend but not to produce Arabic or verbal numbers (comprehension/production dissociation). Another patient made no errors in judging which Arabic number was larger (e.g., 3 vs 8) but performed at chance on the same task involving verbal numbers (e.g. *three* vs *eight*) (Arabic/verbal dissociation). Cases of lexical/syntactic dissociation were also reported. In one patient, when verbal numbers were presented aurally and the patient was asked to write down the Arabic equivalents, the digits were correct but the order of magnitude was incorrect (e.g., *two thousand five hundred* as 2000500). This demonstrated lexical intact processing with syntactic impairment. Other patients are able to perform magnitude comparisons involving spoken number words but are unable to perform the same task with written number words (phonological/graphemic dissociation). From these examples, one can already start to imagine that since different circuits are related to different competences, there will be a wide variability in brain's activation amongst individuals depending on the mental strategy which is preferred.

However, it has been argued that these components are neither enough to characterize human adult perception of numbers nor to explain the competences of quantification or approximation. Therefore, it was suggested that there are separate non-verbal/analogical quantification processes which provide a sense of numerical quantity, i.e, are associated with the semantic of numbers itself (Stanislas Dehaene 1992). In order to prevent ambiguities the "number sense" can be called *numerosity* and the mental representation of a number can been called *numeron* (Gelman & Gallistel, 1978). In this analogue representation the numbers would be manipulated recurring to mental representation of a number line (Stanislas Dehaene 1992).

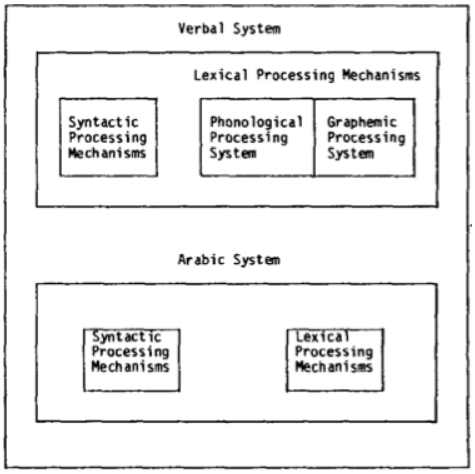

Figure 1-7: Schematic representation of the subsystems comprised in number-comprehension and number-production (adapted from (M. Caramazza 1985)).

1.3.2 Cognitive models for the processing of mental calculation

Calculating involves the integration of various systems, not only those referring to the mental representation of numbers but also those involved in the various stages and processes involved in calculation itself (Sifis Micheloyannis 2005). If one suffers from some kind of impairment of number comprehension/production ability this should lead to a deficit in the performance of a calculation which uses that competence. However, there are systems that concern specifically the process of calculation and one can have no impairment regarding mental representation of numbers but still not be able to calculate (M. Caramazza 1985).

Several models have been proposed which attempt to systematically characterize and interrelate the various mechanisms involved in calculation. M. Caramazza (1985) suggested that the various stages involved in calculation consist of: (1) processing numerical information (numbers and arithmetic symbols); (2) retrieval of basic arithmetic facts (e.g. table facts as 5x4=20); (3) execution of calculation procedures. These operations are held upon an amodal representation of numbers, never directly on numerals or Arabic notation. The conversion between these two modalities is

performed by the number comprehension/production systems mentioned in the previous section. Others have suggested that calculation procedures are accessed through a preferred code (verbal code, visuospacial code, etc) to which all the numerals are initially converted and that can vary from individual to individual (Noel and Seron 1993). This would explain the fact that people tend to perform calculations in the language in which they acquired and practiced arithmetic facts. Campbell and Clark have proposed an *encoding complex model* according to which several codes are integrated and any calculation can be performed according to the input format of the operands. Another suggested model is the *triple-code model* (Stanislas Dehaene 1992). This model is based on the theory that numbers can be represented and manipulated using three different but interconnected codes: the auditory verbal code or *auditory verbal word frame*, which uses general-purpose language modules and where numbers are treated in a way similar to word sequences, a *visual Arabic number form*, where numbers are treated in Arabic format and an *analogue magnitude code*, in which numbers are represented as quantities in an abstract manner similar to a visuo-spatial representation of a number-line. According to Dehaene, each code can be used according to the numerical procedure one wishes to accomplish. In this sense, it totally contradicts the calculation model proposed by McCloskey's, and is more in line with Campbell's model, although in the latter it is argued that the code is selected according to individual's idiosyncratic preferences and in the *triple-code model* the dependence relies on the calculation performed. For example, it was suggested that multiplication tables and counting are stored as verbal associations which are retrieved from memory (e.g. 3x4=12 is stored in a similar manner as a phrase, one doesn't perform the arithmetical calculation to obtain the result), in numerical comparison and approximate calculation the Arabic input is transformed into an analogue magnitude code before the operation can be performed and in multi-digit operations we make use of a spatial image of the operation in Arabic notation. Each representation is interfaced by input-output procedures similar to those presented in McCloskey's model (Stanislas Dehaene 1992).

1.3.3 Arithmetic and brain activity

As stated previously, arithmetical thinking involves the integration of many processes. Many of them are not specific to numbers and also take part in the performance of other tasks, like attention, visual memory, linguistic processing or internal concentration (Thalía Fernández 1995; Laure Zago 2001; O. Gruber 2001; Stanislas Dehaene 2003). In the recent years, brain-imaging techniques have been used in order to get further insight into the anatomical substrate of the various mechanisms involved in arithmetical thinking.

Many studies using brain-imaging techniques reveal predominant activation of the left hemisphere over the right hemisphere in calculation tasks (Linda Rueckert 1996; Margaret G.

Funnell 2007). However, this predominance is not always statically significant, showing a great deal of individual variation. This variability may be related to the strong correlation that exists between strength of handedness and cortical functional asymmetry (Linda Rueckert 1996; Zhang Yun-ting 2005). In fact, previous studies have revealed a strong lateralization of the left hemisphere in right-handed subjects, while left-handed frequently show bilateral activation (Linda Rueckert 1996). In particular, the left parietal cortex area usually shows predominant activity (Thalía Harmony 1999). As the left parietal cortex has been related with storage of verbal information, this activity might be reflect the retrieval of procedural rules and arithmetic facts as well as being involved in the production of internal speech of the sort required for the maintenance of numerical information in working memory (Thalía Harmony 1999). However, the right hemisphere also shows some degree of activation and is believed to be involved in the more semantic aspects of calculation (Gregory A. Troup 1983).

The frontal and prefrontal areas also have been reported as being important in mental calculation processes (J. Cohen 1994; Kazuo Sasaki 1996; Thalía Harmony 1999). Frontal lobes have been described as playing a fundamental role in working memory and attention processes, therefore their activity is probably related to these functions (Thalía Harmony 1999). The Broca's area (located in the left frontal lobe) is strongly associated with the production of speech and often shows activation in arithmetic tasks, therefore it is also suggested that it is involved in the production of internal speech (Thalía Harmony 1999).

Although some structures, as the left parietal cortex and the frontal and prefrontal areas, generally show consistent activation, other structures show varying activation patterns in different tests (Linda Rueckert 1996). Following the fact that the existing models that attempt to explain the process of arithmetical thinking consider different brains systems for different arithmetical tasks, it would not be surprising that different calculations would yield different activation patterns (Linda Rueckert 1996). Various studies have been carried out in order to try to make the link between the theoretical models and the observed activation patterns of the brain. However, the exact interpretation of the results appears difficult since many of the structures which become active are also taking part in other functions as well as in lower levels of numerical processing (O. Gruber 2001). In order to support the triple-code model, Dehaene carried out several studies which aimed at identifying the brain regions associated with the different systems involved in calculation e.g. (S. Dehaene 1999; Stanislas Dehaene 2003; Stanislas Dehaene 2004). Based on results obtained by testing individual's performance on several types of arithmetical tasks (as exact calculation, approximate calculation and number comparison), on animal models of the cerebral bases of number sense and on developmental psychology of basic numerical abilities and their disorders, Dehaene *et al*. suggested possible information pathways involved in the process of mental

calculation. According to Dehaene *et al.*, exact calculation, namely single-digit multiplication, is more related to retrieval of arithmetical facts in a language-specific format as compared to approximation and number comparison tasks, which should rely mostly on non-verbal quantity representation and manipulation networks. In agreement with this, they found that in fact these tasks activated different circuits: exact calculation activated preferably left inferior frontal areas and angular gyrus (traditionally related to language-processing) whereas approximation showed preferably bilateral intraparietal activation. Visual number competences were related to bilateral posterior superior parietal system. Furthermore, within the parietal lobes, the horizontal segment of the intraparietal sulcus (HIPS) was systematically activated whenever numbers were manipulated, independently of number notation and was suggested to be a core quantity system, analogous to an internal number line (S. Dehaene 1999; Stanislas Dehaene 2003; Stanislas Dehaene 2004). Other authors have obtained results in similar experiments which are consistent with these (Zhang Yun-ting 2005; Baldo and Dronkers 2007; Margaret G. Funnell 2007). There is an interesting idea which suggests that this language-independent representation of numerical quantity is related to the preverbal numerical abilities that have been independently established in various animal species and in human infants (S. Dehaene 1999)(Biological foundations of numerical thinking).

On the other hand, Simon (1999) has argued that there is no such thing as an innate "number sense" and that mathematical thinking emerges from the development of nonspecific visuospatial and motor areas (representing a development trace of the finger-counting mechanism that mediates, by extension, the numerical knowledge in adults) in a "brain without numbers". Following this theory, the retrieval of arithmetical facts would engage mainly a left parieto-premotor (motor and visuospacial network) circuit (Laure Zago 2001) and the left anterior insula and the right cerebellar cortex (verbal association network), while computation would yield, in addition to these, mainly activation in a left parieto-frontal network in charge of the holding of the multidigit numbers in visuospatial working memory and a bilateral inferior temporal areas related to the visual mental imagery resolution strategy (Laure Zago 2001). Other tests performed by authors supporting the same model have observed a larger degree of bilateral activation. For example (Thorsten Fehr 2007) observed a common activation of right parietal regions and bilateral frontal regions for all tasks and in particular bilateral parietal activation for more complex tasks.

Finally, it is worth mentioning that an interesting result concerning information direction has been reported by some authors. Based on animal studies, (Nieder 2005; Oana Tudusciuc 2007), Sawamura et al., (2002) suggested that numerosity is first computed in the parietal cortex, and then transmitted and held on-line by prefrontal activity.

2

Brain imaging methods – the special case of EEG

This chapter aims at providing a description of the methods used in the present study, both regarding the acquisition and the processing of the data. It starts by introducing the topic of EEG in the context of functional brain imaging techniques, outlining aspects such as the relation between this technique and neural activity, the recording of the electroencephalographic signal and its main characteristics, and some caveats of the method of EEG. This is followed by an outline of some of the methods used in the processing of the EEG signal, focusing on the ones which were used in the course of this work. Finally, the statistical method of *surrogation* will be introduced, as it was used for the validation of one of the algorithms which were implemented.

2.1 Methods of brain imaging – The EEG method

In the last decades, the development of functional imaging techniques has permitted to get further insight into the anatomy and physiology of the brain. The combination of the experimental strategies of cognitive psychology with these techniques has led to the sprouting of cognitive neuroscience, a science which aims at better understanding the functional organization of the human brain (Raichle 1998).

The non-invasive techniques currently available for functional brain mapping are largely divided into two groups based on their principles. In one hand we have the hemodynamic techniques, which include the positron emission tomography (PET), the single-photon emission computed tomography (SPECT), functional magnetic resonance imaging (fMRI), and the near-infrared spectroscopy (NIRS), and in the other we have the electrophysiological techniques, which include the EEG, the

MEG, and the transcranial magnetic stimulation (TMS). Because each of the above has its unique features in terms of temporal and spatial resolution, it is of special interest to combine them in order to complement each other's information. This multi-modal approach can be divided into two categories: either by using two methods in simultaneous or in separate sessions. The latter has the disadvantage that the experimental conditions cannot be controlled between two sessions, therefore presenting uncontrolled background. However, due to technical reasons, sometimes the simultaneous approach is not feasible and therefore this option has to be taken (Shibasaki 2008).

In this section a brief outline of the above-mentioned techniques will be drawn, giving a special emphasis on EEG, since it consists of the technique used in the present study. Finally, an overview of the multi-modal approach will be presented.

Hemodynamic techniques

The question of neurovascular coupling, i.e., de degree to which brain hemodynamic activity is related to neural activity, has been the subject of discussion for a long time. The experimental studies that have been carried out suggest that the hemodynamic response is correlated to electrical activity at least within a certain range, but showing a spatial spread (Shibasaki 2008).

In brain imaging by PET, positron-emitting isotopes incorporated in radiopharmaceuticals are introduced into the subject intravenously. In the brain, the positrons collide and annihilate local electrons, emitting two oppositely direct photons with the exact same energy. The photon pairs that exit the subject can be detected with a PET scanner, and from a large number of such events it is possible to reconstruct the original distribution of radioisotopes and to map an image of the areas which are being activated either hemodynamically or metabolically. In this way, the PET scan can reveal dynamic effects, such as blood flow. Two tracers that are commonly used are glucose labeled with fluor-18 and water labeled with oxygen-15 (Krane 1988; Shibasaki 2008).

The technique of SPECT is, as PET, a nuclear technique based on the injection of radiopharmaceuticals labeled with isotopes into the body. In SPECT, the common isotopes are technetium 99 and iodine 123. Although SPECT presents lower resolution than PET, it shows other advantages, as using isotopes of longer half-life, which permit to follow their tracing for a longer period of time, and not requiring the presence of a cyclotron nearby.

The fMRI technique was developed in the early 1990's and is based on the principle of blood oxygenation level dependence (BOLD). The BOLD effect was first described in 1990 by Ogawa and co-workers (Ogawa and Lee, 1990; Ogawa et al., 1990) and is based on the following sequence of events: an increase of neural activity is accompanied by an increase of the cerebral metabolic rate of oxygen consumption and a much larger increase in cerebral blood flow. This imbalance leads to a higher oxygenation of the local capillary and venous blood and therefore to a

reduction in the local deoxygenated hemoglobin. This variation will induce the magnetic changes that rely on the basis of the fMRI BOLD signal. However, the precise relationship between neural signals and BOLD is not yet fully understood, which makes the question of the 'inverse problem' (the translation between the fMRI signal and neural activity related to function) complicated. Nonetheless, some advances have been made in terms of formulating the mathematical relations underlying neurovascular coupling. The technique of fMRI shows some advantages over the other noninvasive human brain imaging techniques, which have turned it into a widely used method. These advantages include whole brain coverage, noninterference of spatially separate activation sites and good spatial resolution, which can attain a sub-millimeter scale. However, it does show as well some important limitations, as poor temporal resolution, in the order of seconds, the problem of reconstructing the underlying multi-dimensional neural activity from the scalar vascular fMR signal and the above-mentioned inverse problem: the indirect character of the fMR signal requires a mathematical model to generate functional maps from the signal (P. Ritter 2006). Still related to the technique of MRI, a more recent topic which is revealing interesting results is a technique called diffusion tensor tractography (DTT). This technique is based on the diffusion characteristics of water molecules and has proven to be useful in following white matter tracks (Catani et al., 2005; (Shibasaki 2008). Based on DTT, Catani et al. (2005) were able to detect, beyond the classical arcuate pathway connecting Broca's and Wernicke's areas directly, a previously undescribed, indirect pathway passing through the inferior parietal cortex (Catani et al., 2005).

Finally, there is the technique of NIRS, which has been developed mainly in Japan. The NIRS signal depends on the different optical properties of oxyhemoglobin and deoxyhemoglobin. In brain imaging by this technique, a source irradiates a near-infrared beam into the head through optical fibres, and the signals coming out of the head are detected by optical detectors and transmitted via optical fibres to a photodiode. The NIRS method has the advantages of being able to measure the oxygenated hemoglobin as an index of cerebral blood flow (CBF) continuously and non-invasively, and of not requiring the fixation of the subject's head, making it useful in applications regarding moving subjects and children. The disadvantages include the fact that it only measures cortical activity, not providing a whole brain coverage, and that its spatial resolution is limited to a lobar level (Shibasaki 2008).

Electrophysiological techniques

As stated previously, this group of methods based on electrophysiological principles includes EEG, MEG and TMS.

Transcranial magnetic stimulation (TMS) is used to stimulate both nerve and cortex using external magnetic stimulation, with little or no pain. The lack of pain represents its main advantage

relatively to transcranial electric stimulation (TES), a similar previous technique but which is controversial since it activates pain fibres in the scalp. In TMS, pulsed magnetic field creates current flow in the brain, temporarily exciting or inhibiting specific areas. Depending on stimulation parameters, it is therefore possible to activate or to create transient lesions affecting selective functions of the brain, as vision, language or motor functions. This technique may also be useful for therapy, including psychiatry. An important advantage of this method is its temporal resolution, allowing researchers to assess function on a milli-second scale. It also can be repeated frequently without harm for the patient (Hallett 2000).

Magnetoencephalography (MEG) is a noninvasive technique that detects the weak magnetic fields generated by the large pyramidal neurons of the cerebral cortex using an extremely sensitive magnetic field sensor, the SQUID. The main advantage of the MEG technique is that the magnetic fields are not influenced by the difference in electrical conductivity of the tissues overlying the cerebral cortex, thus, at least theoretically, not being influenced by the skull. However, it presents the disadvantage of only being able to record the current flows from the neurons tangentially oriented with respect to the head surface (Leif Sörnmo 2005; Shibasaki 2008).

Electroencephalography (EEG) is, as MEG, a functional brain imaging technique related to the electrical activity of the apical dendrites of the pyramidal neurons of the cerebral cortex. However, the EEG is the summation of the electrical fields generated by these neurons recorded from the head surface (or from the cortical surface, in the case of electrocorticography (ECoG), instead of the magnetic fields (Shibasaki 2008). As it consists of the technique used in the present study, a more detailed description of the EEG will be presented in the next few paragraphs.

2.1.1 EEG – Electroencephalography

In 1929, Hans Berger recorded the first EEG from the human scalp surface. This was the first step towards the development of a technique that later became an important noninvasive tool in better understanding the human brain. In recent years, the development of the various imaging modalities stated above has led to a decrease in the dominance of the EEG in clinical routine. However, its high temporal resolution, unachieved by the techniques that rely on the hemodynamic response, makes it still a powerful tool in the diagnosis of many diseases such as epilepsy, sleep disorders, and dementia, as well as in the study of human brain physiology and in real-time monitoring in the operating theatre and intensive care unit (Leif Sörnmo 2005).

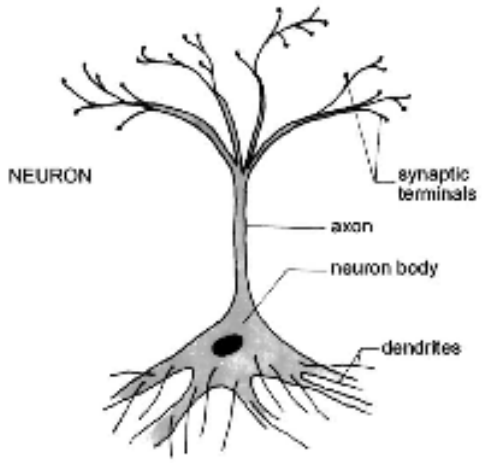

Figure 2-1: Basic structure of a neuron (adapted from (K. B. Durka 2006)

EEG and neural activity

As stated above, the EEG signal is related to the electrical activity of apical dendrites of large pyramidal neurons in the cerebral cortex. The neuron (figure 2.1), or nerve cell, is the basic functional unit of the nervous system (Leif Sörnmo 2005), and together with the glial cells constitutes the two main classes of cells that compose the brain (K. B. Durka 2006). The structure of a neuron is formed by a cell body, called *soma*, from which extend the *dendrites* and the *axon*. The axon is usually a single branch that has a length ranging from 1mm to 1m, like the axons which run from the spinal cord to the feet. Dendrites don't usually have more than 2mm, but one single neuron can have dendrites consisting of several thousands of branches, with each of them receiving a signal from another neuron (Leif Sörnmo 2005), thus establishing contact with up to 10000neurons. In the human brain, there are about 10^{11} neurons (K. B. Durka 2006). The contact between two neurons is established trough *synapses* (figure 2.2), where the terminal part of the axon of one neuron reaches the subsequent neuron, usually by the dendrites or cell body of the latter (Snell 2001).

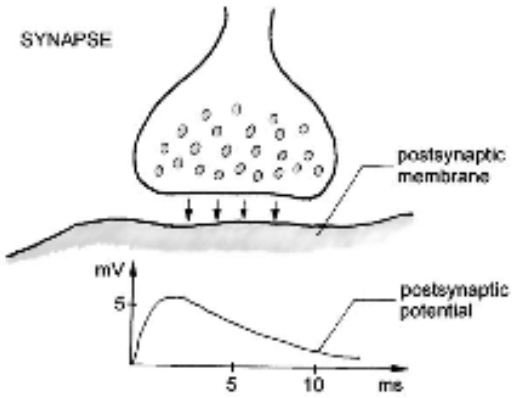

Figure 2-2: Example of chemical synapse and respective excitatory postsynaptic potential (adapted from (K. B. Durka 2006)

The plasma membrane of the neurons has, attached to it, carbohydrate molecules which form the cell coat. These two structures are semipermeable, allowing selective diffusion of certain ions through it. The difference of potential which is observed across the membrane is maintained mainly by the diffusion of K^+ and Na^+ cations (Snell 2001), although there is also a contribution from the Cl^- anions. Ca^+ ions are less abundant but have an important regulatory role (K. B. Durka 2006). Due to the higher permeability of the membrane to K^+ ions than to Na^+, the passive efflux of K^+ to the tissue fluid (where the concentration of this ion is lower) is greater than the influx of Na^+ into the cell (where the concentration of this ion is lower), resulting in a steady potential difference of about -80mV, known as the resting potential. When a cell is stimulated by a certain depolarization, the permeability of the membrane to the Na^+ ions changes, resulting in a rapid influx of this ions into the cell, progressively depolarizing and finally changing the polarity of the membrane to the difference of potential of approximately +40mV. This is called the action potential and lasts about 5 milliseconds. After that, the permeability of the membrane to Na^+ quickly ceases, and is accompanied by an rapid augment of the permeability to K^+ ions, which flow from the cell body into the tissue fluid, restoring the negative resting potential of the membrane (Snell 2001). It is important to refer that this action potential obeys the 'all-or-nothing' rule, this is, for supra-threshold stimuli, a pulse is generated, for subthreshold excitation, the neuron doesn't fire (K. B. Durka 2006). Once generated, the action potential propagates along the axon away from the site of initiation, until arriving at a synapse. At the synapse, the action potential is transmitted onto the following neuron either electrically (electrical synapses), i.e., through gap junctions between the two cells, or, most commonly, mediated by a chemical substance called neurotransmitter (chemical synapse) (figure 2.2) (Leif Sörnmo 2005). The neurotransmitters which arrive at the postsynaptic membrane generate a postsynaptic potential (PSP) which can be excitatory (EPSP), when the postsynaptic membrane becomes depolarized (figure 2.2), or inhibitory (IPSP), when the post-synaptic cell becomes hyperpolarized. Unlike the action potential, the PSP are graded potentials, their amplitudes being proportional to the amount of secreted mediator, which depends on the excitation of the input neuron. EPSP have amplitudes comprehended between 5 to 10 mV and last for 10 to 50 milliseconds (K. B. Durka 2006). Since a neuron can have, as previously mentioned, up to 10000 synaptic contacts with other neurons, it is the summation of the PSP's coming from all these synapses that will determine the excitatory or inhibitory effect on the postsynaptic cell (Snell 2001).

The signal registered in an EEG comes from the summation of the postsynaptic potentials of the neurons in a tissue volume. Although the activity of a single cortical neuron cannot be measured on the scalp due to the thick layers of tissue (fluids, bone, skin) that lie between the cortex and the electrode, the joint activity of millions of cortical neurons produces an electrical field which is sufficiently strong to be measured on the scalp (Leif Sörnmo 2005). The activation of an apical

dendrite produces a brain current flow which generates a current dipole moment. If a number of apical dendrites or neurons which are aligned in the same orientation are activated simultaneously and synchronously, the integration of the current dipoles produced by each of them is probed to be detected by the EEG electrodes. These EEG electrodes detect preferably the normal component of the electric dipoles, which means that the activity of neurons which are normal to the scalp give a larger contribution to the signal than other direction oriented neurons. This is why neuronal activity in the sulci is less reflected in EEG: not only there is majorly a tangential dipole orientation, but also there is a cancellation of dipoles in opposing directions coming from opposing cortical surfaces within the sulci. The largest contribution to the EEG signal comes in most cases from the neocortex, due not only to the proximity of it to the electrodes, but also due to the largely parallel and normal-to-the cortex alignment of pyramidal cells and high number of cortico-cortical synapses facilitating large-scale synchronization (P. Ritter 2006).

Shunting effect and the inverse problem

Another important issue related to the subject of EEG is the fact that electrical fields are strongly influenced by the electrical conductivity of the tissues overlying the cortex. The electrical conductivity of the spinal fluid is higher than that of the brain tissue (about 4 times as high), and the electrical conductivity of the skull is far lower than the former (values of 1/80 and 1/25 have been reported), causing the dispersion of the electrical fields widely over the head surface (Shibasaki 2008). This phenomenon is known by the name of 'shunting effect'. Furthermore, the fact that the structural relationship of the former tissues is not the same all over the head makes this dispersion not uniform, originating a significant distortion of the electrical field distribution. The shunting effect, together with the lack of information regarding different subjects' head geometry and conductivity, and the limited number of EEG channels, makes the so-called 'inverse problem' complicated, i.e., makes the exact location of the current sources from the registered signal difficult to determine (P. Ritter 2006; Shibasaki 2008). This constitutes one important caveat of the EEG technique.

The EEG signal

As previously mentioned, the EEG signal is derived mainly by the post-synaptic potentials. The contribution of the action potentials is very small due to its short duration and to the multi-directional orientation of the axons. Furthermore, because of the capacitive-resistive character of the cell membranes, these act as a low-pass filter, greatly attenuating the higher frequencies typical of action potentials. These facts result in the EEG signal typically presenting frequencies under 50Hz (P. Ritter 2006).

If a group of neurons is activated synchronously the summation of their activity will produce a large amplitude signal, whereas during asynchronous activity of a group of neurons the individual signals will cancel out, resulting in low-amplitude, irregular looking waveforms, even when the excitation involves an identical number of neurons (figure 2.3) (Leif Sörnmo 2005). In normal subjects, the EEG signal has an amplitude ranging from 10 to approximately 100μV. In epilepsy, the amplitudes may increase by almost an order of amplitude (K. B. Durka 2006). The repetition of synchronous activation of a group of neurons results in a rhythmic waveform, which will depend, among other things, on the age and on the mental state of the subject (e.g., attentiveness, sleeping, etc) (Leif Sörnmo 2005). Synchrony among brain networks seems to be a key mechanism for conscious perception and attention (P. Ritter 2006). On the other hand, non-synchronous high frequency/low amplitude rhythms are associated with drowsiness and nondreaming sleep states, when the cortex is involved in processing information and the level of activity of the neurons is relatively high but not directed to any specific task (Leif Sörnmo 2005). It is interesting to observe, for example, that the EEG of lower vertebrates lacks the rhythmical activity found in higher vertebrates recordings (K. B. Durka 2006). Although the meaning of the different brain rhythms is not yet fully understood, some relations between these and mental state have been put forward. The EEG rhythms are usually classified according to five frequency bands:

Delta rhythm: The delta rhythm is characterized by having frequencies under 4 Hz and large amplitude. It is usually found during deep sleep. If this rhythm is registered in the awake adult it may be a sign of, for example, an encephalopathy (Leif Sörnmo 2005);

Theta rhythm: The theta rhythm has frequencies ranging from 4 to 7 Hz and occurs during drowsiness and certain stages of sleep (Leif Sörnmo 2005). In terms of cognition and behaviour, the frequency band corresponding to theta rhythm has been associated with the encoding of new information, episodic memory and syntactic processing (P. Ritter 2006);

Alpha rhythm: This rhythm ranges between 8 to 13 Hz and is usually encountered in normal adults which are relaxed with eyes closed, being suppressed when the eyes are opened . Increased power in this frequency band has been related to working memory and short-term memory load, whereas there seems to be an alpha-desynchronization increasing with long-term memory load and cognitive-task difficulty (P. Ritter 2006). In particular, this rhythm is attenuated by attention, especially visual attention (K. B. Durka 2006);

Beta rhythm: Beta rhythm is a fast rhythm with low amplitude, with frequencies typically ranging from 14 to 30 Hz. It is mainly observed in the frontal and central regions of the scalp and is associated with certain sleep stages (Leif Sörnmo 2005). Synchronization in the beta band is typically associated with visual attention (P. Ritter 2006);

Gamma rhythm: This rhythm corresponds to frequencies above 30 Hz and is associated with

active information processing and finger movement (Leif Sörnmo 2005). Synchronization in this band is related to several types of attention (visual, auditory, etc) (P. Ritter 2006).

In general, one can say that faster rhythms are associated with information and slower rhythms with an idle brain (K. B. Durka 2006). It is important to refer that these rhythms are not present at all times. Sometimes an irregular arrhythmic activity is present, alternating with the above rhythms, which may last from a few seconds to several minutes (Leif Sörnmo 2005). This transient quality is associated with the non-stationary character of the EEG signal, whose statistical properties are ever changing, depending both on time and space. However, for analysis purposes, short epochs of approximately 10 seconds under constant behavioural conditions can be considered to be stationary (Ernst Niedermayer 1999).

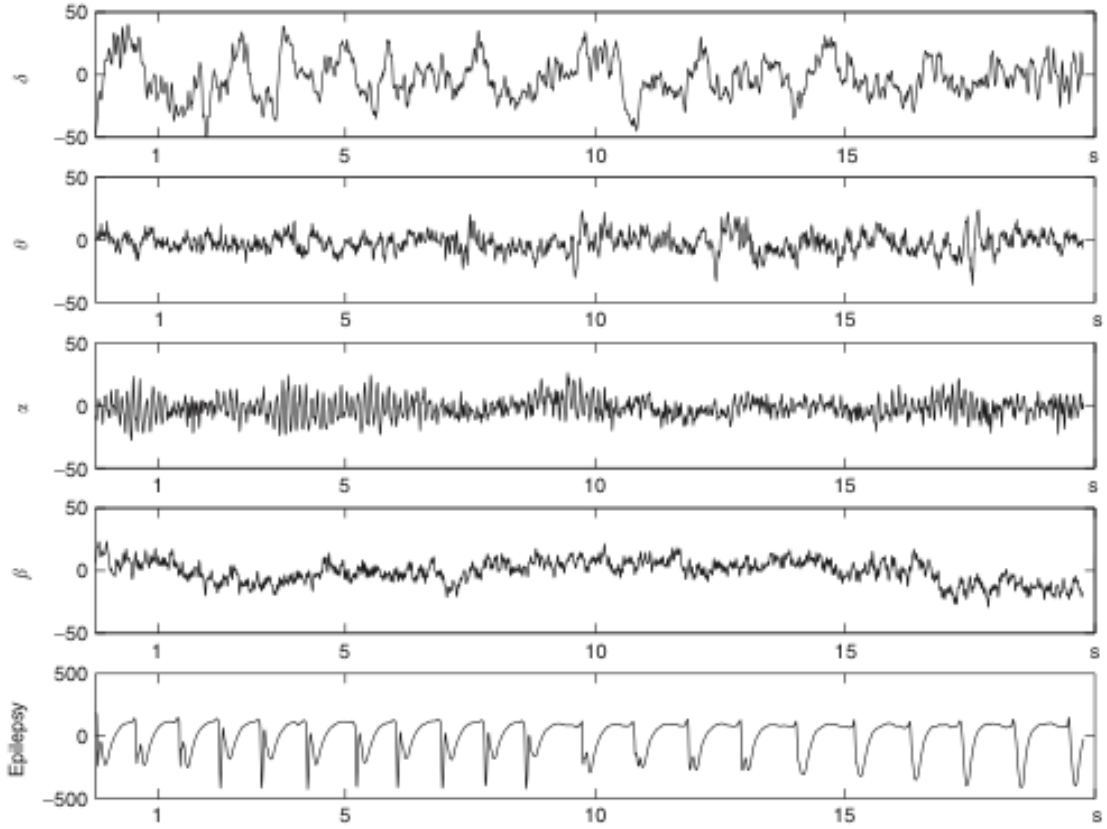

Figure 2-3: Characteristic EEG rhythms. From top to bottom: delta rhythm, theta rhythm, alpha rhythm, beta rhythm and during an epileptic seizure (note that the amplitude scale of the last signal is an order of magnitude bigger) (adapted from Blinowska et al., 2006)

Recording techniques

The usual way to register the EEG signal is using electrodes placed on the scalp. The resistance of this connection should be kept lower than 5 kOhms, therefore the recording site is first cleaned with alcohol and afterwards a conductive gel is put on the electrode (Blinowska & Durka, 2006). The placement of the electrodes is usually made according to the standardized International 10/20 system, which employs 21 electrodes at specific landmarks, so that the distance between them corresponds to either 10 or 20% of the skull perimeter (figure 2.4). According to this system, the letters F, P, T, O, and A stand for, respectively, frontal, parietal, temporal, occipital and auricle. Furthermore, the odd-numbered electrodes are placed on the left side, the even-numbered on the right, and z (zero) on the midline (Leif Sörnmo 2005). In cases where more than 21 electrodes are needed, as for example in brain mapping, electrode sites are placed halfway between these, in the extended 10/20 system (K. B. Durka 2006). In table 2.1 are listed the cortex areas underlying each electrode in the 10/20 system.

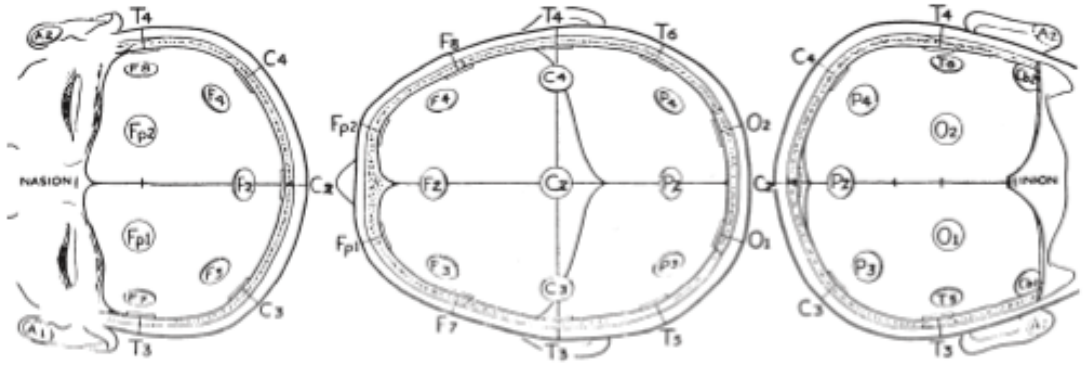

Figure 2-4: International 10/20 system for electrode placing in EEG recording (adapted from (K. B. Durka 2006)

Since the EEG is a measure of potential difference, there is the need to establish a reference. This can be done using more than one montage. In the referential, or unipolar, setup, the signal is measured relatively to the same electrode for all derivations. This common electrode is usually placed on the earlobe, noise, mastoid, chin, neck, or scalp center. In the bipolar montage, the potential difference is measured between two particular scalp electrodes. In the common average setup the activity of the electrodes is measured referenced to the average potential of all electrodes. Finally, there is the Hjorth transform reference, in which the signal from each electrode is referenced to the four closest neighbours (K. B. Durka 2006).

Although the EEG signal is in fact a continuous variation of potential as a function of time, it must be digitalized in order to be computer processed. This can be achieved using an analog-to-digital (AD) converter, which converts the continuous signal into a discrete time series (Ernst

Niedermayer 1999). In order for the statistical properties of the waveforms not to be altered in the course of this process, the signal must be sampled at least 200 Hz, in order to cover, from the Nyquist theorem, the frequencies ranging from 0 to 100 Hz. However, a more detailed analysis of the transient aspects of the waveform requires higher frequencies of acquisition (Leif Sörnmo 2005).

A final important stage regarding EEG signal acquisition is artifact removal. The main problem concerning this issue is the lack of definition regarding what is an EEG artifact. In addition to the neuronal signal, there are many other phenomena which might be interfering with it, as for example muscle activity (EMG), heart activity (ECG), eye movement (EOG), contamination from external magnetic fields, poor electrode contact, subject's movement, etc. In order to distinguish these components from the actual EEG, many times the signals coming from other sources (EMG, ECG, EOG) are registered simultaneously to the EEG in order to facilitate the posterior segregation of artifacts (K. B. Durka 2006).

Table 2-1: Cortical areas underlying each electrode in the 10-20 system (adapted from (Kaiser 2006)

Lobe	**Gyrus**	**Site (Left/Right)**
Frontal	Superior	Fp1/2
	Inferior	F7/8
	Medial	F3/4
	Medial	Fz
	Precentral	C3/4
	Superior	Cz
Temporal	Medial	T3/4
	Medial	T5/6
Parietal	Inferior	P3/4
	Precuneus	Pz
Occipital	Medial	O1/2

2.1.2 Multi-modal approach

Recalling the previous description of hemodynamic and electrophysiological techniques, each of them has its different characteristics, therefore the combined used of two or more of them is expected to complement each other, giving us more information than only one on its own. This multi-modal approach is particularly interesting if a hemodynamic based technique is combined with an electrophysiological based one, since the former provides good spatial resolution and the latter good temporal resolution (Shibasaki 2008). In the next few paragraphs, a brief account of some

combinations of imaging techniques will be presented.

The combined use of EEG and fMRI has been the subject of much attention, especially in what concerns its simultaneous acquisition (P. Ritter 2006; Shibasaki 2008), due not only the fact that it is a very promising technique but also because of the challenge in combining both methods. fMRI employs rapidly changing gradient fields and radiofrequency (RF) electromagnetic fields, which induce significant current flows in the electrodes and wires of the EEG equipment. This creates not only interference, but can also be harmful to the subject due to localized heating and burns. On the other hand, the EEG might also interfere with the MR image quality. Despite these difficulties, some advances has been made in minimizing them, so that nowadays this combined technique can be used both clinically and experimentally, showing interesting results. Some simple general rules which are helpful in overcoming the caveats of this combined method regard minimizing the area comprised by loop wires, avoiding motion and avoiding ferromagnetic substances (P. Ritter 2006). In the clinical context, the simultaneous recording of EEG and MR is extremely useful in the evaluation of patients with medically intractable partial epilepsy (Shibasaki 2008). In Ritter and Villringer (2006) further references for studies regarding the combined use of EEG/MRI can be found.

A combination that is easier to implement and shows much less artifact is the recording of EEG during PET scanning. Experimental studies carried out using this technique include works done by Oohashi et al. (2000), (M. Schreckenberger 2004; N. Oishi 2007).

Furthermore, studies combining different methods in separate sessions have also been carried out. Some examples include works done by (P. Ahlfors 1999; Keiichiro Toma 2002; Christoph Bledowski 2004), combining EEG and fMRI, and by Dale and Halgreen (2001) and (E. Disbrow 2001), combining MEG and fMRI. Because of the technical reasons, the use of MEG and fMRI is only possible in separate sessions.

Finally, due to the complementary characteristics of EEG and MEG, the simultaneous recording of both is also interesting to be applied. An example of such can be found in (C. Tallon-Baudry 1997)

2.2 EEG processing

The development of modern computers has extended the analysis of EEG signals from visual inspection to more complex time series techniques. This time series analysis can be either univariate, i.e. regarding the properties of only one signal, or multivariate, i.e. relating two or more signals, as for example when one estimates interdependencies among different electrodes' recordings. Examples of univariate measures that have been applied in previous studies include correlation

dimension, nonlinear index (Ernesto Pereda 2005), statistical measures such as average amplitude or average frequency, power spectrum, etc (Ernst Niedermayer 1999). More recently, the extraction of information from multivariate techniques has been employed, although one has to apply these methods carefully due to the often noisy, non-stationary and finite character of the signals. Furthermore, within both univariate and multivariate analysis, linear and nonlinear methods can be applied, being it in the time or in the frequency domain (Ernesto Pereda 2005).

Because the present study relied on multivariate time series analysis, a brief account of some of the available multivariate analysis algorithms will be presented in the next few paragraphs. This description will start by the linear methods, followed by the nonlinear methods, focusing in particular the algorithms used in the present study, i.e., the cross-correlation function, the coefficient of determination and the nonlinear regression coefficient. A more extended review on the subject of multivariate analysis can be found in Pereda et al. (2005).

2.2.1 Linear methods

Pearson's product moment correlation coefficient and coefficient of determination

The linear regression coefficient, ρ, commonly known as the Pearson's product moment correlation coefficient, is a well-known signal analytical measure which measures the instantaneous linear relation between two variables, say X and Y. It is defined as

$$\rho = \frac{\mathrm{cov}(X,Y)}{\sqrt{\mathrm{var}(X)\,\mathrm{var}(Y)}}$$

The above formula defines the correlation coefficient for continuous signals, the estimator of which, for sampled signals, is given by

$$r = \frac{\frac{1}{N}\sum_{i=1}^{N}(x_i - \langle x \rangle)(y_i - \langle y \rangle)}{\sqrt{\frac{1}{N}\sum_{i=1}^{N}(x_i - \langle x \rangle)^2 \frac{1}{N}\sum_{i=1}^{N}(y_i - \langle y \rangle)^2}} \quad (1)$$

in which x_i and y_i are the amplitude values of the samples of the X and Y signals, <x> and <y> are the mean of the amplitude values of X and Y and N is the total number of samples (Pijn 1990). The output of this expression ranges between -1 and 1, the former meaning complete linear inverse correlation and the latter meaning complete linear direct correlation. The lower the absolute value of the correlation coefficient, the lower the linear correlation between the two variables, so that a value of 0 (zero) suggests linear independence between X and Y.

Another linear measure related to the above is the coefficient of determination, r^2. If one plots the amplitudes of Y, y_i, against the amplitudes of X, x_i, thus obtaining a scattergram, and uses the least square procedure in order to fit the points with a straight line, ($y = ax + b$), r^2 can be

understood as the proportion of reduction of variance in Y that is obtained by assuming this linear relation between the two sets of values. In other words, the fitted line will provide an explained variance, whereas the points that do not lie on the line will have unexplained variances (not explained by the values of X according to the fitted line). This is translated by the following formula:

$$r^2 = \frac{\text{total variance} - \text{unexplained}}{\text{total variance}},$$

$$\text{or,}\quad r^2 = \frac{\sum_{i=1}^{N} (y_i - \langle y \rangle)^2 - \sum_{i=1}^{N} (y_i - (ax_i + b))^2}{\sum_{i=1}^{N} (y_i - \langle y \rangle)^2}. \quad (2)$$

$$(a,b) \neq (0,0)$$

It is important to notice that r^2 is not necessarily equal to the square of r, defined on expression (1), only when the regression line ($y = ax + b$) passes through the origin. Furthermore, value of r^2 is comprehended between 0 and 1. Finally, it is significant to state that r^2 is a symmetric estimator, i.e., r_{XY} equals r_{YX}, as can be verified by the analysis of expression (2) (Pijn 1990).

Cross-correlation function

If the correlation coefficient, ρ, is calculated as a function of the time shift between X and Y, one obtains the cross-correlation function (Pijn 1990). This algorithm measures the linear correlation between two variables as a function of their delay time (τ), and has been one of the oldest methods to be applied. Furthermore, it can also used to estimate causality: if there is a delay from, say, X to Y, then one may postulate that X causes Y. However, this is not always the case, and therefore one must be careful in the interpretation of the outcome of this function. In fact, either internal delay loops or different distances of the electrodes to the sources might lie at the origin of the observed delay (Ernesto Pereda 2005).

The analytical formula for estimating the correlation between x(t) and y(t), if these are normalized to have zero mean and unit variance, is

$$C_{xy}(\tau) = \frac{1}{N} \sum x(k+\tau)y(k),$$

where N is the total number of samples and τ the time lag between the signals. The value of τ that maximizes the function is usually taken as the delay between the two signals, considering that these are linearly related (as mentioned above, these conclusions must be treated carefully) (Ernesto Pereda 2005). Examples of pioneer studies on EEG using this method can be found for example in

Brazier and Barlow (1956), Brazier and Casby (1952), and Cohn and Leader (1967). Reviews on the application of the cross-correlation function and its variants in cortical neurons' spike trains can be found in (Brody 1999) and Nowak and Bullier (2000).

Coherence

The coherence method is similar to the cross-correlation, in the sense that it is a measure of the linear correlation between two signals, only the former is calculated in the frequency domain whereas the latter refers to the time domain (Pijn 1990). Coherence, sometimes known as coherency, can be estimated using the following expression (Borges 2009):

$$k_{xy}(f) = \frac{W_{xy}(f)}{\sqrt{W_{xx}(f)W_{yy}(f)}},$$

One of the problems of this algorithm relies on the fact that, due to the finite size of the signals, only an estimate of these spectral quantities can be obtained. Thus, some approximate, optimized methods of coherence estimation using averaged epochs of the signals have been developed, as for example the Welch method (Ernesto Pereda 2005; Borges 2009)). Examples of studies using this algorithm can be found, in (Adey et al., 1967; French and Beaumont, 1984; or (H. Zaveri 1999).

Granger causality

The Granger causality, as other linear methods, is based on the assumption that the analyzed signals are linearly related. Though, in the field of economics, there have been some attempts to modify it in order to incorporate the nonlinear properties of the series. It was named after the Nobel Prize winning economist Clive Granger, and parts from the principle that "if X is influencing Y, then adding past values of the first variable to the regression of the second one will improve its prediction performance, which can be assessed by comparing the univariate and bivariate fitting of the AR (autoregressive) models to the signals" (Pereda 2005). This method provides an alternative way for the estimation of causality between two signals, other than through the time delay obtained with the cross-correlation or with the nonlinear regression coefficient algorithms (see Nonlinear regression coefficient). However, results obtained with this method have to be evaluated carefully since the true causality can only be assessed if the sets of the two time series contain all possible information and sources of activities for the problem, which s rarely the case with EEG signals.

2.2.2 Nonlinear methods

Nonlinear regression coefficient

The correlation coefficient, η^2, is analogous to the previously mentioned coefficient of determination, r^2, except that the latter assumes a linear relationship between the samples and the former describes the dependency between X and Y in a non-specific way, i.e., not assuming any previous parametric model. Furthermore, h^2 is an estimator of η^2, which describes the reduction of variance of Y that can be obtained by predicting the Y values from those of X according to the regression curve, i.e.,

$$\eta^2 = \frac{\text{total variance} - \text{unexplained}}{\text{total variance}}$$

The particularity of this method lies in the determination of the regression curve, $\mu_{X|Y}$, based solely on the data points without any *a priori* knowledge of the relationship between the two sets of samples (Pijn 1990). This can be accomplished using the procedure described below.

The first step consists of setting the averages of the samples to zero and plotting (figure 2.5), thus obtaining a scattergram. Afterwards, the ordinate is split into equally sized bins. For each bin, the X value of the midpoint (p_i) and the average of the Y values comprised in the bin (q_i) are calculated, therefore obtaining one (p_i,q_i) point for each bin. These points are then connected by segments of straight lines, thus obtaining a piecewise approximation of the regression curve. This approximation curve shall be designated as $f(x)$. The nonlinear regression coefficient is then calculated using the following formula:

$$h^2 = \frac{\sum_{i=1}^{N}(y_i - < y >)^2 - \sum_{i=1}^{N}\left(y_i - f\left(x_i\right)\right)^2}{\sum_{i=1}^{N}\left(y_i - < y >\right)^2},$$

where N is the number of samples and <y> the average of all y_i (Pijn 1990).

Because of the analogy in concepts of h^2 and r^2, if X and Y are linearly related, the calculation of these two coefficients should yield the same result. However, contrary to what happens with the r^2 coefficient, where the unexplained variance can be precisely determined, in the calculation of the nonlinear regression coefficient this quantity can only be estimated. This means that even if there is in fact a linear relationship between X and Y, h^2 will not necessarily be equal to r^2, although it will approximate this quantity. Furthermore, h^2 is not a symmetric coefficient, which means that h^2_{XY} (nonlinear regression coefficient for Y as a function of X) is not necessarily equal to h^2_{YX} (nonlinear regression coefficient for X as a function of Y). Once again, only if there is a linear relationship between the two sets of values will this equally be verified. In general, this asymmetry will be greater if not only there is a nonlinear relationship between the two variables but also if the inverse of the

nonlinear transformation is not single-valued. Therefore, if one obtains a high asymmetry of h^2, this difference may be 'likely due to a strong nonlinear relationship between X and Y of such type that X is not a single valued function of Y if $h^2_{XY} > h^2_{YX}$ or Y is not a single valued function of X if $h^2_{YX} < h^2_{YX}$' (Pijn 1990). When noise is present in the signal, the asymmetry becomes more enhanced, although it is higher for small amplitude noise (Pijn et al., 1990).

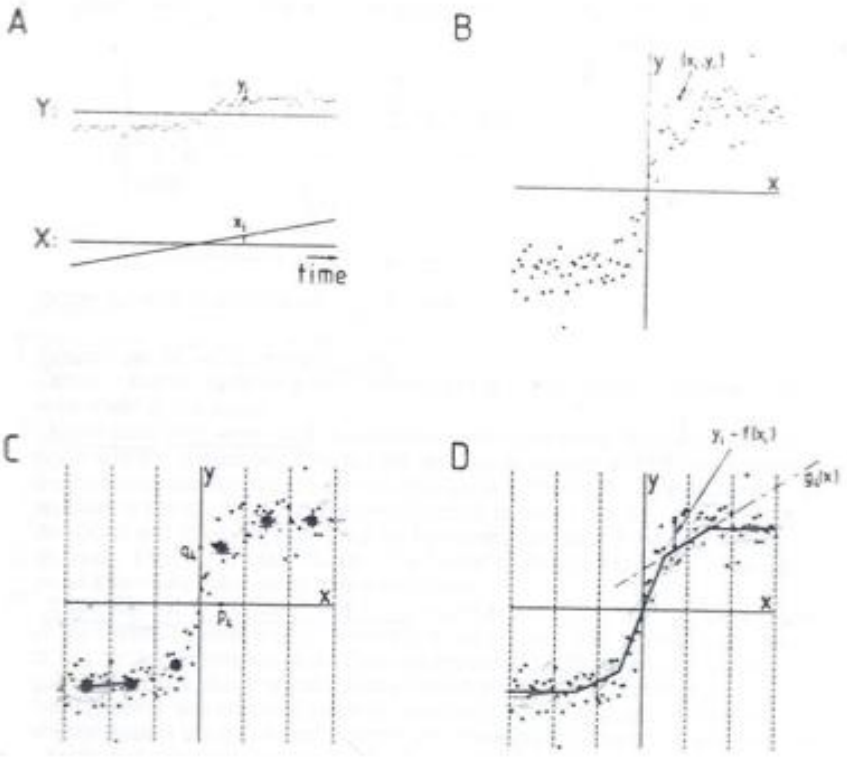

Figure 2-5: Demonstration of the procedure used to calculate the nonlinear regression coefficient, h^2, (adapted from Pijn, 1990). (A) The average of the signals is set to zero. x_i and y_i are the amplitude values of, respectively, X and Y. (B) A scattergram of X and Y is plotted. (C) The ordinate is split in equally sized bins. For each bin, the value of the midpoint in X is called p_j and the average of the Y values within each bin is called q_j. The points (p_j,q_j) are drawn as asterisks. (D) The points (p_j,q_j) are connected by straight lines. The line connecting (p_j,q_j) with (p_{j+1},q_{j+1}) is called $g_j(x)$ and the whole piecewise curve is called $f(x)$. The sum of the square of the deviations in Y is called the unexplained variance, and h^2 is the total variance in Y minus the unexplained variance, divided by the total variance.

Mutual information and Transmission coefficient

The mutual information coefficient, I, is based on the concept of entropy, which in turn can be regarded as a measure of the uncertainty of the outcome. For example, in a uniform distribution, where all the states have equal probabilities, the entropy will be high, whereas a delta-type distribution will have minimum entropy (Pereda 2005). If the entropies of X and Y are noted as, respectively, $H(X)$ and $H(Y)$, and the joint entropy of X and Y noted as $H(X,Y)$, then the expression that defines the mutual information coefficient is (Pijn 1990)

$$I(X,Y) = H(X) + H(Y) - H(X,Y).$$

Conceptually, it is essentially a measure of how much extra information one can get from one signal by knowing the outcomes of the other one. Therefore, if the two signals are independent, $I(X,Y) = 0$. This measure shows the advantage of showing good results in the estimation of the interdependence between experimental signals. However, it presents the disadvantage of requiring a large amount of data, a fact that is sometimes in conflict with the requisite of stationarity in case of experimental signals.

Related to this measure, there is the transmission coefficient, $T(X,Y)$. $T(X,Y)$ measures the proportion of reduction on uncertainty in the knowledge of Y for a given X, i.e.,

$$T(X,Y) = \frac{H(Y) - H(Y/X)}{H(Y)} \Leftrightarrow T(X,Y) = \frac{H(X) + H(Y) - H(Y,X)}{H(Y)}.$$

However, because this measure shows the same caveat as $I(X,Y)$, this is, it requires a large amount of data, it has not found as many electrophysiological applications in EEG signals as other techniques (Pereda 2005).

Phase synchronization

The concept of phase synchronization (PS) relates to two signals being coupled even though their amplitudes remain uncorrelated. In this sense, synchronization refers to phase locking, i.e., the phase difference between two signals remaining constant along time. Thus, in the case of EEG, the concept of phase locking only applies in a statistical sense. In order to extract the phases of the signals, various methods can be applied. A review of these can be found in (Pereda 2005).

2.3 EEG processing – methods used in the present study

The methods used in the present study were the cross-correlation function, $C_{xy}(\tau)$, the coefficient of determination, r^2, and the nonlinear regression coefficient, h^2. In order for them to be applied in the present study in an adequate manner, some kind of algorithm validation and/or parameter definition is needed. This issue will be discussed in this section.

2.3.1 Cross-correlation function validation – surrogation method

Although the cross-correlation function has already been widely used in EEG signal processing (see references in the previous section), and although the algorithm used in the present study was

based on a built-in function of MATLAB (R2008a), *xcorr()*, this algorithm's performance had not been tested specifically for the present EEG signals. In fact, in the validation of a particular algorithm, one must consider not only the properties of the algorithm but also the characteristics of the data that is to be processed by it (L. Faes 2004), since the intrinsic characteristics of the series might be deviating the estimated value of the correlation measure from its expected one (Pereda 2005).

In the implementation of an algorithm that calculates the cross-correlation between two series, it is of interest to test its significance in the sense that nonzero values might appear even in the case of complete uncoupling. One is therefore interested in determining a threshold from which the signals can be considered to be actually coupled. One way to do this is using the surrogation approach (Pereda 2005).

The surrogate method was introduced in 1992 by Theiler et al. originally to test for nonlinearity in time series (Theiler et al., 1992) but is now commonly used to test the significance of some algorithms, as coherence and synchrony measures (Jean-Philippe Lachaux 1999; L. Faes 2001; L. Faes 2004). It is in fact a type of hypothesis test, in which a set of series (the *surrogates*) sharing common properties with the original series but lacking the feature one wishes to test for is generated. In the present case, where one wishes to find a threshold from which the signals can be considered to be coupled, one has to determine the cross-correlation estimator under the null hypothesis (H_0) of full uncoupling, i.e., $C_{xy} = 0$. Based on the distribution of this estimator it is then decided if two particular signals are coupled or uncoupled, i.e., if the null hypothesis of uncoupling is verified or not in a particular case. Different surrogating procedures yield different results, therefore the method of surrogate generation has to be chosen according to the null hypothesis being tested (L. Faes 2004). More details on the procedure of surrogation carried out in this study will be given in Chapter 3. As a final point, it is worth mentioning that, being a statistical test, it is not free from the errors of typical hypothesis testing, as the α (probability of rejecting the null hypothesis when the series are actually uncoupled) and β (probability of not rejecting the null hypothesis when the series are actually coupled) errors (L. Faes 2004).

2.3.2 Coefficient of determination and nonlinear regression coefficient

The algorithms for the calculation of r^2 and h^2 were based on the formulas and procedures described in (Pijn 1990). This work also presents an extensive study of the behaviour of these algorithms according to different types of input signals and validates the results obtained from them in various conditions, therefore no validation procedure was carried out in the present study. However, it is recommended in (Pijn 1990) to calculate the best choice for the number of bins to be used. In fact, the value of the estimation of the nonlinear regression coefficient shows a variation

according to the number of bins in which the ordinate is divided. In most cases, though, the value of h^2 as a function of the number of bins is a function which converges rapidly to its theoretical value, after which it keeps on increasing slowly in the form of a 'plateau' (figure 2.6). A good choice is to chose the number of bins corresponding to the start of the plateau, since fewer bins would lead to an underestimation of h^2 and more bins would only require more computational effort, not altering significantly the estimated value of the nonlinear regression coefficient (Pijn 1990). Further details on the calculation of the number of bins in the present study are presented in Chapter 3.

Until now, the estimators for the coefficient of determination and the linear regression coefficient were only presented in a time-locked frame, i.e., using the signals without shifting them. However, as in the cross-correlation function, these can be calculated as a function of the shift between the time series, this is, as association functions. In this way, both r^2 and h^2 can be used to estimate the lag between the series and thus to make inferences on causality. The studies carried out by Pijn et al. (1990) showed that h^2 is a more robust method than r^2 for the calculation of time shifts with most types of input signals and signal's relationships. Furthermore, the level of significance from which two signals can be considered to be significantly correlated was estimated to be of 20% for both r^2 and h^2, considering a level of significance of $p < 0.001$. Further studies regarding these two correlation measures can be found in (Pijn 1990).

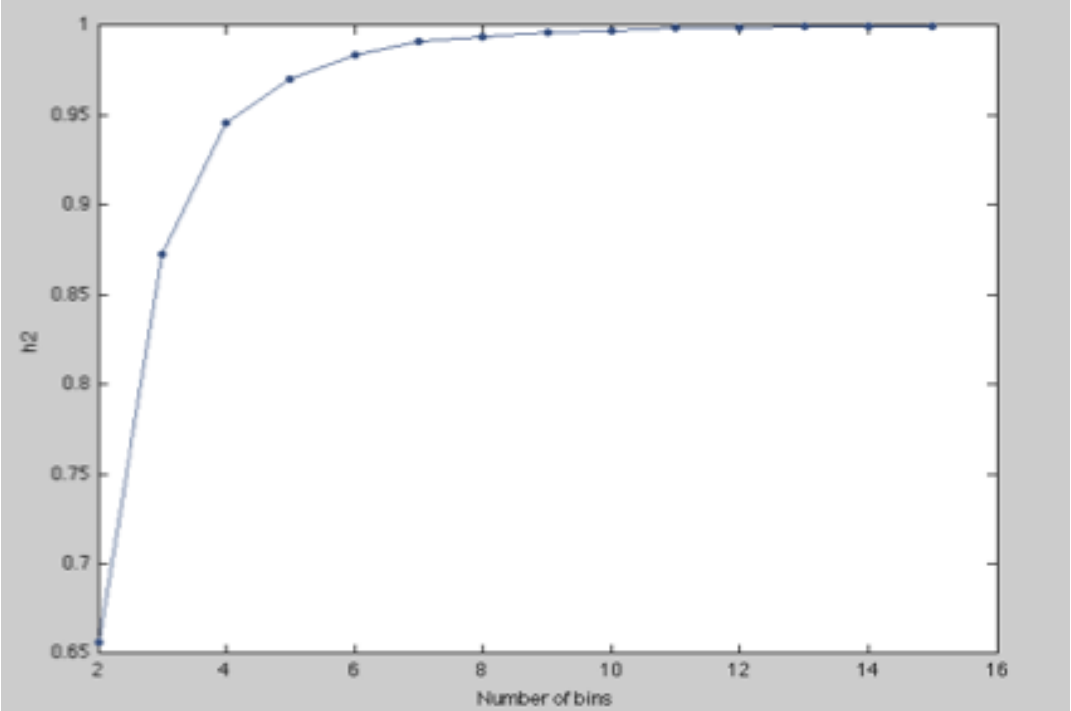

Figure 2-6: Example of a function with the shape of a 'plateau'. In this particular case, h^2 is plotted as a function of the number of bins

3

Methodology

In this chapter the methods used in the present study will be presented. First, the procedures related to the acquisition of the data will be described, followed by an outline of the main algorithms which were implemented and how these were validated.

3.1 Methods – Data acquisition, participants, and experimental paradigm

This study required the collaboration of 15 voluntary participants, who performed an arithmetical task while an EEG record was acquired from them.

3.1.1 EEG Acquisition

The EEG data was recorded from a 32-electrode cap in which the electrodes were distributed according to the International 10/20 system (figure 3.1). The montage used was the average reference montage. The electrodes were the following: FP1, FP2, AF3, AF4, F7, F3, Fz, F4, F8, Fc5, Fc1, Fc2, Fc6, T7, C3, Cz, C4, T8, Cp5, Cp1, Cp2, Cp6, P7, P3, Pz, P4, P8, PO3, PO4, O1, O2 and Oz. The impedance of the electrodes was kept always below 10kOhm, though in the majority of the cases being lower than 5kOhm. This was accomplished by controlling the amount of conductive gel that was put between the electrodes and the scalp. The recordings were sampled at 2048Hz, and three digital filters were applied to the data: a high-pass filter with a cut-off frequency at 1.6Hz, a low-pass filter with a cut-off frequency of 60Hz and a notch filter (50 Hz). EOG artefacts were also removed. In order to carry out these steps the *Biosemi* equipment and commercial versions of *BESA 5.1.8* software were used. The *Biosemi*equipment was used to establish the sampling rate and control the impedance of the electrodes and the *BESA* software was used for processing data (artifact

rejection, filter appliance, etc).

Three recordings were made for each participant: two basal recordings and one during task performance. For the basal recordings the participants were kept in resting state with their eyes opened in one case and with eyes closed in the other, whereas for the task condition they remained with eyes closed and were instructed verbally to start the task which lasted for 3 minutes. As the subjects had not been previously informed about the task they would have to perform, no previous practice was assumed.

As this study aims at understanding the mechanisms underlying mental calculation and because it was assumed that occasional calculating mistakes do not influence these mechanisms, no error control was made.

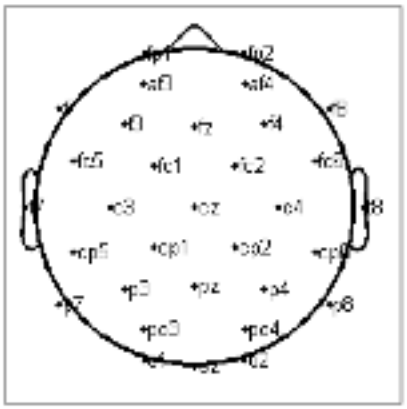

Figure 3-1: Distribution of the electrodes in the present study. (adapted from Borges, 2009)

3.1.2 Participants and experimental paradigm

The 15 volunteers were mainly university students or teachers. All of them were right-handed except for performer CSF who was left-handed, and two were under medication (performers LMBL and CPFRO). Plus, they all had between 23 and 40 years old (mean: 31.9 ± 5.3), and declared not to have any auditory, visual or neurological problem, except for PARS who had obsessive compulsive disorder (OCD). Table 3.1 summarizes the main characteristics and performing details of each participant.

The task performed was the following: with eyes closed, start from 200 and subtract successively 3 for three minutes. The volunteers were told to repeat the procedure (starting again from 200) without interrupting once they arrived at number 2 (i.e., only subtractions with positive integers were executed). After accomplishing the task, they were asked to state which type of strategy they had used perform it.

The present task is quite complex and therefore will not rely solely on arithmetical fact retrieval. Recalling what was said in the first chapter, due to its complexity it is expected that many different

circuits will be involved in this task.

First of all, we can expect that some calculation will be carried out, and therefore some kind of quantity representation circuits will be activated. However, there is a pattern in this calculation that can be followed. As we can see from figure 3.2, for every 10 subtractions there is a repetition regarding the last digit. Thus, once a participant detects it, he or she might continue performing the calculation and keep on subtracting 3 consecutively or can decide to start determining the next element of the series by using a mental strategy based on the pattern, thus relying mostly on rote learning. Many of the participants stated that they had used the pattern regarding the last digits (9, 6, 3). Many volunteers stated they visualized the numbers as in a list, suggesting that many of them also used some kind of visual mental imagery competence. Due to the complexity of the task, it is

$$\underbrace{200 - 197 - 194 - 191 - 188 - 185 - 182 - 179 - 176 - 173} -$$
$$\underbrace{170 - 167 - 164 - 161 - 158 - 155 - 152 - 149 - 146 - 143} - 140...$$

Figure 3-2: First 21st elements of the sequence of numbers. Notice the pattern for each 10 elements of the sequence.

also expected that there will be a constant use of working memory.

As has been described in chapter 1, different mental mechanisms are thought to rely on different brain circuits, although these have not been yet consensually identified. However, some relations have been proposed, and some sites in the cerebral cortex show frequent activation during arithmetic tasks, particularly frontal and parietal regions. Activation of temporal regions has also been reported. The selection of the electrodes' signals to be processed will be based on this previous knowledge.

3.2 EEG Processing – Mathematical algorithms

3.2.1 Cross-Correlation

The first algorithm that was applied was the cross-correlation algorithm.

For a first approach, based on the fact that frontal and parietal locations usually show consistent activation, the electrodes that were chosen for the study were electrodes F4, Fz, F3, P4, Pz, P3. The cross-correlation algorithm was applied not only to determine the degree of coupling between two electrodes but also to determine the direction of propagation, through the determination of the time lag for which the correlation was maximal. After that, the same method was applied but this time for an intra-hemispheric study. The electrodes selected were F4, P4, T7 and O1 for the left hemisphere

and F3, P3, T8 and O2 for the right hemisphere. These studies were done both for the calculation condition and for the basal condition with eyes closed. Since the performers remained with eyes closed during the calculation task, the basal condition with eyes closed was considered to be better for comparison.

In order to compute the cross-correlation and to determine the time lag for which it was maximal, an algorithm was programmed based on the MATLAB R2008A in-built function *xcorr()*.

3.2.2 Surrogation for the validation of the algorithm used to compute cross-correlation

In order to validate this algorithm, the technique of surrogation was used. As stated in the previous chapter, the method selected for the generation of the surrogates should be chosen according to the null hypothesis being tested. In the present case, the null hypothesis is the uncoupling of two time series, i.e., the aim is to determine the threshold for zero correlation, from which two signals can be considered to be coupled. The FT (Fourier transform) surrogates have shown good performance in estimating thresholds for the same null hypothesis but regarding the coherence function (L. Faes 2004), since although they do not maintain the histogram distribution of the original series, they permit to maintain second-order moments (i.e. autocorrelation), which was proven to be more important in this situation (L. Faes 2004). Because the coherence function can be regarded as a particular case of the cross-correlation function, restricted to a particular frequency interval, and because no references to any particular surrogating procedure for the cross-correlation function were found, the FT method was chosen to generate the surrogates in the present case.

Since the purpose of this method was to test for the performance of the algorithm according to the characteristics of a particular pair of signals, the surrogation procedure was carried out for all the combinations of coupling between electrodes F4, Fz, F3, P4, Pz, and P3, i.e., for the pairs F4-Fz, F4-F3, F4-P4, F4-Pz, F4-P3, Fz-F3, Fz-P4, Fz-Pz, Fz-P3, F3-P4, F3-Pz, F3-P3, P4-Pz, P4-P3, and Pz-P3 of each subject. Since in all cases the value of correlation was very low (see figure 3.3), the generalization was made that the algorithm would show similar robustness using the signals from other electrode pairs and therefore no surrogation was carried out using the signals from F4, P4, T7, and O1, nor F3,P3, T8, and O2 (except, of course, for F3-P3 and F4-P4, which had been calculated previously).

The FT surrogates were generated by computing the FFT of each signal, and maintaining the respective moduli while substituting the calculated phases by random phases between $-\pi$ and π. Then, the inverse transform was applied to return to the time domain. After this procedure, the correlation between the signals had been removed, i.e., the surrogate pairs were totally uncoupled. In total, 100 FT surrogate pairs were generated for each pair of signals. For each of the 100 surrogate

pairs, the maximal correlation coefficient was calculated using the algorithm that was being tested, and the frequency histogram was calculated. Since two linearly related signals can be either inversely linearly correlated (in which case the correlation coefficient yields a negative number) or directly linearly correlated (in which case the correlation coefficient yields a positive number), the threshold for zero correlation was calculated for both situations. These thresholds were set by determining, respectively, the $100\alpha/2$ and $100(1-\alpha/2)$ percentiles of the correlation frequency histogram mentioned above, where α is the significance level of the statistical test. Naturally, the calculation of the lower percentile was only significant when it yielded a negative value, since what was being calculated was a threshold for the case of inverse linear couple.

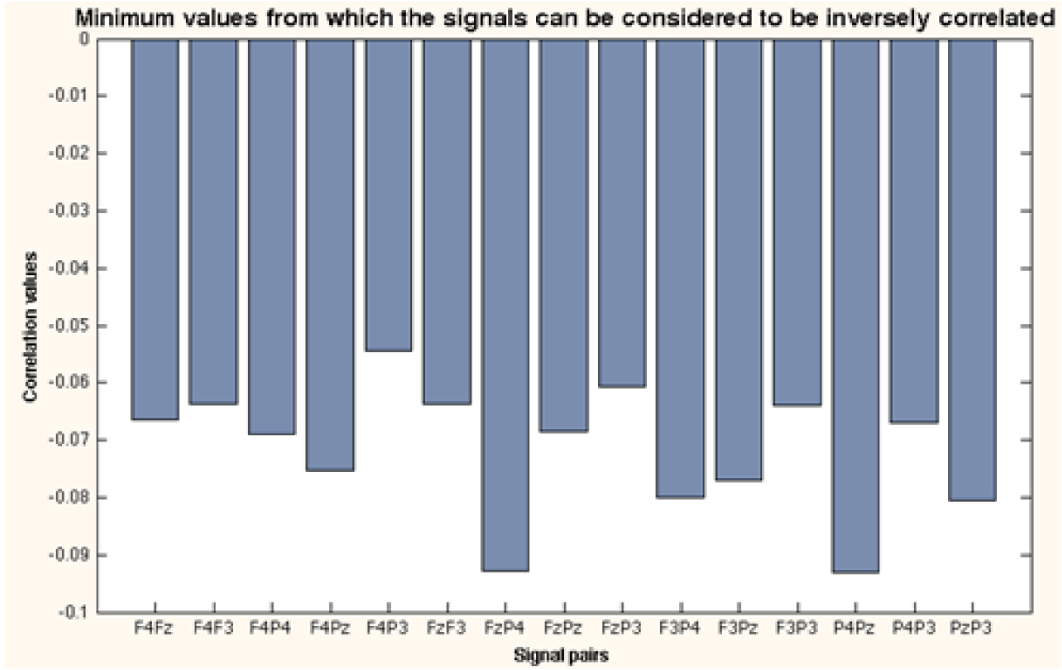

(A)

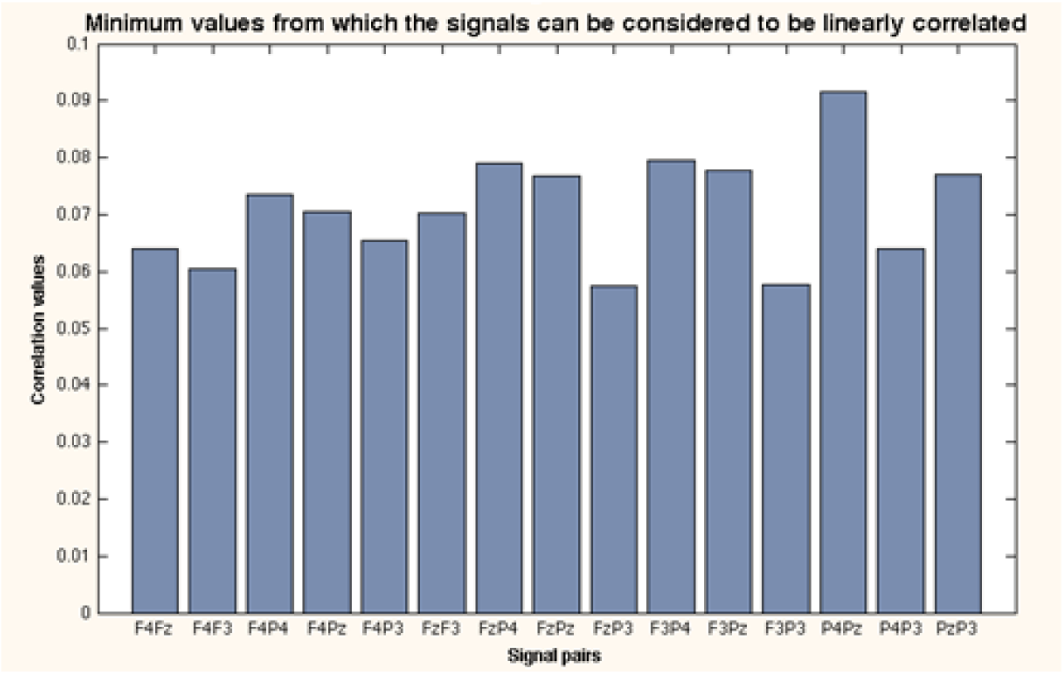

(B)

Figure 3-3: Graphs showing an example of the results of the surrogation procedure. (A) Results of the simulation regarding the estimation of the (negative values) from which two signals can be considered to be inversely linearly correlated. (B) Results of the simulation regarding the estimation of the values from which two signals can be considered to be directly linearly correlated. Notice that all the values are under 0.1. These results were obtained from subject BTL in calculation condition.

The values obtained using the described procedure, with a significance level of $\alpha = 0.001$, were always below 0.1 (in absolute value), which means that, according to this method, correlation values equal to or above this value (in modulus) reveal coupling between the two analysed signals. Furthermore, the fact that the estimated threshold is quite low is a sign of the robustness of the algorithm. Figure 3.3 shows an example of the results obtained for one of the subjects. The remaining cases are similar and can be found in appendix A.

3.2.3 Coefficient of determination and nonlinear regression coefficient

The second part of the study consisted on the implementation of the algorithms that calculated the coefficient of determination, r^2, and the nonlinear regression coefficient, h^2. Since these two coefficients have analogous definitions, one of them being linear and the other being nonlinear, it was considered that the implementation of both would be good for comparison purposes.

Again, the MATLAB software, version R2008a, was used to compute the algorithms. The code generated to compute the nonlinear regression coefficient can be found in appendix B. The electrode pairs selected correspond to the ones showing greater coupling according to the cross-correlation

function. The values of r^2 were, therefore, computed for the following pairs: F4-Fz, F4-P3, Fz-F3, F3-P4, P4-Pz, and Pz-P3, as well as the respective delay values. Regarding the calculation of h^2, since it is an asymmetric estimator, the combinations previously mentioned were computed as well as their symmetricals, i.e.: F4-Fz, Fz-F4, F4-P3, P3-F4, Fz-F3, F3-Fz, F3-P4, P4-F3, P4-Pz, Pz-P4, Pz-P3, and P3-Pz. The respective delay values were also obtained. For the same reason as mentioned previously, these calculations were computed for the records obtained during the arithmetical task and for the basal condition with eyes closed.

Due to computational load, the input signals did not consist of the whole 3 minute recorded signals. Instead, and since stationarity can be assumed for epochs of approximately 10 seconds under constant behavioural conditions (Niedermayer & Lopes da Silva, 1993), the first 10 seconds of the recorded signals were used as input. An advantage of using the first 10 seconds is that the first moments of the task are when the subjects are in more similar situations. This would not happen if an epoch of 10 seconds was chosen in the middle of the task.

3.2.4 Validation of the algorithms used to compute r2 and h2

As mentioned in the previous chapter, (Pijn 1990) present an extensive study of the behaviour of r^2 and h^2 according to different types of input signals and different transformations, validating the results obtained from these estimators in various conditions. Thus, no validation procedure was carried out in the present study. However, it is recommended that before applying the algorithm for the calculation of h^2, the best choice for the number of bins in which the ordinate should be divided should be calculated. In order to do this, the graph showing the variation of h^2 according to the number of bins, m, for $m = 2$ until $m = 15$ was computed, for the case of autocorrelation, i.e., when the expected consists of $h^2 = 1$. The graph obtained is displayed in figure 3.4. Also in this case, and in order to obtain coherent results, epochs of the first 10 seconds were considered. The original signal from which the autocorrelation was calculated came from electrode F4 of patient BTL during calculation condition. Since in (Pijn 1990) had suggested the value for m to be of 10, and due to the fact that the graph obtained in this study corroborates this result, it was assumed that $m = 10$ would be a valid estimate also for this study. All posterior results presented in this study were obtained for this value of m.

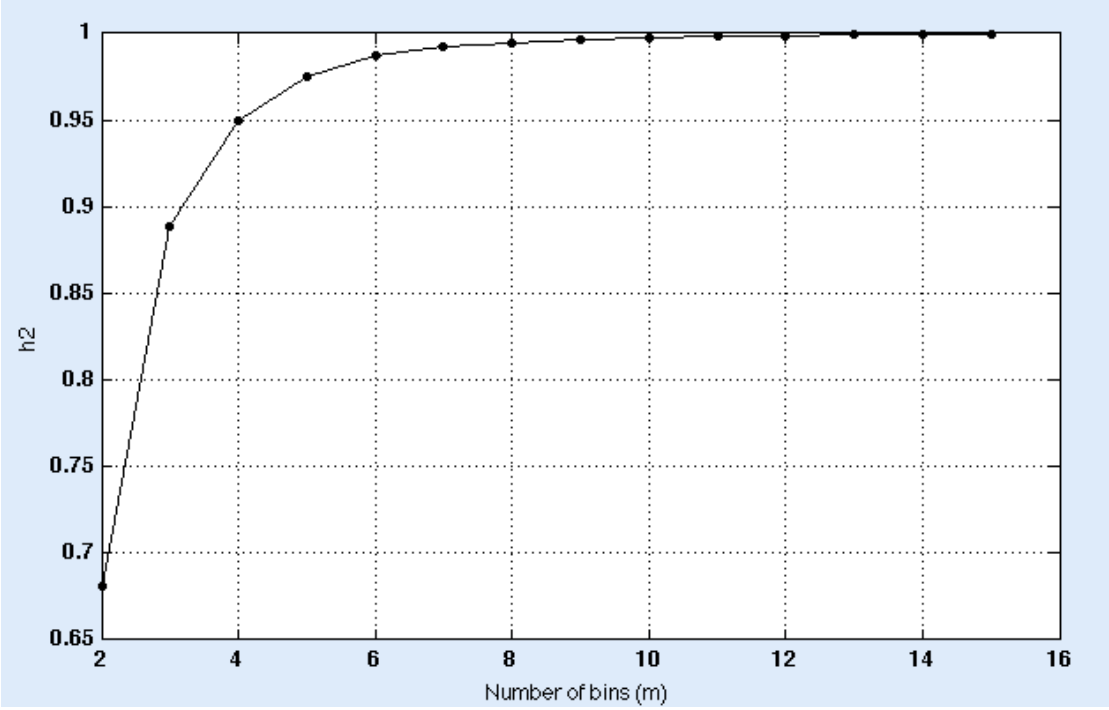

Figure 3-4: Graph showing the variation of the nonlinear regression coefficient, h^2, according to the number of bins, m. Notice that $m = 10$ stands at the beginning of the 'plateau': less bins underestimated the value of h^2 whereas more bins require more computational load without making much difference in terms of the value of the estimation obtained.

3-1 Table summarizing the main characteristics and performing details of the participants (adapted from Borges 2009)

Performer	Code	Gender	Age	Strategy for calculus	Final number	Turns	Academic Level	Notes
1	DRP	M	30	Started by using exclusively calculus; from a certain point followed a pattern; confirmed result in multiples of 30	72	2	Master, Biology and Geology	
2	RAMC	M	23	Only calculus; tried to follow a pattern but quitted; usually visualized the numbers	170	2	5th year, Physics Engineering	
3	PARS	M	29	Calculus	167	2	Bachelor, Biology	Obsessive Compulsive Disorder
4	LMBL	M	37	Only calculus, even after finding a pattern; usually visualized the numbers like in a list	200	2	PhD, Informatics	
5	SGS	F	32	Used the pattern; visualized the results	185	2	Bachelor, Biology	
6	PASS	M	38	Calculus and occasionally pattern	14	1	Master, Physics	
7	OCR	M	40	Calculus; tried to use a pattern but quitted	73	2	PhD, Physics	Native Tongue: Castilian
8	SMGG	F	31	Calculus; used the termination pattern (9, 6, 3); started to perform quicker	180	2	Bachelor, Biology	
9	MFSA	F	37	Calculus and visualization of numbers	148	2	Bachelor, English Teaching	
10	CSF	F	31	Calculus and pattern (9, 6, 3)	184	2	Bachelor, Informatics Teaching	
11	CPFRO	F	35	Showed many difficulties; sometimes subtracted 3, other times 2; used numerical termination (7, 5, 3, 0); great level of mistakes	125	1	Bachelor	
12	BTL	F	33	Calculus and pattern (9, 6, 3)	17	1	Master, Physics	Native Tongue: French
13	RJGT	M	23	Calculus and pattern (9, 6, 3); started to perform quicker after using the pattern; confirmed the result once arriving at zero	146	2	3rd year, Physics Engineering	
14	SRP	F	29	Calculus and pattern (9, 6, 3); started to perform quicker after using the pattern; confirmed the result in multiples of 30	38	2	PhD, Computational Chemistry	
15	LSGA	F	23	Tried to follow a pattern	69	1	4th year, Physics Engineering	

4

Results and Discussion

In this chapter the results of the application of the methods described in the previous chapter will be presented and discussed, starting by the cross-correlation algorithm and followed by the algorithms concerning the association functions of r^2 and h^2. Finally, the results regarding the delays which were estimated between the signals will be discussed.

4.1 Results obtained by applying the cross-correlation function algorithm

As stated in chapter 3, the cross-correlation between the previously mentioned electrode pairs (selected according to the criteria described in the former chapter) was calculated in order to get further insight into which brain areas were coupled, and to estimate the delays between different signals. In this section, the results of this procedure will be first analyzed for the resting condition with eyes closed and then for the condition of mental calculation. This will be followed by a comparison between both conditions. The interpretation of the results concerning the delay values that were estimated will be carried out separately in section 4.3.

Table 4-1: Correlation values regarding the different electrode pairs for the 15 individuals. Basal condition.(see text for colour interpretation)
(*) The signal corresponding to electrode Pz came out as 0 (zero) probably due to an experimental failure, therefore the cross-correlation was not considered for the electrode pairs associated with this signal.

	Pz-P3	P4-P3	P4-Pz	F3-P3	F3-Pz	F3-P4	Fz-P3	Fz-Pz	Fz-P4	Fz-F3	F4-P3	F4-Pz	F4-P4	F4-F3	F4-Fz
BTL	0.711	0.236	0.591	-0.501	-0.459	-0.599	-0.538	-0.457	-0.612	0.968	-0.496	-0.475	-0.604	0.272	0.408
CPFRO	0.732	0.300	0.536	-0.402	-0.480	-0.598	-0.475	-0.376	-0.467	0.580	-0.517	-0.404	-0.350	0.300	0.629
CSF	0.795	0.485	0.768	-0.367	-0.500	-0.609	-0.452	-0.434	-0.464	0.600	-0.525	-0.473	-0.387	0.203	0.496
DRP	0.833	0.581	0.747	-0.407	-0.492	-0.305	-0.576	-0.576	-0.327	0.692	-0.393	0.392	0.231	0.623	0.805
LMBL	0.854	0.673	0.816	-0.438	-0.549	-0.381	-0.498	-0.528	-0.359	0.893	-0.447	-0.464	-0.259	0.840	0.939
LSGA	0.453	0.135	0.546	-0.441	-0.324	-0.714	-0.501	-0.277	-0.590	0.751	-0.606	-0.381	-0.563	0.624	0.843
MFSA	0.786	0.456	0.660	-0.472	-0.547	-0.776	-0.586	-0.511	-0.770	0.773	-0.724	-0.672	-0.749	0.565	0.808
OCR	0.682	0.408	0.669	-0.593	-0.511	-0.706	-0.622	-0.388	-0.582	0.811	-0.689	-0.480	-0.565	0.662	0.821
PARS	0.702	0.294	0.659	-0.433	-0.585	-0.733	-0.553	-0.559	-0.603	0.723	-0.684	-0.678	-0.525	0.402	0.772
PASS	0.494	0.187	0.459	-0.314	-0.391	-0.536	-0.352	-0.204	-0.342	0.589	-0.475	-0.276	-0.261	0.301	0.647
RAMC	0.578	0.230	0.580	-0.503	-0.394	-0.696	-0.509	-0.271	-0.528	0.795	-0.622	-0.459	-0.526	0.613	0.784
RJGT	0.684	0.321	0.675	-0.431	-0.497	-0.694	-0.467	-0.372	-0.501	0.703	-0.674	-0.516	-0.458	0.502	0.735
SGS(*)		0.245		-0.633		-0.520	-0.594		-0.384	0.783	-0.716		-0.363	0.600	0.781
SMGG	0.697	0.402	0.724	-0.598	-0.614	-0.772	-0.648	-0.589	-0.689	0.842	-0.746	-0.688	-0.675	0.728	0.857
SRP	0.631	0.099	0.579	-0.429	-0.490	-0.610	-0.533	-0.398	-0.435	0.720	-0.453	-0.338	-0.267	0.282	0.510

4.1.1 Basal condition – Eyes closed

Fronto-Parietal correlation

The maximal values of cross-correlation between the electrode pairs F4-Fz, F4-F3, F4-P4, F4-Pz, F4-P3, Fz-F3, Fz-P4, Fz-Pz, Fz-P3, F3-P4, F3-Pz, F3-P3, P4-Pz, P4-P3, and Pz-P3 of each subject in the basal condition with eyes closed are summarized in table 4.1. The averages of these values and respective variances were also calculated for each pair, and are displayed in table 4.2. The formulas used to calculated the variance and the index of dispersion, D, were, respectively, (3) and (4). The index of dispersion (%) gives an estimate of the variability of the correlation values among individuals.

$$\sigma^2 = \frac{\sum\left(x-\bar{x}\right)^2}{(n-1)} \qquad (3) \qquad\qquad D = \frac{\mu(mean)}{\sigma^2}\times 100\% \qquad (4)$$

Table 4-2: Mean values for the cross-correlation between electrode pairs considering the 15 individuals, and respective variances and indexes of dispersion. Basal condition. (see text for colour interpretation)

	MEAN (μ)	**VAR** (σ^2)	**D (%)** (σ^2/μ)
F4-Fz	0.722	0.023	3.19
F4-F3	0.501	0.038	7.53
F4-P4	0.452	0.027	5.94
F4-Pz	0.478	0.016	3.32
F4-P3	0.584	0.014	2.37
Fz-F3	0.748	0.012	1.61
Fz-P4	0.510	0.017	3.37
Fz-Pz	0.424	0.014	3.41
Fz-P3	0.527	0.006	1.07
F3-P4	0.617	0.019	3.04
F3-Pz	0.488	0.006	1.25
F3-P3	0.464	0.008	1.69
P4-Pz	0.644	0.010	1.56
P4-P3	0.337	0.027	7.87
Pz-P3	0.688	0.014	2.02

The first observation that can be made, regarding table 4.1, is that within each pair of electrodes, the sign of the correlation (which indicates if the signals are directly linearly correlated, if the sign is positive, or inversely linearly correlated, if the sign is negative) is maintained for all subjects, except for subject DRP in pairs F4-Pz and F4-P4 (coloured in orange). This reveals a certain degree of coherence among the results.

In table 4.2, the mean and variances were calculated considering the absolute values displayed in the previous table, since it was considered that what was relevant in this case was to determine the average degree of coupling in each pair, independently of them being directly or inversely related. Furthermore, this procedure was maintained for all the calculations of averages and variances displayed in this chapter.

The pairs of electrodes showing a correlation equal or superior to 0.5 have been coloured in blue and green. The blue corresponds to the six pairs showing higher correlation values, and the green are the remaining ones. Furthermore, the same pairs that have been coloured in blue in this case have also been indicated in the previous table. The values of the indexes of dispersion are relatively low, which was interpreted as an indication that the mean values which were obtained can be used for comparison purposes, despite the whole set of values showing some dispersion.

These results will be later compared to the task condition, when the subjects are performing the calculations.

Intra-Hemispheric correlation

Table 4.3 shows the results that were obtained for the maximal correlation values regarding the electrode pairs T7-O1, P3-O1, P3-T7, F3-O1, F3-T7, and F3-P3. These electrodes are all located in the left hemisphere. Regarding the right hemisphere, table 4.4 shows the results obtained for electrode pairs T8-O2, P4-O2, P4-T8, F4-O2, F4-T8, and F4-P4.

As has been done in table 4.1, the values that don't follow the tendency of the majority in terms of signal (+ or -) have been coloured in orange.

In tables 4.5 and 4.6, the mean values, respective variances, and indexes of dispersion have been summarized, as has been done for the fronto-parietal study. Once again, the pairs of electrodes showing correlation values above 0.5 have been coloured in blue. In both cases, the most correlated pairs are the parieto-occipital pair (P-O) and fronto-occipital pair (F-O).

As has succeeded previously, once again the indexes of dispersion are relatively low, therefore it was considered that the mean values could be used for comparison purposes. Regarding the comparison of values between both hemispheres, there is not one predominant hemisphere showing significantly more coupling than the other, although, for the fronto-temporal pair (F-T), the left hemisphere shows more coupling than the right. Furthermore, the order of the pairs within each hemisphere in terms of correlations is the same, i.e., in descending order, P-O, F-O, F-P, F-T, T-O,

and P-T. Another point which is interesting to mention is that the pairs showing correlations under 0.300 are the ones that show most inconsistencies in terms of signal (see tables 4.3 and 4.4). Because the averages were calculated using the absolute values of the correlations, the explanation cannot be that the averages are lower because of this variability in terms of signal. Instead, the explanation might be that because these pairs are not very connected, they have more independent behaviour and therefore there is more variability in terms of signal. In fact, these two facts corroborate each other.

These values will be used for posterior comparison with the calculation condition.

Table 4-3: Correlation values regarding the different electrode pairs for the 15 individuals (left hemisphere). Basal condition. (see text for colour interpretation)

	BTL	CPFRO	CSF	DRP	LMBL	LSGA	MFSA	OCR	PARS	PASS	RAMC	RJGT	SGS	SMGG	SRP
F3-P3	-0.501	-0.402	-0.367	-0.407	-0.438	-0.441	-0.472	-0.593	-0.433	-0.314	-0.503	-0.431	-0.633	-0.598	-0.429
F3-T7	-0.357	0.309	0.083	0.343	0.436	0.387	0.175	0.319	0.233	0.259	0.508	0.221	0.255	0.499	0.272
F3-O1	-0.825	-0.497	-0.541	-0.346	-0.277	-0.658	-0.602	-0.740	-0.607	-0.483	-0.613	-0.567	-0.642	-0.689	-0.570
P3-T7	0.189	-0.075	-0.193	0.238	0.432	0.123	0.175	-0.274	-0.132	-0.180	-0.202	-0.079	-0.155	-0.282	0.159
P3-O1	0.639	0.692	0.707	0.927	0.824	0.457	0.414	0.719	0.674	0.369	0.574	0.532	0.669	0.673	0.689
T7-O1	0.302	-0.120	-0.164	0.278	0.627	-0.225	0.137	-0.182	-0.185	0.106	-0.156	-0.077	-0.183	0.326	0.106
	BTL	**CPFRO**	**CSF**	**DRP**	**LMBL**	**LSGA**	**MFSA**	**OCR**	**PARS**	**PASS**	**RAMC**	**RJGT**	**SGS**	**SMGG**	**SRP**

Table 4-4: Correlation values regarding the different electrode pairs for the 15 individuals (right hemisphere).Basal condition. (see text for colour interpretation)

	T8-O2	P4-O2	P4-T8	F4-O2	F4-T8	F4-P4
BTL	-0.177	0.748	-0.141	-0.556	0.127	-0.604
CPFRO	-0.056	0.408	0.112	-0.359	0.097	-0.350
CSF	0.249	0.661	0.128	-0.527	-0.129	-0.387
DRP	0.401	0.878	0.368	0.227	0.553	0.231
LMBL	0.655	0.845	0.547	-0.242	0.427	-0.259
LSGA	-0.192	0.536	-0.157	-0.645	0.348	-0.563
MFSA	0.206	0.856	0.151	-0.695	0.183	-0.749
OCR	-0.168	0.802	-0.170	-0.759	-0.159	-0.565
PARS	0.161	0.785	-0.114	-0.668	0.238	-0.525
PASS	0.157	0.428	0.126	-0.433	0.180	-0.261
RAMC	0.137	0.508	0.163	-0.634	0.186	-0.526
RJGT	0.274	0.437	0.210	-0.516	-0.139	-0.458
SGS	-0.201	0.571	-0.117	-0.662	0.287	-0.363
SMGG	0.331	0.703	0.376	-0.700	0.436	-0.675
SRP	-0.082	0.560	0.125	-0.420	0.088	-0.267

Table 4-5: Mean values for the cross-correlation between electrode pairs considering the 15 individuals, and respective variances and indexes of dispersion (left hemisphere). Basal condition.(see text for colour interpretation)

	MEAN (μ)	**VAR** (σ^2)	**D (%)** (σ^2/μ)
F3-P3	0.464	0.008	1.69
F3-T7	0.310	0.014	4.40
F3-O1	0.577	0.020	3.39
P3-T7	0.193	0.008	4.17
P3-O1	0.637	0.022	3.47
T7-O1	0.211	0.019	8.79

Table 4-6: Mean values for the cross-correlation between electrode pairs considering the 15 individuals, and respective variances and indexes of dispersion (right hemisphere). Basal condition.(see text for colour interpretation)

	MEAN (μ)	**VAR** (σ^2)	**D (%)** (σ^2/μ)
F4-P4	0.452	0.027	5.94
F4-T8	0.238	0.020	8.40
F4-O2	0.536	0.028	5.26
P4-T8	0.200	0.016	8.12
P4-O2	0.648	0.028	4.26
T8-O2	0.230	0.022	9.40

4.1.2 Task condition – Mental calculation

The study of the mental calculation condition will be carried out analogously to the basal condition.

Fronto-Parietal correlation

The results of the correlation values for the mental calculation condition are summarized in table 4.7. The blue and orange coloured values stand for the same as stated previously. Furthermore, the subjects who used only calculus and no mental strategy using the pattern have also been indicated, as well as those who studied physics (see legend of the tables). This was done because it was considered that subjects who were, or were studying to be physical engineers might have different

activation patterns than the others, who worked in less numerical areas. However, in terms of correlation values, no significant differences were found, neither regarding the comparison between physical engineers and the other subjects, nor regarding the comparison between subjects who used only calculus and those who followed a pattern (see table 4.7).

Table 4-7: Correlation values regarding the different electrode pairs for the 15 individuals. Task condition. Red: subjects who used only calculus; Underlined: physical engineers (see text for remaining colour interpretation).

	Pz-P3	P4-P3	P4-Pz	F3-P3	F3-Pz	F3-P4	Fz-P3	Fz-Pz	Fz-P4	Fz-F3	F4-P3	F4-P4	F4-F3	F4-Fz
BTL	0.660	0.201	0.615	-0.386	-0.456	-0.672	-0.416	-0.372	-0.546	0.773	-0.545	-0.565	0.539	0.724
CPFRO	0.459	0.289	0.282	-0.502	-0.424	-0.484	-0.541	-0.279	-0.425	0.647	-0.630	-0.387	0.442	0.741
CSF	0.763	0.412	0.729	-0.340	-0.473	-0.581	-0.434	-0.388	-0.408	0.627	-0.647	-0.369	0.162	0.595
DRP	0.801	0.574	0.690	-0.251	-0.346	-0.131	-0.427	-0.455	0.158	0.679	-0.232	0.143	0.636	0.769
LMBL	0.855	0.552	0.707	-0.655	-0.635	-0.763	-0.677	-0.565	-0.704	0.849	-0.764	-0.689	0.745	0.920
LSGA	0.455	0.275	0.594	-0.571	-0.421	-0.767	-0.480	-0.178	-0.611	0.674	-0.645	-0.629	0.687	0.837
MFSA	0.283	0.268	0.296	-0.321	-0.346	-0.684	-0.463	-0.352	-0.698	0.705	-0.639	-0.540	0.406	0.722
OCR	0.581	0.252	0.642	-0.420	-0.479	-0.702	-0.445	-0.239	-0.510	0.758	-0.624	-0.478	0.572	0.770
PARS	0.701	0.195	0.584	-0.396	-0.561	-0.627	-0.418	-0.407	-0.418	0.502	-0.585	-0.301	0.261	0.601
PASS	0.456	0.167	0.489	-0.140	-0.347	-0.572	-0.360	-0.250	-0.367	0.507	-0.556	-0.211	-0.127	0.592
RAMC	0.672	0.503	0.719	-0.183	-0.276	0.162	-0.335	-0.368	-0.177	0.721	-0.190	0.178	0.620	0.765
RJGT	0.729	0.429	0.698	-0.506	-0.528	-0.716	-0.571	-0.451	-0.600	0.749	-0.718	-0.554	0.535	0.764
SGS	0.344	0.146	0.318	-0.373	-0.425	-0.539	-0.319	-0.496	-0.456	0.773	-0.584	-0.222	0.467	0.658
SMGG	0.552	0.195	0.654	-0.375	-0.494	-0.629	-0.431	-0.422	-0.520	0.778	-0.540	-0.450	0.364	0.580
SRP	0.617	0.121	0.553	-0.285	-0.390	-0.617	-0.434	-0.356	-0.486	0.720	-0.615	-0.488	0.295	0.714

Furthermore, subjects CPFRO and PARS also had special conditions, since the former made a great level of mistakes and the latter had obsessive compulsive disorder (OCD). However, no significant difference was found between the correlation values of these subjects and the others.

Table 4-8. Mean values for the cross-correlation between electrode pairs considering the 15 individuals, and respective variances and indexes of dispersion.Task condition. (see text for colour interpretation)

	MEAN (μ)	**VAR** (σ^2)	**D (%)** (σ^2/μ)
F4-Fz	0.717	0.009	1.32
F4-F3	0.457	0.035	7.69
F4-P4	0.412	0.030	7.37
F4-Pz	0.407	0.018	4.36
F4-P3	0.568	0.025	4.33
Fz-F3	0.697	0.009	1.35
Fz-P4	0.472	0.025	5.40
Fz-Pz	0.372	0.011	2.87
Fz-P3	0.450	0.008	1.87
F3-P4	0.576	0.037	6.37
F3-Pz	0.440	0.009	1.99
F3-P3	0.380	0.019	5.12
P4-Pz	0.571	0.024	4.26
P4-P3	0.305	0.023	7.45
Pz-P3	0.595	0.028	4.77

Table 4.8 shows the means, variances and respective indexes of dispersion that were obtained for each one of the fronto-parietal electrode pairs. The colour code is the same as previously mentioned. Once again, the indexes of dispersion are relatively low, from which it was assumed that the calculated descriptive values could be used for comparison purposes (from this point on, whenever this shall be true it shall be omitted; whenever this condition shall not be verified this fact shall be mentioned in the text). Here, only 6 pairs showed correlation values above 0.5. These are, in descending order, F4-Fz, Fz-F3, Pz-P3, F3-P4, P4-Pz, and F4-P3.

Table 4-9: Correlation values regarding the different electrode pairs for the 15 individuals (left hemisphere). Task condition. Red: subjects who used only calculus; Underlined: physical engineers (see text for remaining colour interpretation).

	T7-O1	P3-O1	P3-T7	F3-O1	F3-T7	F3-P3
BTL	-0.117	0.589	-0.089	-0.621	0.258	-0.386
CPFRO	-0.139	0.644	0.082	-0.434	0.085	-0.502
CSF	0.090	0.566	0.118	-0.459	0.064	-0.340
DRP	0.284	0.888	0.255	-0.184	0.359	-0.251
LMBL	-0.173	0.707	-0.204	-0.722	0.174	-0.655
LSGA	-0.239	0.451	-0.111	-0.553	0.440	-0.571
MFSA	0.154	0.178	0.148	-0.402	0.196	-0.321
OCR	0.216	0.398	0.111	-0.526	0.144	-0.420
PARS	-0.178	0.637	-0.072	-0.520	0.517	-0.396
PASS	0.095	0.446	0.208	-0.354	0.431	-0.140
RAMC	0.526	0.822	0.397	-0.196	0.599	-0.183
RJGT	0.172	0.618	0.108	-0.630	0.292	-0.506
SGS	-0.073	0.525	0.079	-0.623	0.232	-0.373
SMGG	-0.237	0.534	0.150	-0.594	0.337	-0.375
SRP	0.090	0.612	0.141	-0.492	0.068	-0.285

Table 4-10: Correlation values regarding the different electrode pairs for the 15 individuals (right hemisphere). Task condition. Red: subjects who used only calculus; Underlined: physical engineers (see text for remaining colour interpretation).

	T8-O2	P4-O2	P4-T8	F4-O2	F4-T8	F4-P4
BTL	-0.153	0.648	0.133	-0.549	0.299	-0.521
CPFRO	0.114	0.574	0.100	-0.652	0.099	-0.387
CSF	0.148	0.522	0.126	-0.509	0.127	-0.369
DRP	0.529	0.860	0.538	0.108	0.614	0.143
LMBL	-0.159	0.749	-0.228	-0.745	-0.189	-0.689
LSGA	0.083	0.599	-0.084	-0.696	0.163	-0.629
MFSA	0.157	0.808	0.137	-0.562	0.172	-0.540
OCR	0.218	0.782	0.232	-0.647	-0.077	-0.478
PARS	-0.137	0.603	0.092	-0.556	0.271	-0.301
PASS	0.125	0.465	0.225	-0.431	0.287	-0.211
RAMC	0.505	0.711	0.466	-0.156	0.589	0.107
RJGT	-0.081	0.588	0.105	-0.579	0.158	-0.539
SGS	0.150	0.633	-0.091	-0.601	0.141	-0.357
SMGG	-0.153	0.648	0.133	-0.549	0.299	-0.521
SRP	0.125	0.595	0.201	-0.591	0.105	-0.342

Table 4-11: Mean values for the cross-correlation between electrode pairs considering the 15 individuals, and respective variances and indexes of dispersion (left hemisphere). Task condition.(see text for colour interpretation)

	MEAN (μ)	**VAR** (σ^2)	**D (%)** (σ^2/μ)
F3-P3	0.380	0.019	5.12
F3-T7	0.280	0.028	9.85
F3-O1	0.487	0.024	4.92
P3-T7	0.152	0.007	4.90
P3-O1	0.574	0.030	5.14
T7-O1	0.186	0.013	6.91

Table 4-12: Mean values for the cross-correlation between electrode pairs considering the 15 individuals, and respective variances and indexes of dispersion (right hemisphere). Task condition.(see text for colour interpretation)

	MEAN (μ)	**VAR** (σ^2)	**D (%)** (σ^2/μ)
F4-P4	0.409	0.030	7.21
F4-T8	0.239	0.027	11.31
F4-O2	0.529	0.032	6.01
P4-T8	0.193	0.019	9.64
P4-O2	0.652	0.012	1.84
T8-O2	0.189	0.019	9.95

Intra-Hemispheric correlation

Tables 4.9 and 4.10 show, respectively, the correlation values obtained for the situation of mental calculation for the left and the right hemispheres. The respective descriptive values are displayed in tables 4.11 and 4.12.

Contrary to what had happened in the basal condition, here it is possible to identify a predominant hemisphere in terms of coupling, which is the right hemisphere. This is true especially in what regards the three most coupled pairs, which are the same as in the basal condition, i.e., from the most to the least, the parieto-occipital pair (P-O), the fronto-occipital pair (F-O), and the fronto-parietal pair (F-P). In fact, these pairs show a higher degree of coupling in the right hemisphere than in the left. Furthermore, the order of coupling among the pairs is the same for both hemispheres, and is the same as in the basal condition (P-O > F-O > F-P > F-T > T-O > P-T). Regarding the subjects

who were or were studying to be physical engineers, the subjects who used only calculus, the subject who made a lot of mistakes (CPFRO), and the subject who had OCD (PARS), no special pattern or outstanding behaviour was identified. I also looked for a pattern, especially regarding the occipital regions (associated with vision and visualization), among the subjects who had stated they had used visualization skills, but I didn't find any consistent results. Nevertheless, there is a tendency for these subjects to show high correlation in pairs involving the occipital region, but this tendency is not conclusive.

4.1.3 Basal condition vs. Task condition

Fronto-Parietal correlation

One of the first points that stand out from the results which have been displayed is that there are many similarities in coupling between the basal condition and the task condition. Another surprising point is that there seems to be a higher degree of coupling in the basal condition than in the task condition. In fact, not only do the most coupled pairs show similar values in both cases, but also in the basal condition more pairs show correlations above 0.5 (9 pairs), against only 6 pairs in the task condition. Furthermore, these 6 pairs are the same that show the highest degree of coupling in the basal condition, although not in the same order. However, in both situations there is higher coupling among the frontal areas, followed by a high coupling among the parietal areas and finally a high degree of coupling between fronto-parietal areas located in opposite hemispheres, i.e., F3-P4 and F4-P3.

Intra-Hemispheric correlation

Regarding the values obtained within the hemispheres, there is, once again, some similarity between the two conditions, in the sense that the order of coupling among the pairs is the same for both the basal and the mental calculation situations. However, one can observe that there is a reduction in the coupling of the pairs within the left hemisphere in the calculation situation, whereas the right hemisphere tends to maintain its coupling values.

4.2 Results obtained by applying the coefficient of determination (r2) association function algorithm and the nonlinear regression coefficient (h2) association function algorithm

In this section, the results regarding signal coupling obtained through the application of the coefficient of determination association function algorithm and the nonlinear regression coefficient association function algorithm will be presented. First, the analysis of the estimated values regarding r^2 will be presented, followed by the analysis of the values regarding h^2, and finally a comparison

between both. It is worth mentioning that the coefficient of determination association function algorithm and the nonlinear regression coefficient association function algorithm were only applied to the 6 pairs of the fronto-parietal network that had shown highest degree of coupling according to the study made with the cross-correlation function, due to computational load (each value of the nonlinear regression coefficient took 10 minutes to acquire). Another important point to keep in mind is that, recalling what has been said in chapter 3, following Pijn 1990, both the values of r^2 and h^2 from which two signals can be considered to be significantly coupled is 0.2.

Table 4-13: Coefficient of determination values regarding the different electrode pairs for the 15 individuals. Basal condition.
(*) The signal corresponding to electrode Pz came out as 0 (zero) probably due to an experimental failure, therefore the coefficient of determination was not considered for the electrode pairs associated with this signal

	Pz-P3 P3-Pz	P4-Pz Pz-P4	F3-P4 P4-F3	Fz-F3 F3-Fz	F4-P3 P3-F4	F4-Fz Fz-F4	
BTL	0.468	0.201	0.532	0.753	0.227	0.710	BTL
CPFRO	0.451	0.227	0.272	0.272	0.302	0.455	CPFRO
CSF	0.568	0.563	0.167	0.187	0.106	0.260	CSF
DRP	0.797	0.636	0.115	0.472	0.217	0.688	DRP
LMBL	0.758	0.663	0.151	0.812	0.261	0.884	LMBL
LSGA	0.162	0.207	0.403	0.480	0.262	0.654	LSGA
MFSA	0.639	0.385	0.550	0.528	0.380	0.664	MFSA
OCR	0.354	0.342	0.403	0.312	0.277	0.278	OCR
PARS	0.467	0.345	0.495	0.461	0.405	0.544	PARS
PASS	0.310	0.235	0.302	0.249	0.151	0.298	PASS
RAMC	0.304	0.486	0.459	0.543	0.428	0.600	RAMC
RJGT	0.443	0.357	0.459	0.376	0.363	0.491	RJGT
SGS(*)			0.249	0.432	0.515	0.514	SGS(*)
SMGG	0.535	0.591	0.612	0.775	0.610	0.801	SMGG
SRP	0.386	0.322	0.347	0.501	0.165	0.179	SRP

4.2.1 Coefficient of determination, r2

Table 4.13 shows the results obtained for r^2 in the basal condition, and table 4.14 the respective averages, variances, and indexes of dispersion that are obtained using the data coming from the 15 individuals.

Table 4-14: Mean values for the coefficient of determination estimated between electrode pairs considering the 15 individuals, and respective variances and indexes of dispersion.Basal condition.

	MEAN (μ)	**VAR** (σ^2)	**D (%)** (σ^2/μ)
F4-Fz **Fz-F4**	0.535	0.044	8.22
F4-P3 **P3-F4**	0.311	0.019	6.24
Fz-F3 **F3-Fz**	0.477	0.036	7.52
F3-P4 **P4-F3**	0.368	0.024	6.51
P4-Pz **Pz-P4**	0.397	0.026	6.66
Pz-P3 **P3-Pz**	0.474	0.031	6.51

The observation of table 4.13 doesn't suggest any particular difference among individuals. However, the table is displayed for future comparison with the calculation condition.

Regarding table 4.14, the first observation that can be made is that the values of coupling between the pairs are generally lower than those that had been obtained using the cross-correlation function. This is not surprising, since the coefficient of determination is a squared decimal quantity, and therefore the values are expected to be lower than regular cross-correlations. Though, it is worth noticing that despite the values being lower, they are still all above 0.2, and therefore all the pairs can be considered to be significantly correlated. Furthermore, the order of coupling, from the most coupled pair to the least coupled one, is the following: F4-Fz, Fz-F3, Pz-P3, P4-Pz, F3-P4, and F4-P3. This order does not correspond to any of the previous that were obtained for the cross-correlation algorithm. However, it is very similar in the sense that, also in this case, the frontal areas show the most coupling, followed by the parietal areas, and finally the fronto-parietal network from

opposite hemispheres.

Tables 4.15 and 4.16 summarize the results obtained for r^2 for the mental calculation condition.

The observation of table 4.15 reveals an accentuated decrease in some of the pairs in comparison to the basal condition, namely in pairs P4-Pz of subject CPFRO, F3-P4 and F4-P3 of subject DRP, P4-Pz of subject MFSA, and F3-P4 and F4-P3 of subject RAMC. Among these subjects, only CPFRO shows particular characteristics. In fact, this subject revealed great level of errors, which could be associated with the low correlations observed in the parietal areas. However, the other subjects who also showed low levels of coupling values in some pairs don't have any particular characteristic which distinguishes them from the others, thus these low values can be correlated with some other phenomena or be simply due to poor performance of the algorithm in some cases. However, it is worth noticing that subject DRP had already showed some odd behaviour in the study performed using the cross-correlation algorithm, therefore this corroborates the idea that it might be interesting to further examine this subject.

Regarding table 4.16, and comparing it to table 4.14, which presents the equivalent results for the rest condition, one can see that the order of coupling, from the more coupled pair to the least, has changed. In the mental calculation condition, the frontal areas are still the ones showing the highest degree of coupling, but this time not followed by the parietal areas, because the parietal pair P4-Pz shows the least degree of correlation among the selected pairs. This lower activity of the right parietal side could be an indication of low right parietal involvement in comparison to the other selected brain areas.

Table 4-15: Coefficient of determination values regarding the different electrode pairs for the 15 individuals. Task condition.

	Pz-P3 P3-Pz	P4-Pz Pz-P4	F3-P4 P4-F3	Fz-F3 F3-Fz	F4-P3 P3-F4	F4-Fz Fz-F4	
BTL	0.380	0.350	0.272	0.451	0.266	0.394	BTL
CPFRO	0.451	0.063	0.214	0.364	0.336	0.563	CPFRO
CSF	0.631	0.526	0.373	0.395	0.420	0.354	CSF
DRP	0.488	0.340	0.025	0.381	0.007	0.570	DRP
LMBL	0.737	0.439	0.585	0.680	0.549	0.762	LMBL
LSGA	0.160	0.348	0.680	0.564	0.327	0.763	LSGA
MFSA	0.101	0.042	0.365	0.307	0.279	0.364	MFSA
OCR	0.417	0.324	0.405	0.338	0.391	0.436	OCR
PARS	0.419	0.200	0.394	0.325	0.340	0.378	PARS
PASS	0.212	0.241	0.229	0.246	0.373	0.295	PASS
RAMC	0.355	0.455	0.031	0.463	0.031	0.535	RAMC
RJGT	0.330	0.336	0.382	0.494	0.355	0.489	RJGT
SGS	0.175	0.170	0.428	0.601	0.388	0.441	SGS
SMGG	0.202	0.272	0.390	0.572	0.274	0.305	SMGG
SRP	0.458	0.281	0.451	0.524	0.349	0.510	SRP

Table 4-16: Mean values for the coefficient of determinationestimated between electrode pairs considering the 15 individuals, and respective variances and indexes of dispersion.Task condition

	MEAN (μ)	**VAR** (σ^2)	**D (%)** (σ^2/μ)
F4-Fz **Fz-F4**	0.477	0.021	4.39
F4-P3 **P3-F4**	0.312	0.019	6.05
Fz-F3 **F3-Fz**	0.447	0.015	3.46
F3-P4 **P4-F3**	0.348	0.031	8.94
P4-Pz **Pz-P4**	0.292	0.018	6.25
Pz-P3 **P3-Pz**	0.338	0.040	11.84

4.2.2 Nonlinear regression coefficient, h2

Tables 4.17 and 4.18 display the results relative to h^2.

The first observation that can be made regarding both tables is that the values of the pairs are the same or very similar whatever is the order considered, i.e., the value of, for example, F4-Fz (0.540), is equal to the value of Fz-F4. As had been stated in chapter 2, this symmetry is an indication of linearity, i.e., it suggests that the coupling between the pairs is linear. Furthermore, comparing these results with the ones obtained for r^2, one finds out that these are also very similar, thus corroborating the idea of linearity. Again, recalling what was stated in chapter 2, when two signals are linearly coupled, h^2 tends to approximate r^2, which is what happens in this case. It is also interesting to see that, in fact, the order of coupling obtained using this algorithm for the basal condition is the same as for r^2 in the same condition, this is, in descending order: F4-Fz/Fz-F4, Fz-F3/F3-Fz, Pz-P3/P3-Pz, P4-Pz/Pz-P4, F3-P4/P4-F3, and F4-P3/P3-F4.

The values regarding the calculation task condition are presented in tables 4.19 and 4.20. Again, the same symmetry that had been verified in the resting situation is verified in the calculation condition (e.g., $F4-Fz=Fz-F4$), and a high similarity between h^2 and r^2 for this condition is also found. This suggests that the correlations within the different pairs of electrodes are mostly linear also in the case where the subjects are engaged in performing an arithmetic task. The order of

coupling among the pairs, in descending order, is F4-Fz/Fz-F4, Fz-F3/F3-Fz, F3-P4/P4-F3 or Pz-P3/P3-Pz, F4-P3/P3-F4, and P4-Pz/Pz-P4, following a similar tendency as r^2 in the same condition. Furthermore, the same subjects who had presented unusually low values of correlation for certain pairs when computing r^2 were also found, for the same pairs, in the case of the computation of h^2.

4-17: Nonlinear regression coefficient values regarding the different electrode pairs for the 15 individuals. Basal condition.

	P3-Pz	Pz-P3	Pz-P4	P4-Pz	P4-F3	F3-P4	F3-FZ	Fz-F3	P3-F4	F4-P3	FZ-F4	F4-Fz	
BTL	0.465	0.470	0.202	0.202	0.538	0.535	0.752	0.754	0.231	0.235	0.712	0.712	**BTL**
CPFRO	0.454	0.455	0.234	0.229	0.274	0.275	0.284	0.274	0.299	0.308	0.448	0.456	**CPFRO**
CSF	0.588	0.585	0.558	0.575	0.237	0.213	0.278	0.197	0.159	0.120	0.258	0.266	**CSF**
DRP	0.801	0.798	0.647	0.639	0.129	0.119	0.469	0.473	0.223	0.219	0.687	0.689	**DRP**
LMBL	0.773	0.759	0.679	0.665	0.150	0.157	0.812	0.813	0.262	0.283	0.889	0.883	**LMBL**
LSGA	0.161	0.165	0.214	0.213	0.464	0.478	0.520	0.482	0.272	0.267	0.658	0.655	**LSGA**
MFSA	0.654	0.643	0.382	0.387	0.574	0.598	0.549	0.539	0.387	0.383	0.677	0.665	**MFSA**
OCR	0.352	0.359	0.370	0.350	0.395	0.405	0.318	0.316	0.283	0.281	0.287	0.288	**OCR**
PARS	0.507	0.531	0.375	0.374	0.514	0.514	0.497	0.463	0.424	0.412	0.531	0.545	**PARS**
PASS	0.321	0.342	0.220	0.241	0.321	0.318	0.255	0.258	0.171	0.163	0.323	0.314	**PASS**
RAMC	0.313	0.308	0.500	0.486	0.462	0.460	0.548	0.544	0.429	0.430	0.602	0.604	**RAMC**
RJGT	0.450	0.444	0.355	0.361	0.464	0.463	0.378	0.379	0.367	0.367	0.493	0.493	**RJGT**
SGS					0.256	0.252	0.445	0.469	0.518	0.523	0.551	0.544	**SGS**
SMGG	-5.856	2.928	2.928	-2.928	2.928	-2.928	0.000	0.000	0.000	0.000	0.000	0.000	**SMGG**
SRP	0.410	0.388	0.342	0.333	0.341	0.350	0.493	0.501	0.176	0.175	0.187	0.185	**SRP**

4-18: Mean values for the nonlinear regression coefficient estimated between electrode pairs considering the 15 individuals, and respective variances and indexes of dispersion. Basal condition.

	MEAN (μ)	**VAR** (σ^2)	**D (%)** (σ^2/μ)
F4-Fz	0.540	0.043	7.89
FZ-F4	0.540	0.043	7.97
F4-P3	0.319	0.019	5.93
P3-F4	0.321	0.018	5.56
Fz-F3	0.483	0.035	7.25
F3-FZ	0.492	0.032	6.52
F3-P4	0.383	0.025	6.45
P4-F3	0.382	0.023	6.05
P4-Pz	0.403	0.026	6.47
Pz-P4	0.405	0.027	6.66
Pz-P3	0.485	0.030	6.26
P3-Pz	0.485	0.032	6.55

Table 4-19: Nonlinear regression coefficient values regarding the different electrode pairs for the 15 individuals. Task condition.

	P3-Pz	Pz-P3	Pz-P4	P4-Pz	P4-F3	F3-P4	F3-FZ	Fz-F3	P3-F4	F4-P3	FZ-F4	F4-Fz
BTL	0.377	0.382	0.333	0.353	0.284	0.297	0.449	0.463	0.268	0.269	0.415	0.400
CPFRO	0.147	0.166	0.084	0.067	0.223	0.219	0.383	0.373	0.341	0.337	0.575	0.564
CSF	0.626	0.631	0.524	0.530	0.380	0.378	0.394	0.403	0.422	0.424	0.370	0.360
DRP	0.499	0.492	3.490	0.346	0.039	0.031	0.376	0.393	0.024	0.015	0.588	0.574
LMBL	0.747	0.737	0.427	0.440	0.587	0.586	0.682	0.681	0.557	0.551	0.772	0.762
LSGA	0.164	0.167	0.348	0.355	0.681	0.682	0.567	0.566	0.336	0.329	0.766	0.764
MFSA	0.103	0.142	0.076	0.054	0.398	0.371	0.374	0.429	0.306	0.355	0.478	0.482
OCR	0.410	0.440	0.391	0.350	0.378	0.411	0.357	0.360	0.388	0.396	0.457	0.441
PARS	0.437	0.421	0.197	0.203	0.396	0.396	0.316	0.329	0.353	0.344	0.422	0.397
PASS	0.204	0.214	0.249	0.248	0.239	0.238	0.239	0.256	0.389	0.378	0.289	0.301
RAMC	0.356	0.359	0.456	0.455	0.033	0.035	0.463	0.464	0.036	0.034	0.537	0.535
RJGT	0.341	0.341	0.344	0.341	0.388	0.385	0.494	0.496	0.363	0.357	0.488	0.489
SGS	0.179	0.189	0.179	0.186	0.433	0.431	0.600	0.609	0.375	0.400	0.450	0.444
SMGG	0.204	0.206	0.278	0.275	0.408	0.393	0.573	0.574	0.280	0.277	0.316	0.307
SRP	0.460	0.462	0.279	0.287	0.453	0.451	0.525	0.530	0.349	0.355	0.526	0.523

Table 4-20: Mean values for the nonlinear regression coefficientestimated between electrode pairs considering the 15 individuals, and respective variances and indexes of dispersion.Task condition.

	MEAN (μ)	**VAR** (σ^2)	**D (%)** (σ^2/μ)
F4-Fz	0.489	0.019	3.97
FZ-F4	0.497	0.020	3.93
F4-P3	0.322	0.019	5.85
P3-F4	0.319	0.018	5.74
Fz-F3	0.462	0.013	2.89
F3-FZ	0.453	0.014	3.19
F3-P4	0.354	0.030	8.60
P4-F3	0.355	0.030	8.53
P4-Pz	0.299	0.018	5.96
Pz-P4	0.301	0.017	5.51
Pz-P3	0.357	0.032	9.03
P3-Pz	0.350	0.035	9.97

4.3 Estimation of the delays between signals

All the association functions described above were also used to estimate the delay between different signals, by calculating the time lag for which these association functions were maximal. However, no conclusive results were obtained. The values that were obtained were mostly 0 (zero) for all cases, which could mean that the signals were synchronous. However, the lack of consistency among the results obtained for different subjects using the same algorithm and according to different algorithms used on the same subject seems to be evidence that none of these algorithms show in fact enough robustness for the estimation of time delays. The tables containing these results can be found in appendix C.

4.4 Discussion of the results

Comparing the results obtained with different procedures, some interesting points stand out. In the following paragraphs a brief presentation of the main findings will be carried. The integration of these within the different theories that have been previously defended by other authors will be carried out in the next chapter.

First of all, the results that were obtained in this study suggest linear coupling among the different areas, since not only are the values estimated for the coefficients of determination and for the nonlinear regression coefficient very similar, but also the nonlinear regression coefficient shows a high degree of symmetry, which has been associated with linear coupling (Pijn et al 1990). This was observed both for the basal condition as well as for the task condition.

Regarding the correlations that were estimated, the frontal pairs always showed the highest degree of coupling. Once again, this was found in both conditions and according to all the algorithms that were implemented.

Concerning the results obtained with the cross-correlation function, some interesting comparisons between the intra and inter-hemispheric coupling can be made. For instance, one can observe that both in rest and in task conditions, the highest coupling is found among the frontal, parietal and occipital regions (F-P-O). In fact, despite the frontal and occipital regions being quite far away from each other, a higher correlation is found between these two regions than, for example, between homologous areas situated in opposite hemispheres. For instance, the following values were obtained:

(basal condition)		**(calculation condition)**	
F3-F4: 0.501	**F3-O1:** 0.577	**F3-F4:** 0.457	**F3-O1:** 0.487
P3-P4: 0.337	**F4-O2:** 0.536	**P3-P4:** 0.305	**F4-O2:** 0.529

These results can also be seen as an indication of the robustness of the algorithm used, since very distant areas show more coupling than areas that are physically much nearer each other. Therefore, one can say that the effects of volume conduction are not influencing this study to a very large extent.

Still regarding the results obtained with the cross-correlation algorithm, among all the pairs that show correlation values above 0.5, the order, from the most coupled to least coupled, is the following:

(basal condition)	**(calculation condition)**
Fz-F3	F4-Fz
F4-Fz	Fz-F3
Pz-P3	P4-O2
P4-O2	Pz-P3
P4-Pz	F3-P4
P3-O1	P3-O1
F3-P4	P4-Pz
F4-P3	F4-P3
F3-O1	F4-O2
F4-O2	
Fz-P3	
Fz-P4	
F4-F3	

Concerning all the algorithms in general, it is also observed that F3-P4 > F4-P3 for both conditions. Furthermore, the pair P4-Pz is the 4th most correlated for all algorithms, in the basal condition. However, in the calculation condition, the coupling of this pair always decreases relatively to the other pairs.

Overall, the general tendency seems to be that in the basal condition many areas show significant coupling, and in the calculation condition the coupling is maintained in some of these areas and reduced in the others.

5

General Conclusions

Despite the data that has been analysed in the course of this study, 15 subjects, not being sufficient to reach statistical significance, some important observations regarding the results that were obtained can be made.

First of all, an important point that has already been mentioned, is the fact that the coupling between the signals revealed linearity.

Secondly, regarding the differences observed in terms of coupling between the basal condition and between the mental task condition, it was interesting to see that the latter did not reveal any particular increase in coupling in relation to the former. In fact, what was observed was that in the basal condition many areas showed significant correlation, but when the subjects were performing the calculations the coupling among some areas showed a decrease while other areas simply maintained the same level of correlation. This seems as though the brain becomes 'concentrated' in some areas while other areas become less involved. Furthermore, it might be an explanation of why, when one is concentrated in one task, one becomes less aware and less attentive to the other things that are happening.

Recalling what was described in chapter 1, concerning the results that have been achieved by other authors, we can arrive at the conclusion that, in the present study, the areas that seem to maintain the coupling level in both conditions correspond to the ones that usually show more activation with other imaging techniques in similar tasks. For example, here the highest coupling is found between the frontal areas, bilaterally, and a strong fronto-parietal correlation can also be found, especially between opposite hemispheres (F3-P4 and P4-F3). This is in concordance with other results that have been observed in other studies, and which have suggested a strong participation of frontal and parietal areas in mental calculation, with the involvement of both hemispheres in more complex tasks (such as this one). Furthermore, concerning the differences between the two hemispheres, despite both showing similar levels of coupling in rest condition,

during the accomplishment of this task the right hemisphere shows predominant levels of coupling, in particular regarding the connection of frontal and parietal areas with the occipital areas. Despite the task of mental calculation being traditionally associated with activation of the left hemisphere, right hemisphere activation has been shown in more complex tasks, and some authors even defend the involvement of the right parietal areas in some kind of numerical quantity system. The results of this study are in concordance with the idea that, in fact, some tasks of mental calculation strongly engage the right hemisphere. Other areas that have been suggested to take part in mental calculation by other authors are the temporal areas, especially left temporal areas during arithmetic fact retrieval. Bilateral temporal areas also have been suggested to take part in visual mental imagery resolution strategies. However, this study does not show evidence supporting the involvement of this area. In fact, temporal areas show low levels of coupling, at least with other areas of the same hemisphere. It might be interesting to determine if there is an inter-hemispheric involvement of temporal zones. The occipital areas, though, show high levels of coupling with frontal and parietal areas of the same hemisphere. Occipital areas are traditionally associated with vision and visualization skills.

Regarding the estimation of delays and inferences on causality between signals, no conclusive results were achieved. An interesting approach would be to implement algorithms especially tailored for testing for causality and delays between signals. Since these results have shown linear coupling among different networks, one algorithm that could be used is the Granger causality. Furthermore, it would be interesting to try to look for synchronies in phase (PS). Regarding the further exploration of the algorithms and results of this study, it would be interesting to make comparisons between the relative values of correlation instead of only the absolute values, as has been done presently. The computation of relative values might outstand some tendencies in the results difficult to detect using absolute values. It would also be interesting to compute the correlations between the signals coming from other electrodes and to further explore inter-hemispheric coupling.

Finally, regarding the limitations of this work, it is subject to the same caveats as the other similar studies. Concerning the technique used, EEG, the signal is unavoidably contaminated by artefacts, and the calculation of coupling is influenced by volume conduction, especially when determining the coupling between two signals coming from electrodes that are near each other. Regarding the data and the paradigm, some variability among individuals was found. The paradigm was quite complex, involving both computation ad arithmetic fact retrieval. This is interesting in the sense that it tests for individual's performance in complex arithmetic tasks, but also shows the caveat of involving different skills without being able to distinguish them.

Bibliography

Baddeley, A. (1992). "Working memory." Science **255**(5044): 556-559.

Baldo, J. V. and N. F. Dronkers (2007). "Neural correlates of arithmetic and language comprehension: A common substrate?" Neuropsychologia **45**(2): 229-235.

Borges, A. F. T. (2009). Spectral and Coherence Estimates on Electroencephalogram recordings during arithmetical tasks. Physics Department. Lisbon, Universidade Nova de Lisboa. **Master Thesis**.

Brody, C. D. (1999). "Correlations Without Synchrony." Neural Computation **11**: 1537-1551.

C. Tallon-Baudry, O. B., C. Wienbruch, B. Ross, C. Pantev (1997). "Combined EEG and MEG recordings of visual 40 Hz responses to illusory triangles in human." Neuroreport **8**(5): 1103-1107.

Christoph Bledowski, D. P., Karsten Hoechstetter, Michael Scherg, Michael Wibral, Rainer Goebel, and David E. J. Linden (2004). "Localizing P300 Generators in Visual Target and Distractor Processing: A Combined Event-Related Potential and Functional Magnetic Resonance Imaging Study " The Journal of Neuroscience **24**(42): 9353-9360.

E. Disbrow, T. R., D. Poeppel, L. Krubitzer (2001). "Evidence for interhemispheric processing of inputs from the hands in human S2 and PV." J Neurophysiol **85**: 2236–2244.

Eric R. Kandel, J. H. S., Thomas M. Jessell (2000). Principles of neural science, McGraw-Hill, Health Professions Division.

Ernesto Pereda, R. Q. Q., Joydeep Bhattacharya (2005). "Nonlinear multivariate analysis of neurophysiological signals." Neurobiology **77**: 1.37.

Ernst Niedermayer, L. D. S. (1999). Electroencephalography: Basic Principles, Clinical Applications and Related Fields. W. Wilkins. **1154**.

Gregory A. Troup, J. L. B., and Norman C. Nettleton (1983). "The Lateralization of arithmetic and number processing: a review." Intern. J. Neuroscience **19**: 231-242.

H. Zaveri, W. W., J. Sackellares, A. Beydoun, R. Duckrow, S. Spencer (1999). "Measuring the coherence of intracranial electroencephalograms." Clinical Neurophysiology **110**: 1717-1725.

Hallett, M. (2000). "Transcranial magnetic stimulation and the human brain." Nature **406**(6792): 147-150.

illustrations, B. (2005). Anatomy and Functins of the Brain. Richmond, VA, Golgeon Group, Inc.

J. Cohen, S. F., T. Braver, B. Casev, D. Servan-Schreiber, and D. Noll (1994). "Activation of the Prefrontal Cortex in a Nonspatial Working Memory Task with Functional MRI." Human Brain Mapping **1**: 293-304.

Jean-Philippe Lachaux, E. R., Jacques Martinerie, and Francisco J. Varela (1999). "Measuring phase synchorony in brain signals." Human Brain Mapping **8**: 194-208.

Juliana V. Baldo, N. F. D. (2006). "Neural correlates of arithmetic and language comprehension: A common substrate?" Neuropsychologia.

K. B. Durka, P. W. (2006). Encyclopedia of Biomedical Engineering ch. Electroencephalography (EEG), John Wiley & Sons, Inc,.

Kaiser, D. A. (2006). "What is quantitative eeg?" Journal of Neurotherapy **10**(4).

Kazuo Sasaki, T. T., Satoru Nishikawa, Nobuyuki Nishitani, Tsutomu Ishihara (1996). "Frontal mental theta wave recorded simultaneously with magnetoencephalography and electroencephalography." Neusoscience Research **26**: 79-81.

Keiichiro Toma, T. M., Ilka Immisch, Tatsuya Mima, Daniel Waldvogel, Benjamin Koshy, Takashi Hanakawa, Holly Shill, and Mark Hallett (2002). "Generators of Movement-Related Cortical Potentials: fMRI-Constrained EEG Dipole Source Analysis." NeuroImage **17**: 161-173.

Krane, K. S. (1988). Introductory Nuclear Physics. USA, Wiley.

L. Faes, G. N., R. Antolini (2001). "Investigating thr Level of the Significance of the Coherence Function in Cardiovascular Variability Analysis." Computers in Cardiology **28**: 481-484.

L. Faes, G. P., A. Porta, R. Maestri, and G. Nollo (2004). "Surrogate Data Analysis for Assessing the Significance of the Coherence Function." IEEE Transactions on Biomedical Engineering **51**(7): 1156-1166.

Laure Zago, M. P., Emmanuel Mellet, Fabrice Crivello, Bernard Mazoyer, and Nathalie Tzourio-Mazoyer (2001). "Neural Correlates of Simple and Complex Mental Calculation." Neuroimage **13**: 314-327.

Leif Sörnmo, P. L. (2005). Bioelectrical signal processing in cardiac and neurological applications. San Diego, USA, Elsevier Academic Press.

Linda Rueckert, N. L., Arnaud Partiot, Ildebrando Appollonio, Irene Litvan, Denis Le Bihan, and Jordan Grafman (1996). "Visualizing Cortical Activation during Mental Calculation with Functional MRI." Neuroimage **3**: 97-103.

M. Caramazza, a. A. B. (1985). "Cognitive Mechanisms in Number Processing and Calculation: Evidence from Dyscalculia." BRAIN AND COGNITION **4**: 171-196.

M. Schreckenberger, C. L.-A., M. Lochmann, K. Mann, T. Siessmeier, H. Buchholz, P. Bartenstein, G. Gründer (2004). "The thalamus as the generator and modulator of EEG alpha rhythm: a combined PET/EEG study with lorazepam challenge in humans." Neuroimage **22**(2): 637-644.

Margaret G. Funnell, M. K. C., Michael S. Gazzaniga (2007). "The calculating hemispheres: Studies of a split-brain patient." Neuropsychologia **45**: 2378-2386.

N. Oishi, T. M., K. Ishii, K. O. Bushara, T. Hiraoka, Y. Ueki, H. Fukuyama, M. Hallett, (2007). "Neural correlates of regional EEG power change." Neuroimage **36**(4): 1301-1312.

Nieder, A. (2005) "Counting Ounting on Neurons: The Neurobiology of Numerical Competence." NATURE REVIEWS - NEUROSCIENCE, 14.

Noel, M.-P. and X. Seron (1993). "Arabic number reading deficit: A single case study or when 236 is read (2306) and judged superior to 1258." Cognitive Neuropsychology **10**(4): 317 - 339.

O. Gruber, P. I., H. Steinmetz, and A. Kleinschmidt (2001). "Dissociating Neural Correlates of Cognitive Components in Mental Calculation." **11**(4): 350-359.

Oana Tudusciuc, a. A. N. (2007). "Neuronal population coding of continuous and discrete quantity in the primate posterior parietal cortex." Neuroscience **104**(36): 14513-14518.

P. Ahlfors, G. V. S., A. M. Dale, J. W. Belliveau, A. K. Liu, A. Korvenoja, J. Virtanen, M. Huotilainen, R. B. Tootell, H. J. Aronen, R. J. Limoniemi (1999). "Spatiotemporal activity of a cortical network for processing visual motion revealed by MEG and fMRI." J Neurophysiol **82**: 2545-2555.

P. Ritter, a. A. V. (2006). "Simultaneous eeg-fmri." Neuroscience and Biobehavioral Reviews **30**: 823–838.

Pereira, C. M. Q. (1998). Processamento de Dados Electroencefalográficos - Aplicações à Epilepsia.

Physpharm. (2009). "The Physiology of the Senses - Transformations For Perception and Action - Lecture 5 - The Cerebral Association Cortex." Retrieved 16/08, 2010, from www. physpharm.fmd.uwo.ca.

Pijn, J. P. M. (1990). Quantitative evaluation of EEG signals in epilepsy. Department of Experimental Zoology. Amsterdam, Universiteit van Amsterdam. **Doctor:** 172.

Raichle, M. (1998). "Behind the scenes of functional brain imaging: a historical and physiological perspective." Proc. Natl. Acad. Sci. USA **95** (3): 765-772.

Rochel Gelman, a. B. B. (2005). "Number and language: how are they related?" Cognitive Sciences **9**(1): 6-10.

S. Dehaene, E. S., P. Pinel, R. Stanescu, S. Tsivkin (1999). "Sources of Mathematical Thinking: Behavioral and Brain-Imaging Evidence." Science **284**: 970-974.

Shepherd, G. M. (1994). Neurobiology. New York, USA, Oxford University Press.

Shibasaki, H. (2008). "Human brain mapping:hemodynamic response and electrophysiology." Clinical Neurophysiology **119**: 731-743.

Sifis Micheloyannis, V. S., Michalis Vourkas, Cornelis J. Stam, Panagiotis G. Simos (2005). "Neural networks involved in mathematical thinking: evidence from linear and non-linear analysis of electroencephalographic activity." Neuroscience letters **373**: 212-217.

Simon, T. (1999). "The foundations of numerical thimking in a brain without numbers." Cognitive Sciences **3**(10): 363-366.

Snell, R. S. (2001). Clinical Neuroanatomy for Medical Students - Chapter 7-9. Washington, D.C., Lippincott Williams & Wilkins.

Stanislas Dehaene, M. P., Philippe Pinel, and Laurent Cohen (1992). "Varieties of numerical abilities." Cognition **44**: 1-42.

Stanislas Dehaene, M. P., Philippe Pinel, and Laurent Cohen (2003). "Three Parietal Circuits for Numbers Processing." Cognitive Neuropsychology **20**(3/4/5/6): 487–506.

Stanislas Dehaene, N. M., Laurent Cohen, and Anna J. Wilson (2004). "Arithmetic and the brain." Cognitive Neuroscience **14**: 218-224.

Thalía Fernández, T. H., Mario Rodríguez, Jorge Bernal, Juan Silva, Alfonso Reyes, Erzsébet Marosi (1995). "EEG activation patterns during the performance of tasks

involving different components of mental calculation." Electroencephalography and clinical Neurophysiology **94**: 175-182.

Thalía Harmony, T. F., Juan Silva, Jorge Bosch, Pedro Valdés, Antonio Fernández-Bouzas, Lídice Galán, Eduardo Aubert, Daniel Rodríguez (1999). "Do specific EEG frequencies indicate different processes during mental calculation?" Neuroscience **266**: 25-28.

Thorsten Fehr, C. C., Manfres Herrmann (2007). "Common brain regions underlying different arithmetic operations as revealed by conjunct fMRI-BOLD activation." Brain Research **1172**: 93-102.

Zhang Yun-ting, Z. Q., zhang Jing, and Li Wei (2005). "Laterality of brain areas associated with arithmetic calculations revealed by functional magnetic resonance imaging." Chinese Medical Journal **118**(8): 633-638.

Appendix A

Surrogation carried out for subject BTL

Minimum values from which the signals can be considered to be inversely correlated (eyes closed)

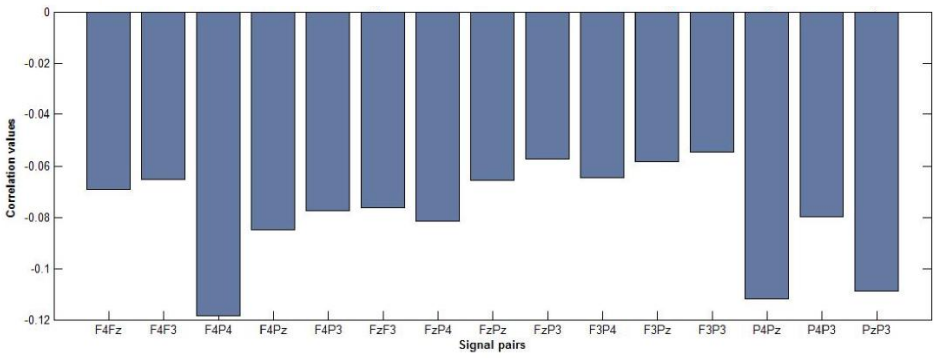

Minimum values from which the signals can be considered to be directly correlated (eyes closed)

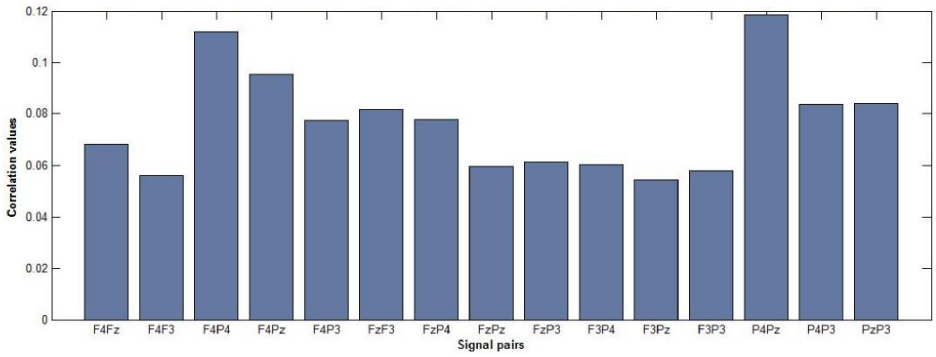

Surrogation carried out for subject CPFRO

Minimum values from which the signals can be considered to be inversely correlated (calculation)

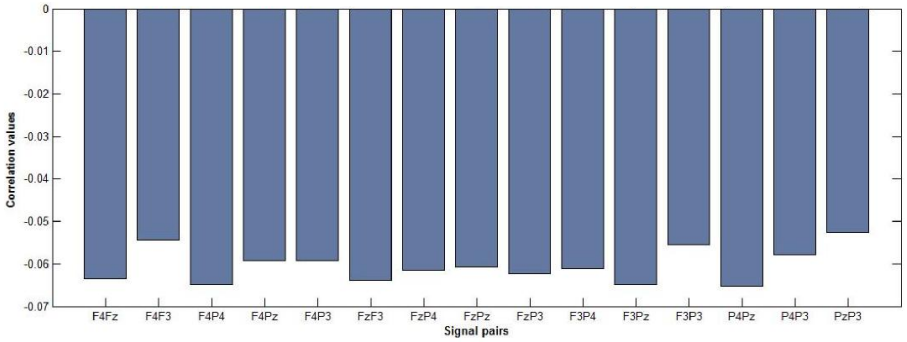

Minimum values from which the signals can be considered to be directly correlated (calculation)

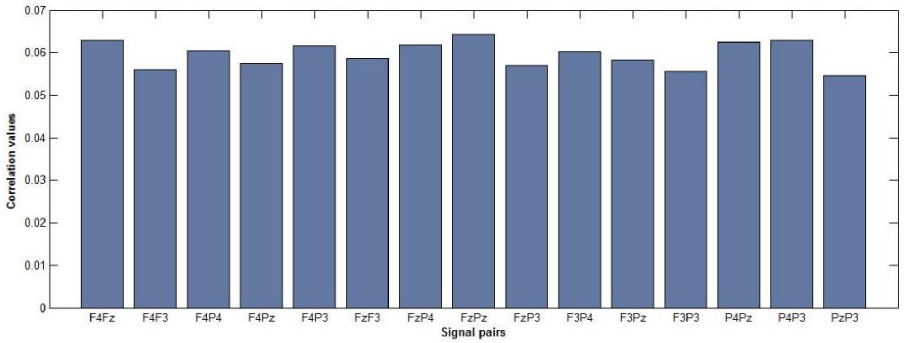

Minimum values from which the signals can be considered to be inversely correlated (eyes closed)

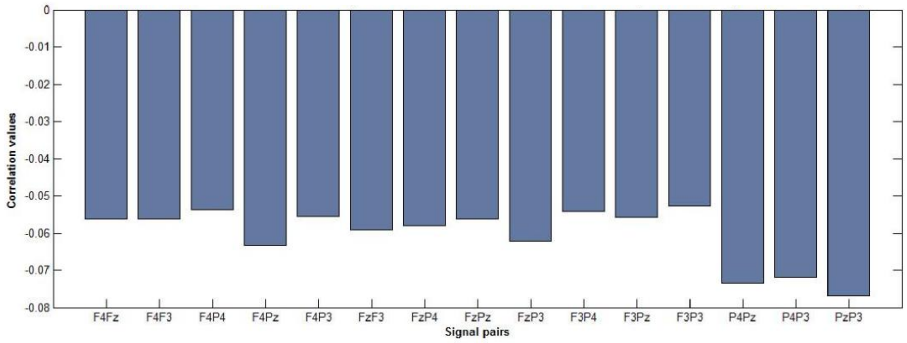

Minimum values from which the signals can be considered to be directly correlated (eyes closed)

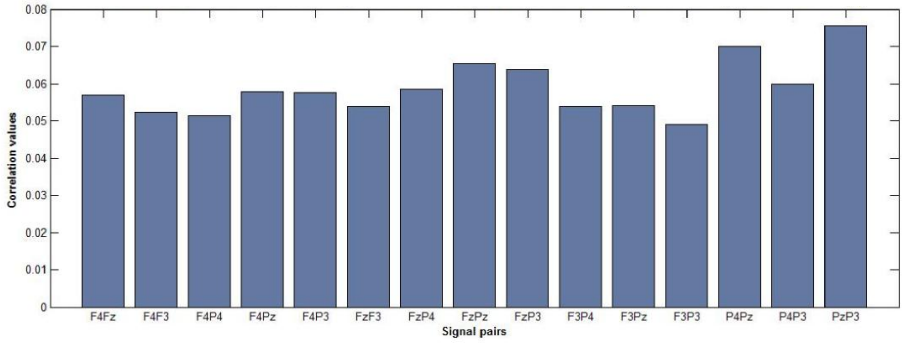

Surrogation carried out for subject CSF

Minimum values from which the signals can be considered to be inversely correlated (calculation)

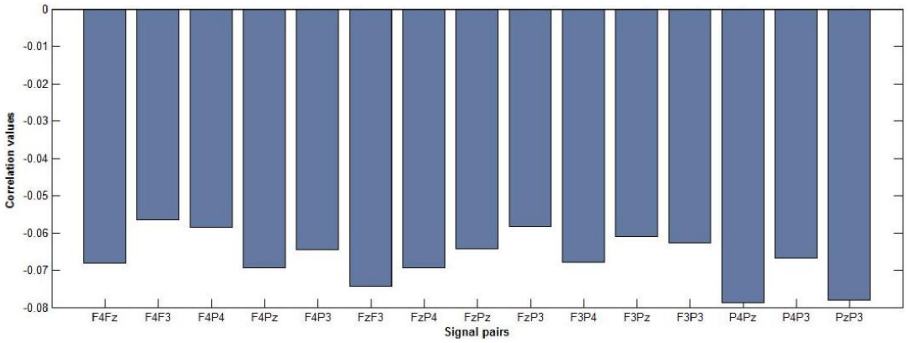

Minimum values from which the signals can be considered to be directly correlated (calculation)

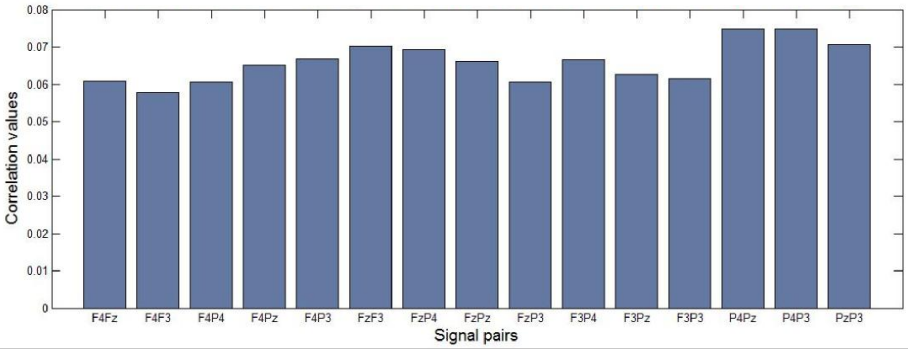

Minimum values from which the signals can be considered to be inversely correlated (eyes closed)

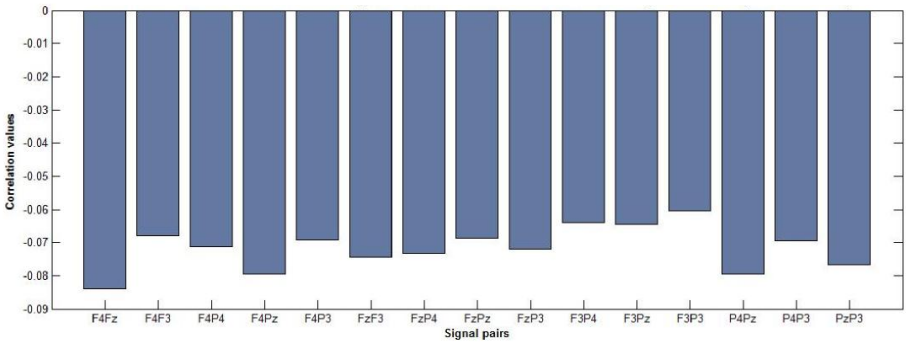

Minimum values from which the signals can be considered to be directly correlated (eyes closed)

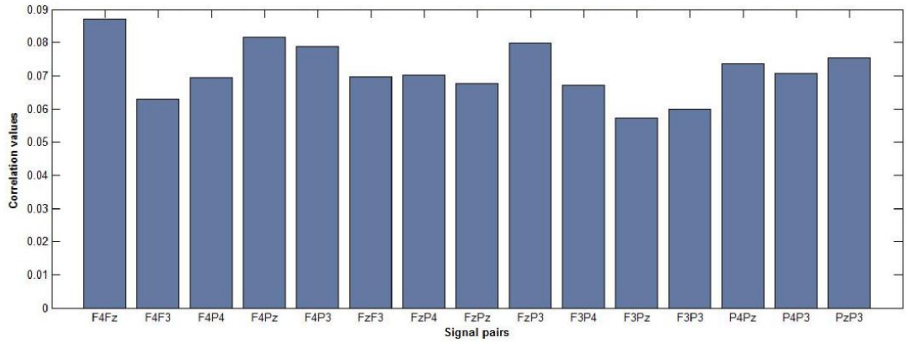

Surrogation carried out for subject DRP

Minimum values from which the signals can be considered to be inversely correlated (calculation)

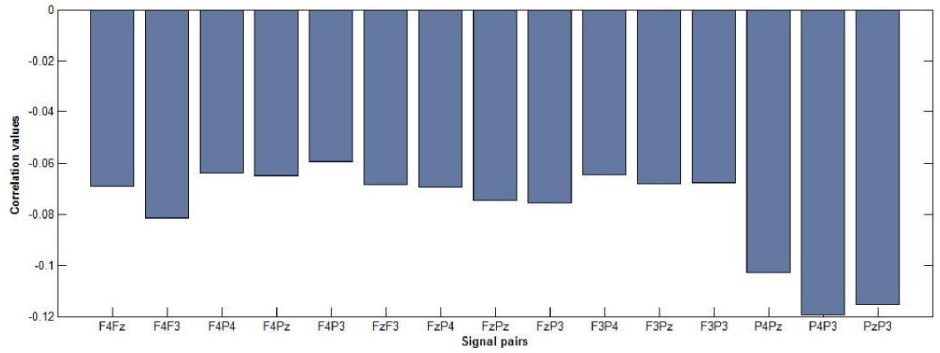

Minimum values from which the signals can be considered to be directly correlated (calculation)

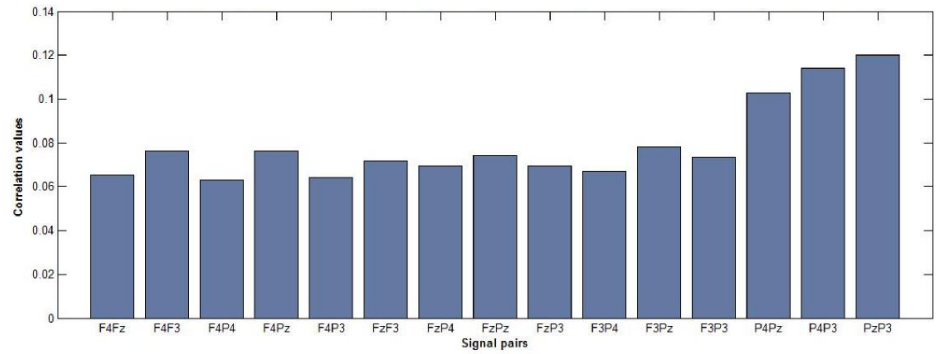

Minimum values from which the signals can be considered to be inversely correlated (eyes closed)

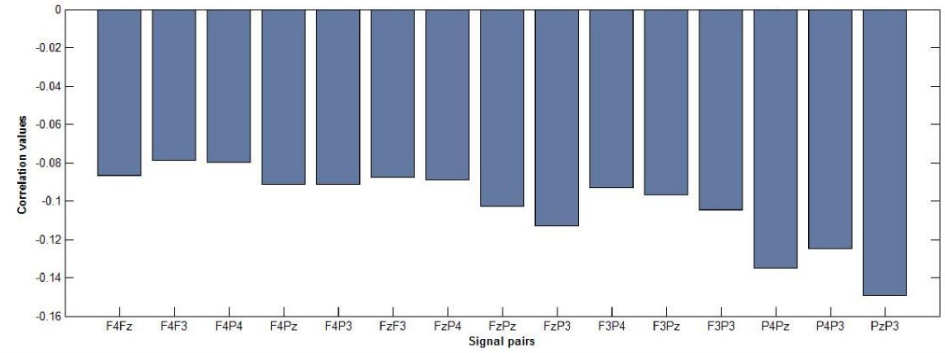

Minimum values from which the signals can be considered to be directly correlated (eyes closed)

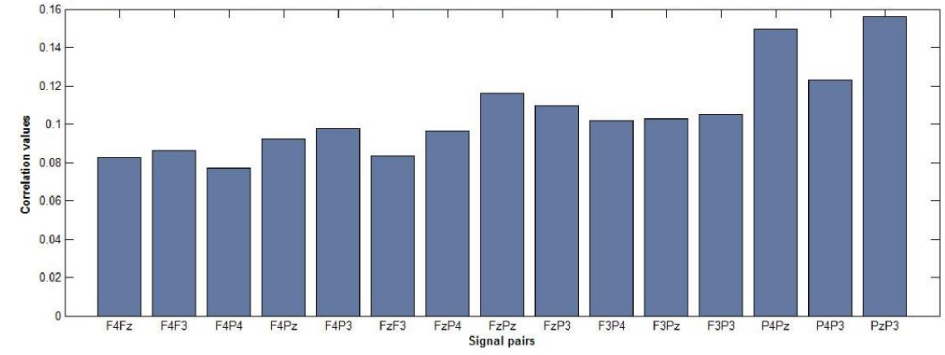

Surrogation carried out for subject LMBL

Minimum values from which the signals can be considered to be inversely correlated (calculation)

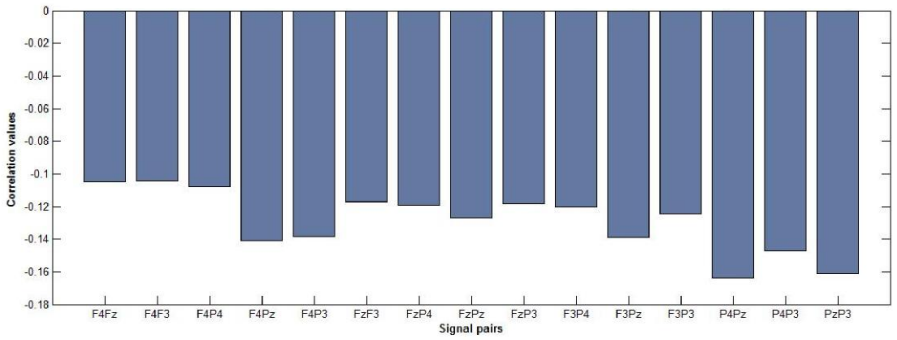

Minimum values from which the signals can be considered to be directly correlated (calculation)

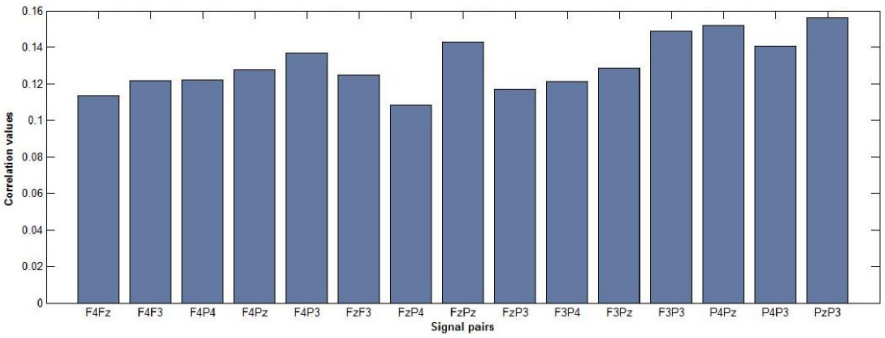

Minimum values from which the signals can be considered to be inversely correlated (eyes closed)

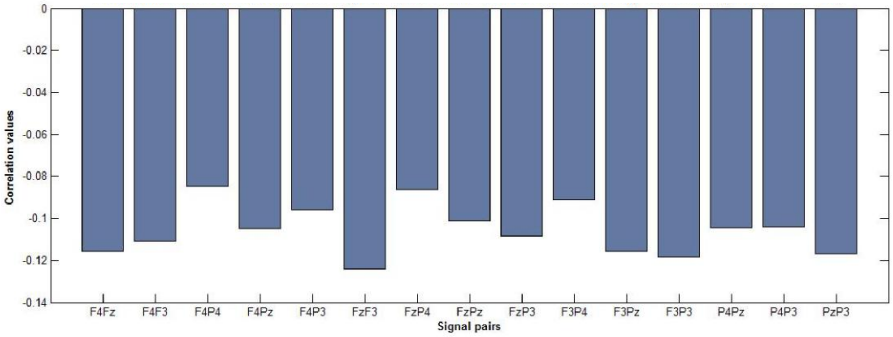

Minimum values from which the signals can be considered to be directly correlated (eyes closed)

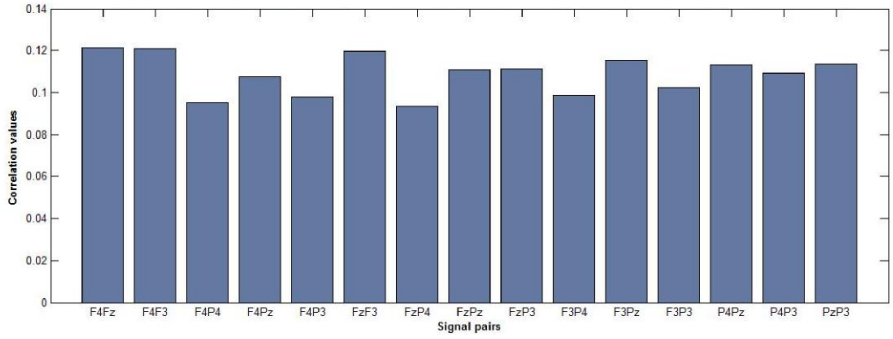

Surrogation carried out for subject LSGA

Minimum values from which the signals can be considered to be inversely correlated (calculation)

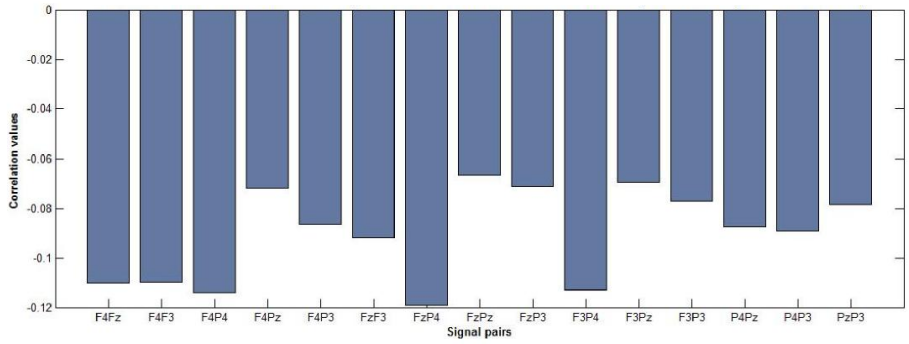

Minimum values from which the signals can be considered to be directly correlated (calculation)

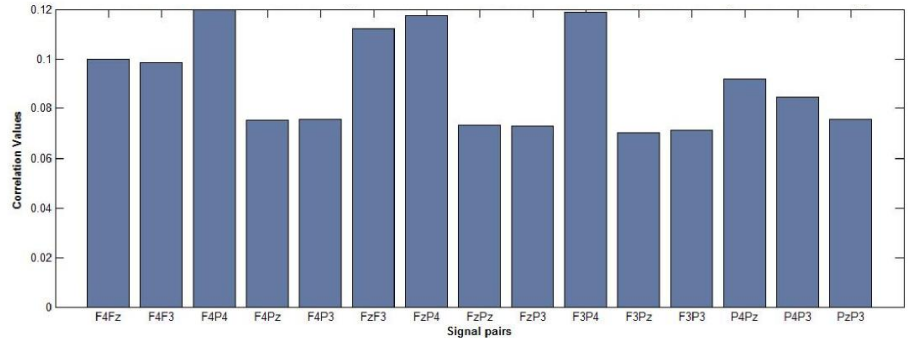

Minimum values from which the signals can be considered to be inversely correlated (eyes closed)

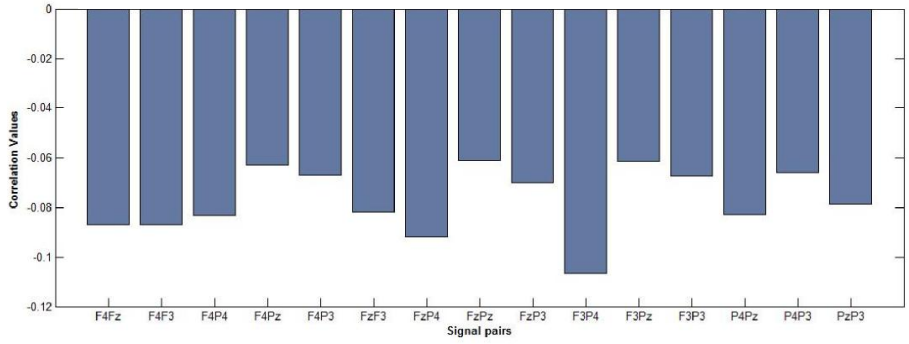

Minimum values from which the signals can be considered to be directly correlated (eyes closed)

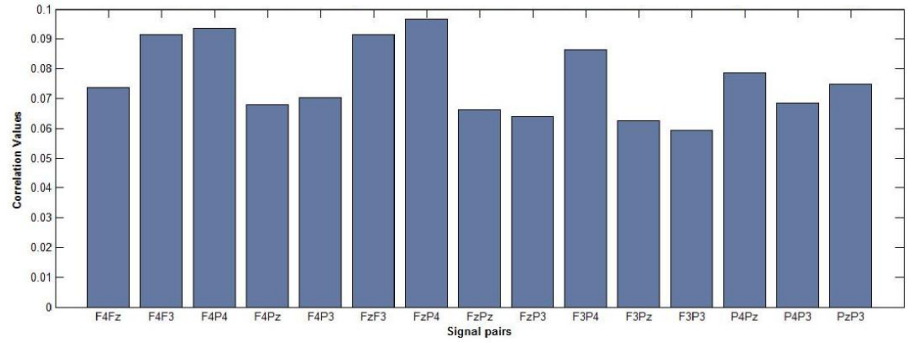

Surrogation carried out for subject OCR

Minimum values from which the signals can be considered to be inversely correlated (calculation)

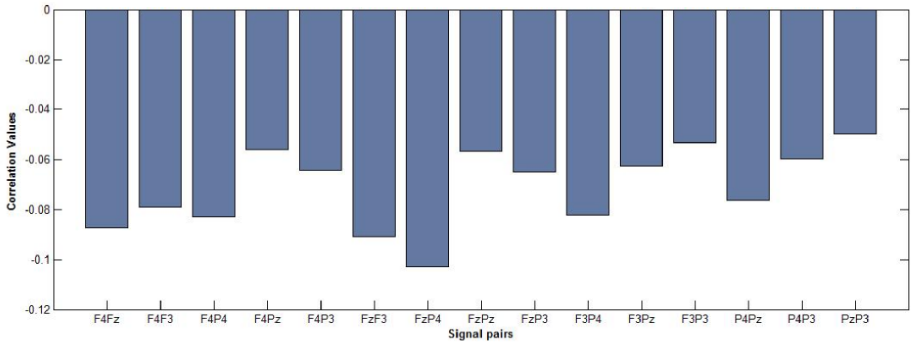

Minimum values from which the signals can be considered to be directly correlated (calculation)

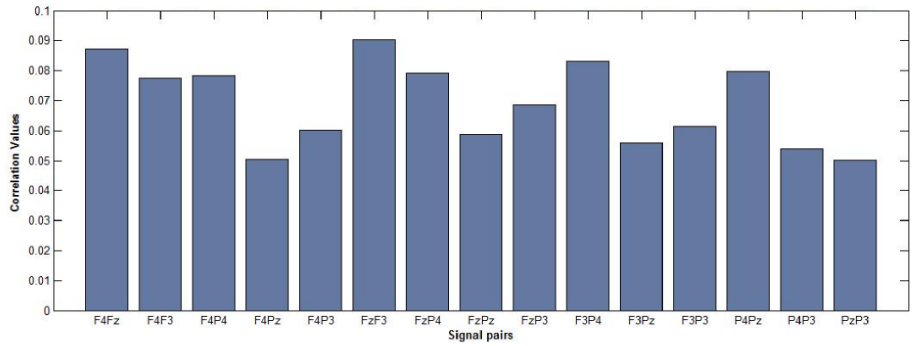

Minimum values from which the signals can be considered to be directly correlated (eyes closed)

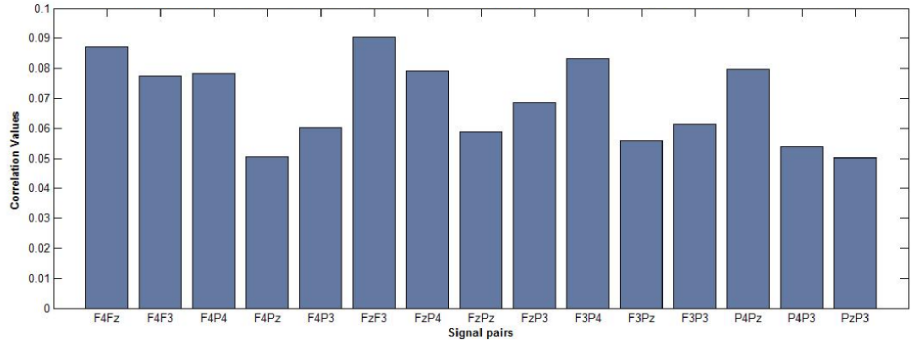

Surrogation carried out for subject PARS

Minimum values from which the signals can be considered to be inversely correlated (calculation)

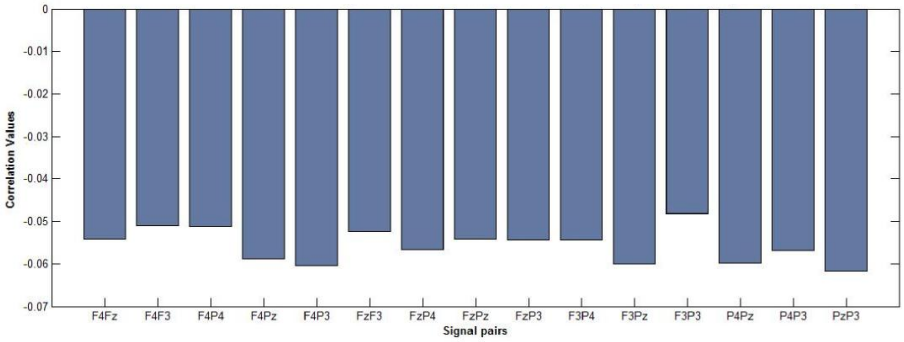

Minimum values from which the signals can be considered to be directly correlated (calculation)

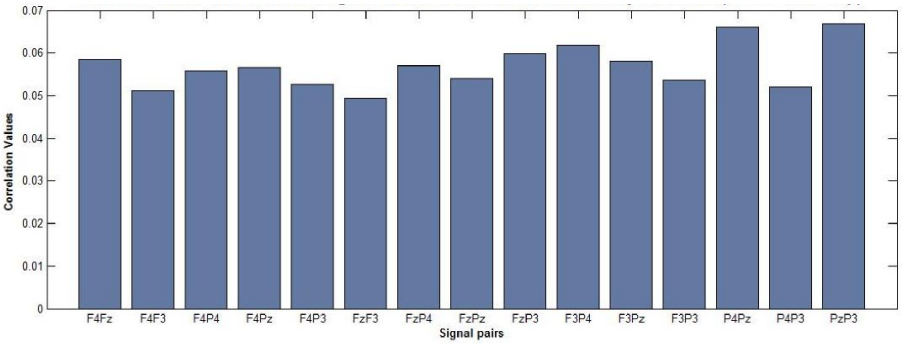

Minimum values from which the signals can be considered to be inversely correlated (eyes closed)

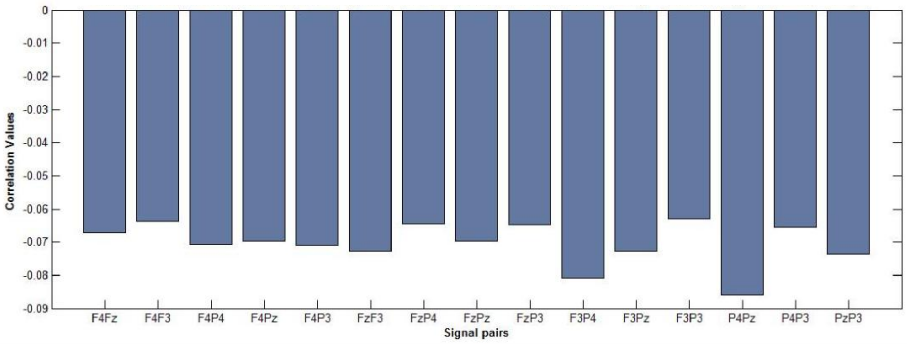

Minimum values from which the signals can be considered to be directly correlated (eyes closed)

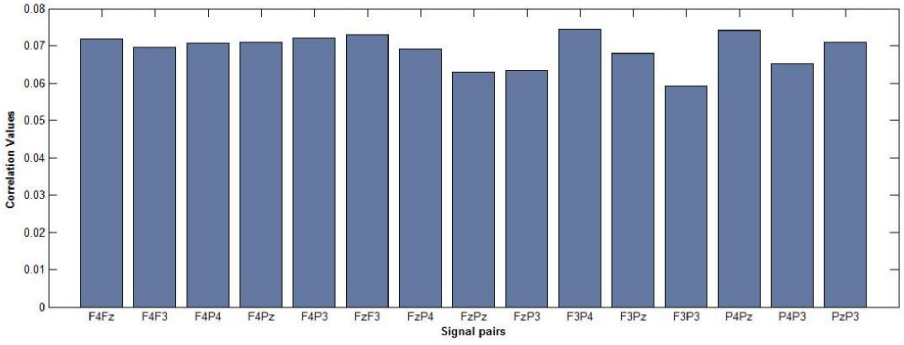

Surrogation carried out for subject PASS

Minimum values from which the signals can be considered to be inversely correlated (calculation)

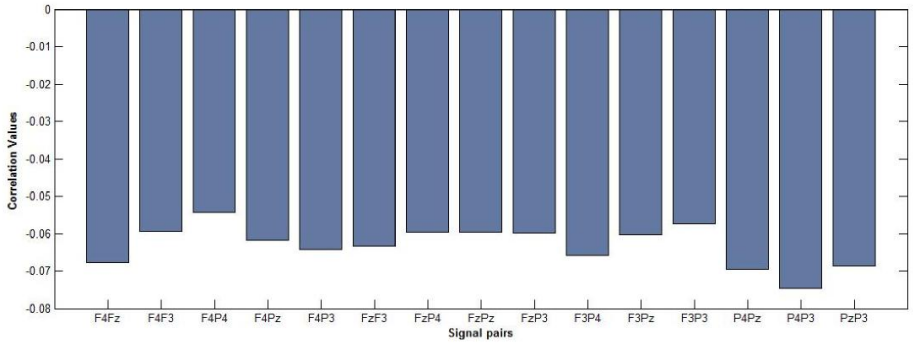

Minimum values from which the signals can be considered to be directly correlated (calculation)

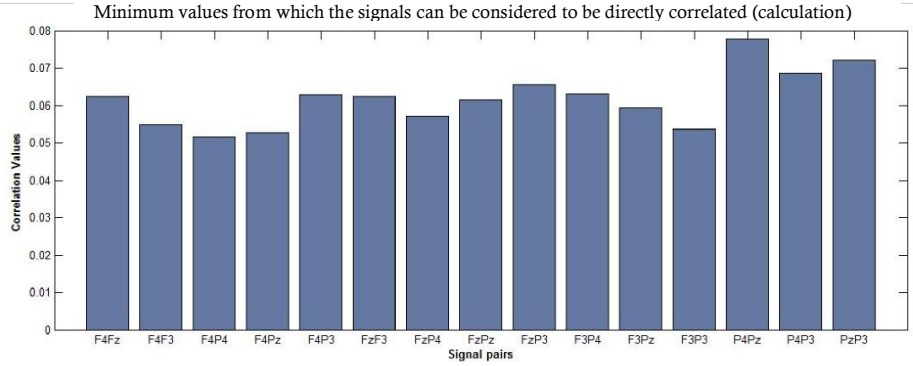

Minimum values from which the signals can be considered to be inversely correlated (eyes closed)

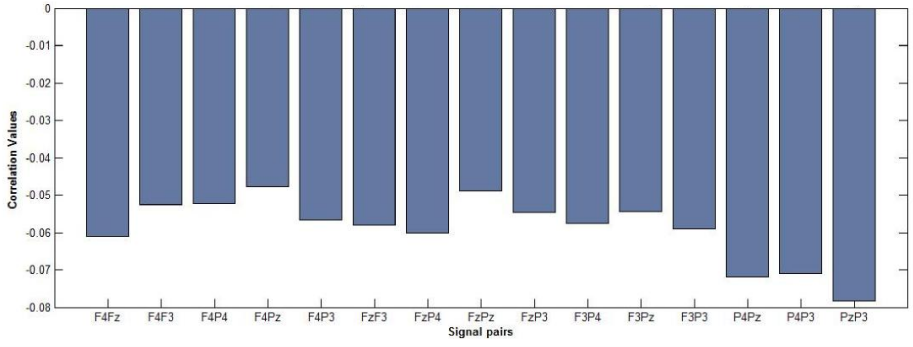

Minimum values from which the signals can be considered to be directly correlated (eyes closed)

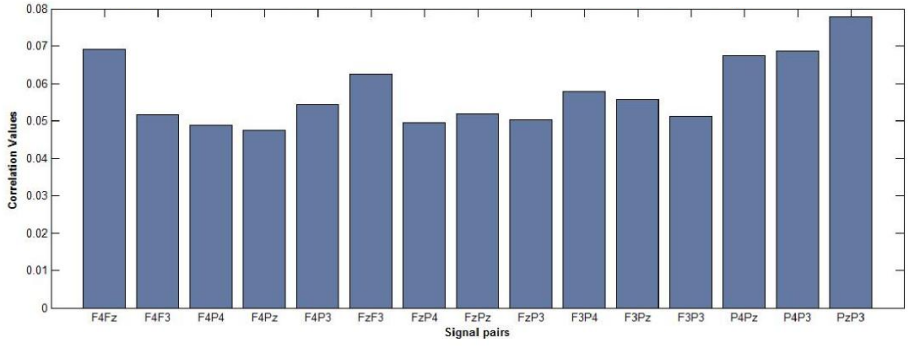

Surrogation carried out for subject RAMC

Minimum values from which the signals can be considered to be inversely correlated (calculation)

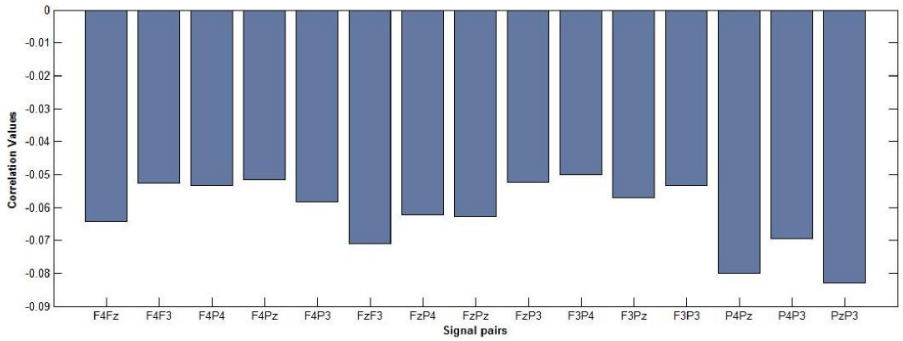

Minimum values from which the signals can be considered to be directly correlated (calculation)

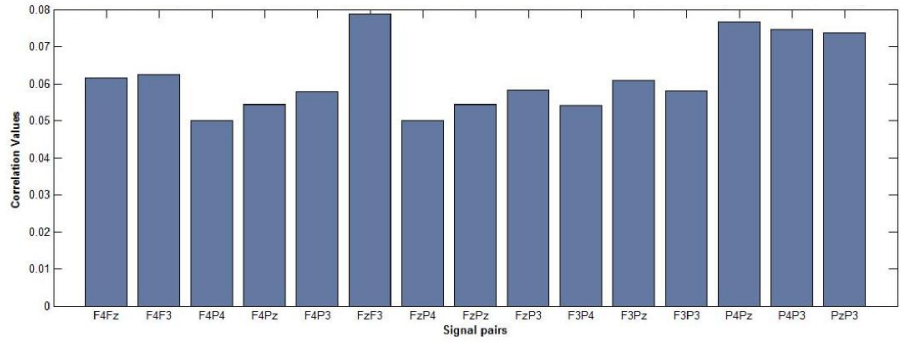

Minimum values from which the signals can be considered to be inversely correlated (eyes closed)

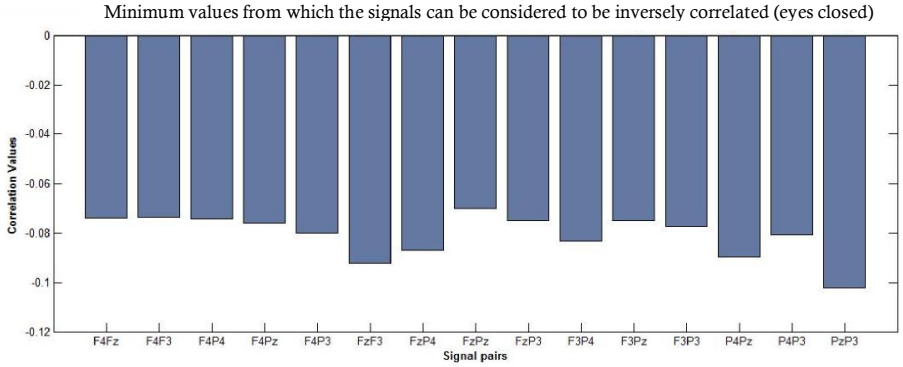

Minimum values from which the signals can be considered to be directly correlated (eyes closed)

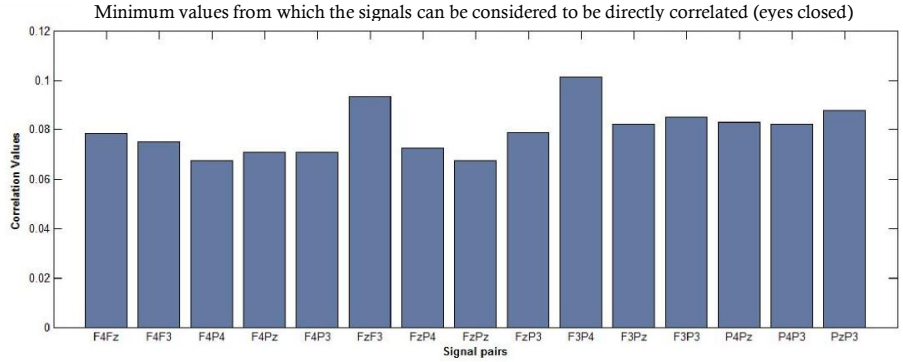

Surrogation carried out for subject RJGT

Minimum values from which the signals can be considered to be inversely correlated (calculation)

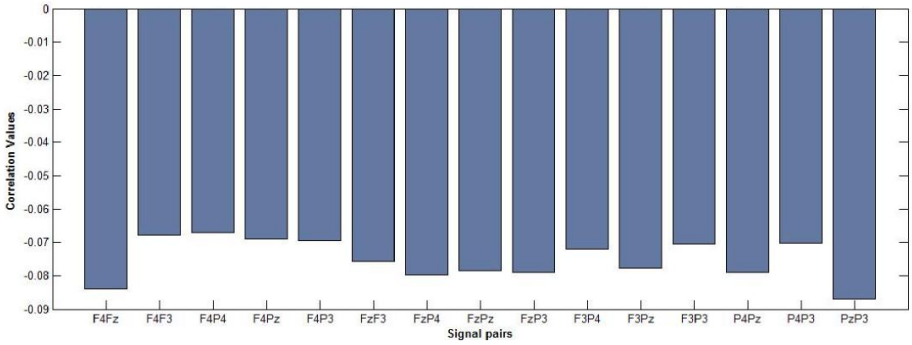

Minimum values from which the signals can be considered to be directly correlated (calculation)

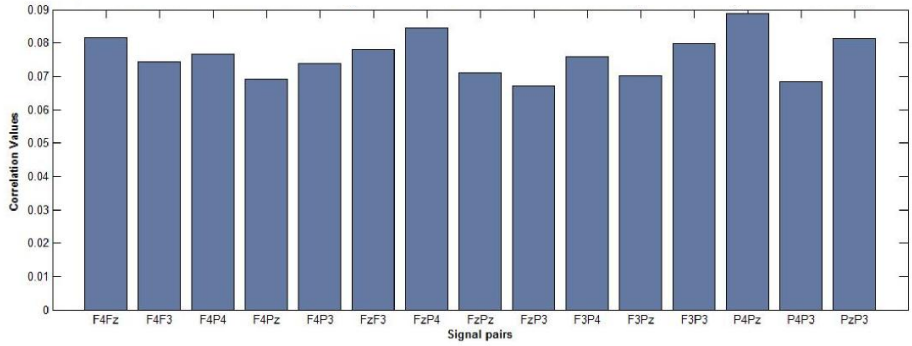

Minimum values from which the signals can be considered to be inversely correlated (eyes closed)

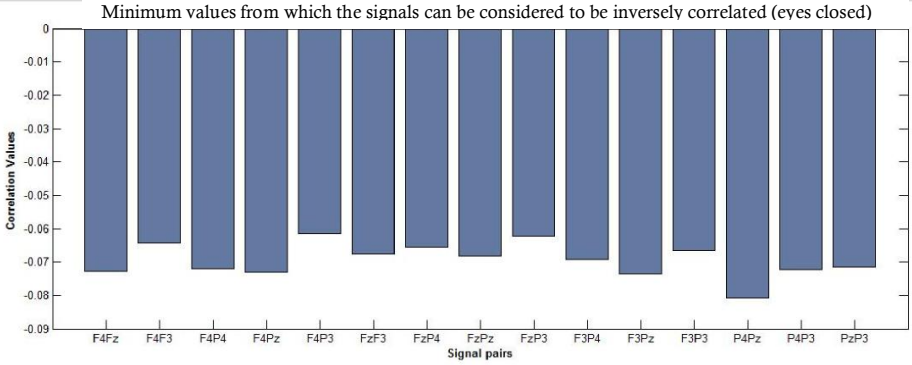

Minimum values from which the signals can be considered to be directly correlated (eyes closed)

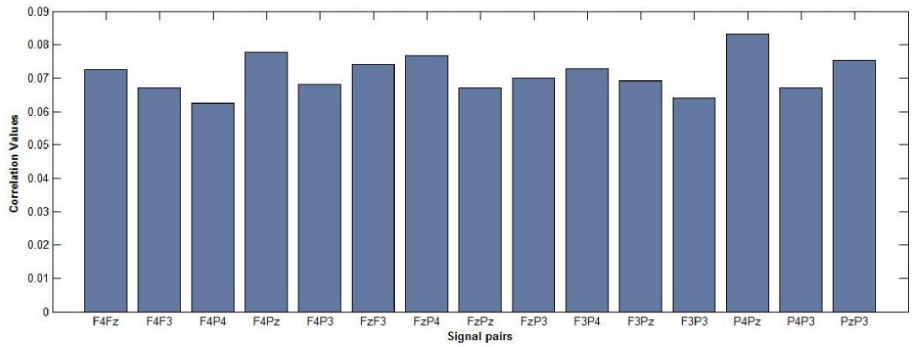

Surrogation carried out for subject SGS

Minimum values from which the signals can be considered to be inversely correlated (calculation)

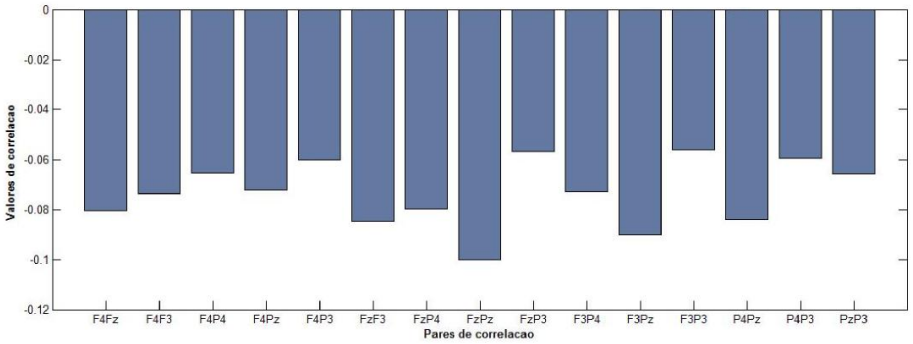

Minimum values from which the signals can be considered to be directly correlated (calculation)

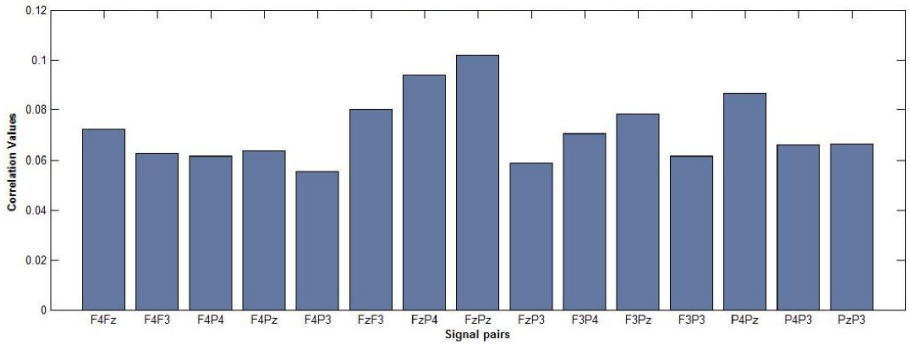

Minimum values from which the signals can be considered to be inversely correlated (eyes closed)

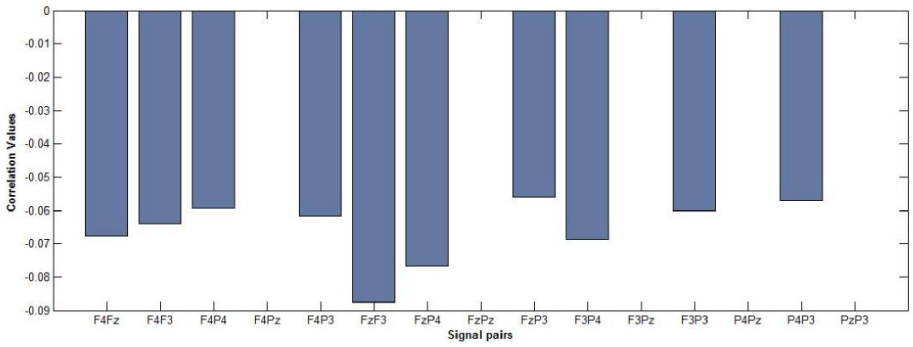

Minimum values from which the signals can be considered to be directly correlated (eyes closed)

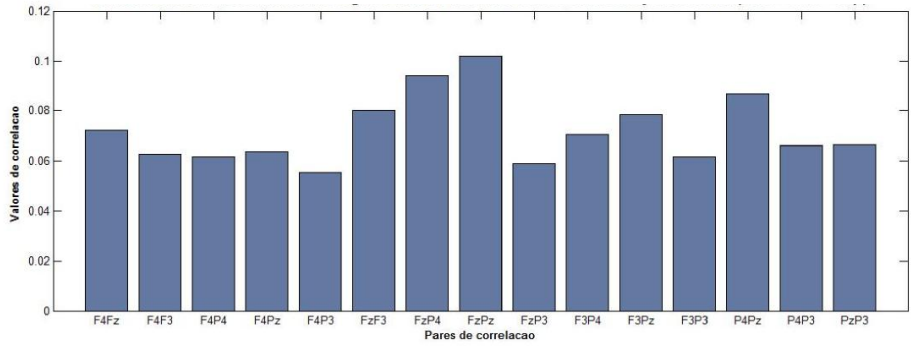

Surrogation carried out for subject SMGG

Minimum values from which the signals can be considered to be inversely correlated (calculation)

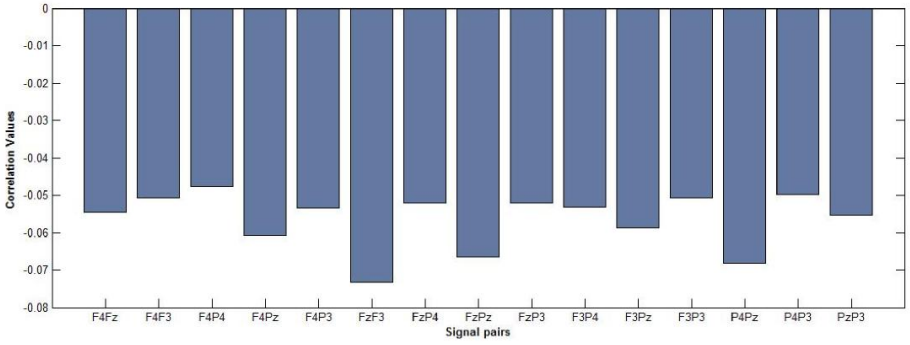

Minimum values from which the signals can be considered to be directly correlated (calculation)

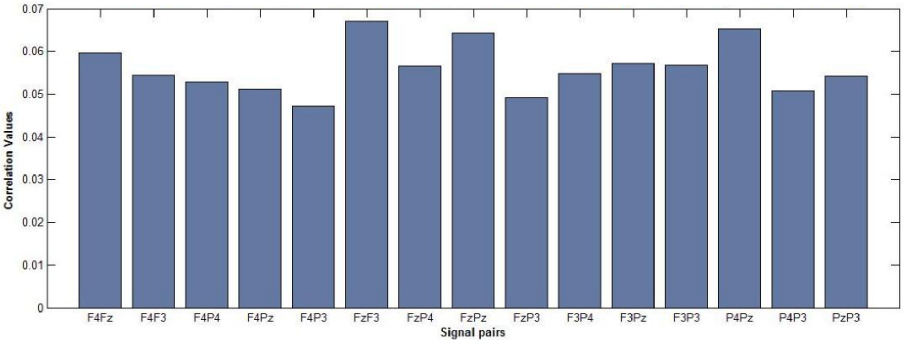

Minimum values from which the signals can be considered to be inversely correlated (eyes closed)

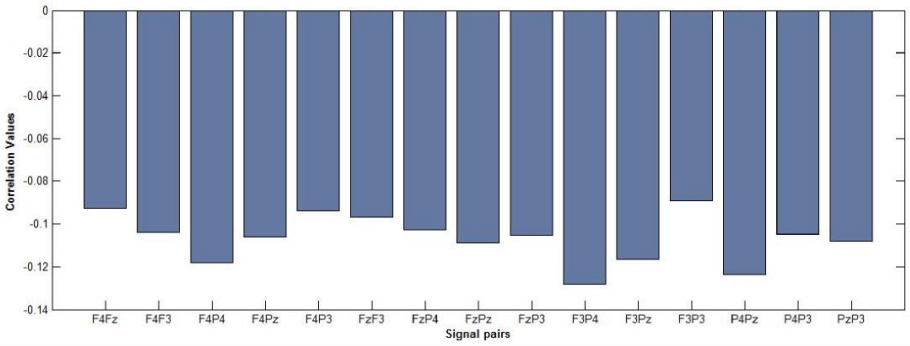

Minimum values from which the signals can be considered to be directly correlated (eyes closed)

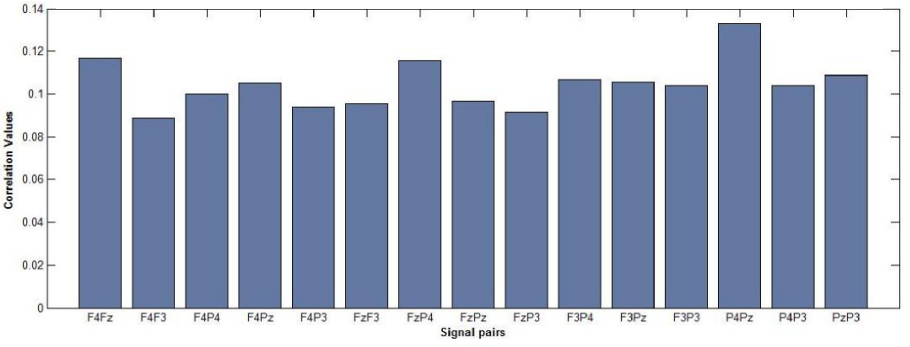

Surrogation carried out for subject SRP

Minimum values from which the signals can be considered to be inversely correlated (calculation)

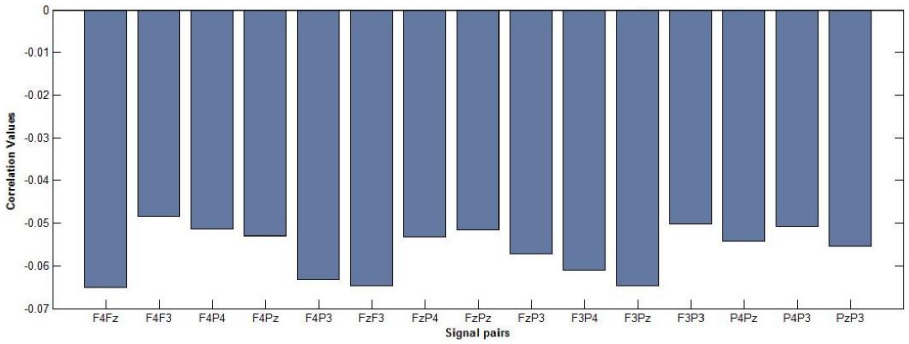

Minimum values from which the signals can be considered to be directly correlated (calculation)

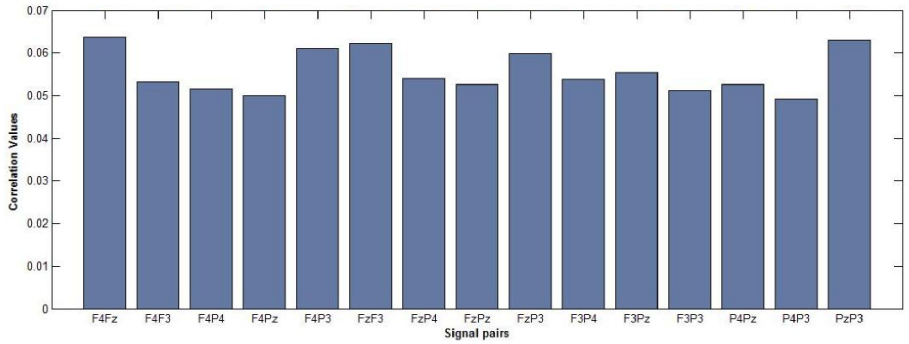

Minimum values from which the signals can be considered to be inversely correlated (eyes closed)

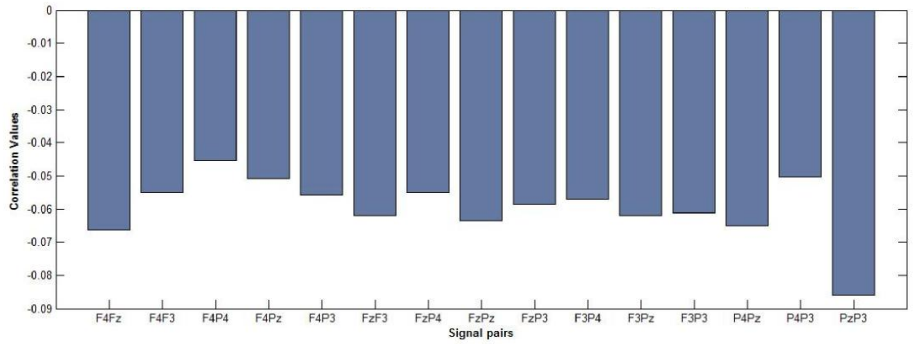

Minimum values from which the signals can be considered to be directly correlated (eyes closed)

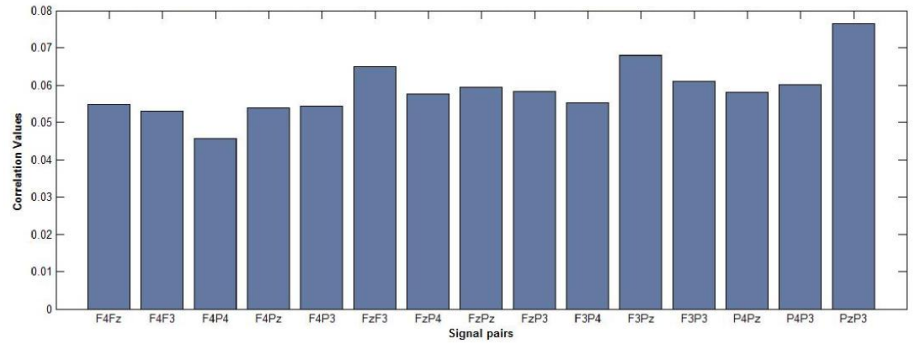

Appendix B

```
% Estimation of h2

clear all;
load tese1.mat BTL_calc;


% Signal selection
signal_eeg = OCR_calc;


% Number of samples
signal_size = size(signal_eeg);
num_samples = signal_size(1, 1);

% Fraction of signal to analise
samples_calc = floor(num_samples/18);

% Data selection
i=1;
data{i}.values = 27;
data{i}.name = 'F4';
i=i+1;
data{i}.values = 31;
data{i}.name = 'Fz';
i=i+1;
data{i}.values = 4;
data{i}.name = 'F3';
i=i+1;
data{i}.values = 19;
data{i}.name = 'P4';
i=i+1;
data{i}.values = 13;
data{i}.name = 'Pz';
i=i+1;
data{i}.values = 12;
data{i}.name = 'P3';
i=i+1;
data{i}.values = 7;
data{i}.name = 'T7';
i=i+1;
data{i}.values = 24;
```

```
data{i}.name = 'T8';
i=i+1;
data{i}.values = 15;
data{i}.name = 'O1';
i=i+1;
data{i}.values = 16;
data{i}.name = 'Oz';
i=i+1;
data{i}.values = 17;
data{i}.name = 'O2';

data1 = 1; %1 1 2 3 4 5
data2 = 2; %2 6 3 4 5 6

% Parametre definition
sampling_freq = 0.488;
samples_per_shift = 6;
num_bins = 5;
shift_max_ms = 100;
shift_max_samples = floor(shift_max_ms/sampling_freq);
num_shifts = floor(shift_max_samples/samples_per_shift);


% Setting the average to zero
x = signal_eeg(1:samples_calc, data{data1}.values) -
                    mean(signal_eeg(1:samples_calc,
data{data1}.values));
y = signal_eeg(1:samples_calc, data{data2}.values) -
                    mean(signal_eeg(1:samples_calc,
data{data2}.values));

result.name = [data{data1}.name data{data2}.name];

% Initializing variables
shift = -num_shifts;
delays_array = zeros(num_shifts*2+1, 1);
h2_array = zeros(num_shifts*2+1, 1);
aux3 = 1;


y = circshift(y, -shift_max_samples);

while shift<=num_shifts

    % Finding the minimum and maximum values of dataI and dataK

    max_x = max(x);
    min_x = min(x);

    max_y = max(y);
    min_y = min(y);


    % Calculating the x coordinates
    interval_x = (max_x - min_x)/num_bins;
    midpoint_x = min_x + interval_x/2;
```

```
index_x = min_x;

midpoints_x = zeros(num_bins, 1);
midpoints_x(1) = midpoint_x;


% Calculating the y coordinates
averages_y = zeros(num_bins, 1);

aux2 = 1;
k=1;
while k<=num_bins

    aux1 = 1;
    y_values = [];

    i=1;
    while i<=length(x)

        if (x(i)>=index_x && x(i) < (index_x+interval_x))

            y_values(aux1) = y(i);
            aux1 = aux1+1;

        end
        i=i+1;
    end

    index_x = index_x + interval_x;
    averages_y(aux2) = mean(y_values);
    aux2 = aux2 + 1;

    k=k+1;
end

i=2;
while i<=num_bins

    midpoints_x(i) = midpoints_x(i-1) + interval_x;

    i=i+1;
end

% Plotting
figure(1);
plot(x, y, 'b. ', midpoints_x, averages_y, 'gd-');


% CALCULATING H2

% Initializing variables
total_var = 0;
explained_var = 0;
m = zeros(num_bins-1, 1);
```

```
clear diference expected_y

i=1;
while i<=length(y)

    diference = y(i) - mean(y);
    total_var = total_var + diference.^2;

    i=i+1;
end

k=1;
while k<=(num_bins-1)

    m(k) = (averages_y(k+1)-averages_y(k))/interval_x;

    i=1;
    while i<=length(x)

        if x(i)>=midpoints_x(k) && x(i)<midpoints_x(k+1)

            expected_y = m(k)*(x(i)-midpoints_x(k))+averages_y(k);
            diference_exp = y(i) - expected_y;
            explained_var = explained_var + diference_exp.^2;


        end

        i=i+1;
    end
    k=k+1;

end

i=1;
while i<=length(x)

    if x(i)<midpoints_x(1)

        expected_y = m(1)*(x(i)-midpoints_x(1))+averages_y(1);
        diference = y(i) - expected_y;
        explained_var = explained_var + diference.^2;

    end

    if x(i)>=midpoints_x(length(midpoints_x))

        expected_y = m(length(m))*(x(i)-
                            midpoints_x(length(midpoints_x)))+

                                averages_y(length(midpoints_x));
        diference = y(i) - expected_y;
        explained_var = explained_var + diference.^2;

    end
```

```
        i=i+1;
    end

    % h2
    h2 = (total_var - explained_var)/total_var;
    h2_array(aux3) = h2;
    delays_array(aux3) = shift*sampling_freq*samples_per_shift;

    % shift vectors
    y = circshift(y, samples_per_shift);
    y = y(1:(length(y)-samples_per_shift), 1);
    x = x(1:(length(x)-samples_per_shift), 1);

    % increment variables
    aux3 = aux3+1;
    shift = shift+1;

end


% Plotting
figure(2);
plot(x, y, 'b. ', midpoints_x, averages_y, 'gd-', x_teste,
                                                    y_esperados, 'm.
');
figure(3);
graph_h2 = plot(delays_array, h2_array, 'b.-');

% Finding maximum h2 and time lag
[h2_max, index_max] = max(abs(h2_array));

delay_max2 = delays_array(index_max);

fprintf('%s / %d / %d \n', result.name, h2_max, delay_max2);
```

Appendix C

Time delays obtained for basal condition with cross-correlation algorithm

	Fz-P3	Fz-P4	F4-F3	Pz-P3	P4-Pz	F3-P4	Fz-F3	F4-P3	F4-Fz	
BTL	0.000	0.976	0.488	-0.488	-0.976	0.488	0.000	-0.488	0.000	BTL
CPFRO	-0.976	0.976	4.392	0.976	-1.952	0.000	0.000	0.000	0.488	CPFRO
CSF	0.000	0.488	-0.976	0.000	0.000	0.000	0.000	0.000	0.000	CSF
DRP	2.928	-1.952	0.000	2.440	0.488	3.416	-0.976	4.880	0.488	DRP
LMBL	-9.272	-10.736	0.000	-1.952	0.976	-12.200	-0.488	-10.736	0.000	LMBL
LSGA	0.488	-0.488	0.488	2.928	-1.464	-0.488	0.000	0.488	0.488	LSGA
MFSA	0.976	0.000	0.000	0.488	0.976	-0.488	0.000	0.976	0.000	MFSA
OCR	0.976	0.488	0.000	0.000	0.976	0.488	0.000	0.488	0.000	OCR
PARS	0.976	-0.976	2.440	1.464	-0.976	-0.976	0.000	1.464	0.976	PARS
PASS	1.952	-0.976	0.488	3.416	0.488	-0.976	-0.488	0.488	0.000	PASS
RAMC	1.952	1.952	0.488	-0.488	0.000	0.976	0.488	0.488	0.000	RAMC
RJGT	0.000	0.000	0.000	0.000	-0.976	0.000	0.000	0.000	0.488	RJGT
SGS	0.488	4.392	1.464	-195886	-195886	2.440	0.976	0.488	0.000	SGS
SMGG	-0.488	-0.976	1.464	3.416	-3.416	-1.952	0.976	0.000	0.488	SMGG
SRP	0.488	0.488	-0.976	0.488	-0.976	0.488	-0.488	0.000	0.000	SRP

Time delays obtained for calculation condition with cross-correlation algorithm

	Pz-P3	P4-Pz	F3-P4	Fz-F3	F4-P3	F4-Fz	
BTL	0.000	-1.464	0.488	0.488	0.488	0.488	**BTL**
CPFRO	4.880	-2.440	0.976	0.000	0.000	0.000	**CPFRO**
CSF	0.000	0.000	0.000	0.000	0.000	0.000	**CSF**
DRP	1.464	0.488	-86.376	-0.488	-87.840	0.000	**DRP**
LMBL	-0.976	-2.440	1.464	0.000	-0.488	0.000	**LMBL**
LSGA	0.976	0.488	0.488	0.488	0.488	0.000	**LSGA**
MFSA	0.488	0.000	-0.488	0.000	0.000	0.000	**MFSA**
OCR	0.000	0.000	0.000	0.000	0.000	0.000	**OCR**
PARS	0.488	0.000	0.000	-0.488	0.000	0.488	**PARS**
PASS	1.952	0.488	-0.976	-0.488	0.000	0.000	**PASS**
RAMC	-0.976	-0.488	122.488	-0.488	78.080	0.000	**RAMC**
RJGT	0.000	-0.976	0.000	0.000	0.000	0.488	**RJGT**
SGS	0.000	-1.464	0.488	0.488	0.000	0.000	**SGS**
SMGG	0.976	-1.464	-0.976	0.000	0.976	-0.488	**SMGG**
SRP	0.000	0.000	0.488	0.000	0.488	0.000	**SRP**

Time delays obtained for basal condition with r2 association function algorithm

	Pz-P3 P3-Pz	P4-Pz Pz-P4	F3-P4 P4-F3	Fz-F3 F3-Fz	F4-P3 P3-F4	F4-Fz Fz-F4
BTL	0.000	0.000	0.000	0.000	0.000	0.000
CPFRO	0.000	0.000	0.000	0.000	0.000	0.000
CSF	0.000	0.000	0.000	0.000	0.000	0.000
DRP	2.928	2.928	-2.928	0.000	0.000	0.000
LMBL	-2.928	0.000	-64.416	0.000	-11.712	0.000
LSGA	0.000	-2.928	0.000	0.000	0.000	0.000
MFSA	0.000	2.928	0.000	0.000	2.928	0.000
OCR	0.000	0.000	0.000	0.000	0.000	0.000
PARS	0.000	0.000	0.000	0.000	0.000	0.000
PASS	0.000	0.000	0.000	0.000	0.000	0.000
RAMC	0.000	0.000	0.000	0.000	0.000	0.000
RJGT	0.000	0.000	0.000	0.000	0.000	0.000
SGS			0.000	0.000	0.000	0.000
SMGG	2.928	-2.928	-2.928	0.000	0.000	0.000
SRP	0.000	0.000	0.000	0.000	0.000	0.000

Time delays obtained for calculation condition with r2 association function algorithm

			BTL	CPFRO	CSF	DRP	LMBL	LSGA	MFSA	OCR	PARS	PASS	RAMC	RJGT	SGS	SMGG	SRP
Pz-P3 P3-Pz		Pz-P3	0.000	0.000	0.000	0.000	0.000	2.928	0.000	0.000	0.000	0.000	0.000	0.000	0.000	0.000	0.000
P4-Pz Pz-P4		P4-Pz	0.000	-2.928	0.000	0.000	-5.856	2.928	0.000	0.000	0.000	0.000	0.000	0.000	0.000	0.000	0.000
F3-P4 P4-F3		F3-P4	0.000	0.000	0.000	-99.552	0.000	0.000	0.000	0.000	0.000	0.000	-46.848	0.000	0.000	0.000	0.000
Fz-F3 F3-Fz		Fz-F3	0.000	0.000	0.000	0.000	0.000	0.000	0.000	0.000	0.000	0.000	0.000	0.000	0.000	0.000	0.000
F4-P3 P3-F4		F4-P3	0.000	0.000	0.000	-99.552	0.000	0.000	0.000	0.000	0.000	0.000	-29.280	0.000	0.000	0.000	0.000
F4-Fz Fz-F4		F4-Fz	0.000	0.000	0.000	0.000	0.000	0.000	0.000	0.000	0.000	0.000	0.000	0.000	0.000	0.000	0.000

Time delays obtained for basal condition with h2 association function algorithm

	P3-Pz	Pz-P3	Pz-P4	P4-Pz	P4-F3	F3-P4	F3-FZ	Fz-F3	P3-F4	F4-P3	FZ-F4	F4-Fz
BTL	0.000	0.000	0.000	0.000	0.000	0.000	0.000	0.000	0.000	0.000	0.000	0.000
CPFRO	0.000	0.000	0.000	0.000	0.000	0.000	0.000	0.000	0.000	0.000	0.000	0.000
CSF	0.000	0.000	0.000	0.000	0.000	0.000	0.000	0.000	0.000	0.000	0.000	0.000
DRP	-2.928	2.928	-2.928	2.928	2.928	-2.928	0.000	0.000	0.000	0.000	0.000	0.000
LMBL	0.000	-2.928	0.000	0.000	64.416	-64.416	0.000	0.000	11.712	-11.712	0.000	0.000
LSGA	0.000	0.000	2.928	-2.928	0.000	0.000	0.000	0.000	0.000	0.000	0.000	0.000
MFSA	0.000	0.000	-2.928	2.928	0.000	0.000	0.000	0.000	-2.928	2.928	0.000	0.000
OCR	0.000	0.000	0.000	0.000	0.000	0.000	0.000	0.000	0.000	0.000	0.000	0.000
PARS	0.000	0.000	0.000	0.000	0.000	0.000	0.000	0.000	0.000	0.000	0.000	0.000
PASS	0.000	0.000	0.000	0.000	0.000	0.000	0.000	0.000	0.000	0.000	0.000	0.000
RAMC	0.000	0.000	0.000	0.000	0.000	0.000	0.000	0.000	0.000	0.000	0.000	0.000
RJGT	0.000	0.000	0.000	0.000	0.000	0.000	0.000	0.000	0.000	0.000	0.000	0.000
SGS					-2.928	0.000	0.000	0.000	0.000	0.000	0.000	0.000
SMGG	0.540	0.536	0.590	0.592	0.614	0.614	0.776	0.774	0.616	0.615	0.800	0.802
SRP	0.000	0.000	0.000	0.000	0.000	0.000	0.000	0.000	0.000	0.000	0.000	0.000

Time delays obtained for calculation condition with h2 association function algorithm

	BTL	CPFRO	CSF	DRP	LMBL	LSGA	MFSA	OCR	PARS	PASS	RAMC	RJGT	SGS	SMGG	SRP
F4-Fz	0.000	0.000	0.000	0.000	0.000	0.000	0.000	0.000	0.000	0.000	0.000	0.000	0.000	0.000	0.000
FZ-F4	0.000	0.000	0.000	0.000	0.000	0.000	0.000	0.000	0.000	0.000	0.000	0.000	0.000	0.000	0.000
F4-P3	0.000	0.000	0.000	-46.848	0.000	0.000	0.000	0.000	0.000	0.000	-32.208	0.000	0.000	0.000	0.000
P3-F4	0.000	0.000	0.000	-17.568	0.000	0.000	0.000	0.000	0.000	0.000	29.280	0.000	0.000	0.000	-2.928
Fz-F3	0.000	0.000	0.000	0.000	0.000	0.000	0.000	0.000	0.000	0.000	0.000	0.000	0.000	0.000	0.000
F3-FZ	0.000	0.000	0.000	0.000	0.000	0.000	0.000	0.000	0.000	0.000	0.000	0.000	0.000	0.000	0.000
F3-P4	0.000	0.000	0.000	-99.552	0.000	0.000	0.000	0.000	0.000	0.000	-49.776	0.000	0.000	0.000	0.000
P4-F3	0.000	0.000	0.000	-61.488	0.000	0.000	0.000	0.000	0.000	0.000	43.920	0.000	0.000	0.000	0.000
P4-Pz	0.000	-2.928	0.000	0.000	-5.856	2.928	0.000	0.000	0.000	0.000	0.000	0.000	0.000	0.000	0.000
Pz-P4	0.000	2.928	0.000	0.000	5.856	-2.928	0.000	0.000	0.000	0.000	0.000	0.000	0.000	0.000	0.000
Pz-P3	0.000	0.000	0.000	0.000	0.000	2.928	0.000	0.000	0.000	0.000	0.000	0.000	0.000	0.000	0.000
P3-Pz	0.000	0.000	0.000	0.000	0.000	-2.928	0.000	0.000	0.000	0.000	0.000	0.000	0.000	0.000	0.000